Practical Evaluation of the Structural Integrity of Welded Joint Structures Towards the Improvement of the Hull Construction Quality Standards

EZZARHAN, BIN ABDULLAH

KYUSHU UNIVERSITY

Kyushu University

Graduate School of Engineering
Department of Civil and Structural Engineering

Practical Evaluation of the Structural Integrity of Welded Joint Structures Towards the Improvement of the Hull Construction Quality Standards

By:
EZZARHAN BIN ABDULLAH

Under Supervision of:
Assoc. Prof. Koji GOTOH

A Thesis Submitted to the Graduate Studies Office in Fulfillment of the Requirements for the Degree of Doctor of Engineering in Civil and Structural Engineering at Kyushu University, Fukuoka, Japan

July 2014

Certificate

The undersigned reviewing committee members hereby certify that EZZARHAN BIN ABDULLAH defended his thesis entitled **"Practical Evaluation of The Structural Integrity of Welded Joint Structures Towards the Improvement of the Hull Construction Quality Standards"** on July 2014 and the thesis was accepted in fulfillment of the requirement for the degree of Doctor of Engineering at Kyushu University.

Koji GOTOH

(Associate Professor, Faculty of Engineering, Kyushu University)

Takao YOSHIKAWA

(Professor, Faculty of Engineering, Kyushu University)

Akiji SHINKAI

(Professor, Faculty of Engineering, Kyushu University)

Yoshimi SONODA

(Professor, Faculty of Engineering, Kyushu University)

ACKNOWLEDGEMENTS

ABSTRACT

The suggestion for improvement of hull construction quality standard e.g; Japan Shipbuilding and Quality Standard (JSQS) become the overall focus of the study. Welded joint with defect such as undercut and large gap size will be highlighted. Numerical work and experimental studies will be conducted in order to confirm such geometrical parameter to investigate the structural integrity in terms of mechanical and fatigue performance.

In numerical studies, butt welded joint with undercut defects and various geometrical parameter will be investigated. Geometrical parameter such as plate thickness, weld bead height, weld bead width, flank angle and weld toe radius will be discussed. In addition, different geometrical shape like U and V-shape of undercut will be included. Furthermore, the important of stress concentration factor (SCF) and stress gradient (χ) in the evaluation of fatigue strength will be highlighted with various geometrical parameter. Re-tensile plastic generation (RPG) stress criterion by Toyosada was applied in order to estimate the fatigue performance. At the end of the numerical study, practical formula with suggested allowable limit will be established for engineer or inspector procedure. From the numerical work, such shape factor can be ignored by considering undercut breadth and depth.

Investigation of the structural integrity and the fatigue performance of the non-load-carrying fillet welded joint with large gap sizes made by CO_2 gas shielded was conducted by experimental work. The study was made to suggest for the extension of construction quality standards. Many codes, classifications and standards were published the requirements of welding gap size. However, most publication was based on experimental and empirical results from the welded joints made by manual metal arc welding. Therefore the present study would become as references in order to future development of the publications. The fatigue test results for the welded specimen with large gap presents higher performance compared to the fatigue design S-N curves proposed by the International Institute of Welding (IIW) and UK-HSE.

KEY WORDS: welded joint with gaps; non-load-carrying, fatigue performance; CO2, hot spot stress.

Table of content   **Page**

CHAPTER 1

CHAPTER 1

Introduction

1.1 Background

An international standard has been published in order to ensure the standardization between countries in the world in many aspects but mainly for worldwide business. Any product in the market, which full fill the requirements of the international codes and standards normally will get benefit in the business trade. Towards the globalization, most of the codes and standards in the world are getting normalized in order to offer cost benefit as well as structural integrity and safety guarantee.

Designers, engineers and inspectors were kind of the group whose depends to the established international code and standards to perform their job. Therefore, the code and standards are really important to keep updated in order to be suitable based on current need and situations. The numerical study of the performance of butt welded joint was done in accordance to various codes and standards. Here, the undercut defect become as a focus in determining the effect to structural integrity. Some of the codes specify undercut depth with plate thickness consideration, but some were ignored. In recent ship building industries, some parts of the plate thickness can goes up to 100mm. Therefore, determining the allowable undercut depth over plate thickness become the important criteria. This is because by considering the plate thickness, certain allowable undercut depth is not sufficient. Shipbuilding company and ship owner raised this issue, especially for structural inspection during construction and maintenance work. Therefore, the study is vital to confirm whether the existing allowable limit is sufficient or some improvement can be made.

The next chapter discussed in this thesis is the continuity of study. The overall aspect of the study will be focusing on the defect which is presented to the welded structure. Two kinds of defects will be highlighted in the study were undercut and large gap size. Other welding defects such as pores, lack of fusion and misalignment are not covered in the present study. Undercut presents in welded joint have been discussed earlier is related to the improvement of JSQS (2010) and IACS Rec. 47 (2010). Therefore, next study will

focus the influence of weld gap size on the fatigue performance of non-load-carrying fillet welded joint. As mentioned in The Welding Institute (TWI) website, poor fit up, lack of tolerance of drawings, incompetence workshop practices and improper dimensioning will introduce an excessive gap between base plate and stiffener. In this case, fatigue performance of welded specimens with zero, 20mm and 25mm gap made by semi-automatic CO_2 gas shielded welding will be discussed. The introduction of fully CO_2 welding joint was at the right time since very limited study was made related to the performance of the type of welding. In addition, the welding joint is widely applied to shipbuilding industries, especially in Japan due to its cost benefit and high strength performance. For that reason, the study made in this thesis will benefit to industrial player, especially for shipyards which are one of the major contributors to Japan's economy.

1.2 Outline

1.2.1 Chapter 1

In this chapter, an introduction about the whole chapter of the study will be presented. A brief explanation in short about the improvement of the code and standard is mentioned in order to give an idea to readers. The important aspect of this study also highlighted in brief.

1.2.2 Chapter 2

The objective of the study will be explained in this chapter. The continuity between numerical study and experimental was briefly discussed in order to harmonize between both studies. The chapter also includes a literature survey as well as explanations about international standards, codes and classification related to the study. In addition, the effect of geometrical parameter such as flank angle, weld bead width and plate thickness will be highlighted. Furthermore, type of stresses which normally applied for welded joints had been discussed according to available standards. Finally, the methodology of fatigue and mechanical tests were explained briefly to provide importance information related to experimental work which was conducted in this study.

1.2.3   Chapter 3

This chapter will discuss about the important of stress concentration and stress gradient in order to evaluate the structural strength at initial level. Practical equation related to butt welded joint geometrical parameter will be highlighted. The numerical study will be focused on the available international standards and code related to undercut of welded joints. The main objective of the study is to suggest for the improvement of JSQS and IACS Rec. 47 related to undercut parameter as specified in the code. In addition, the influence of stress concentration factor and stress gradient to the fatigue performance of butt welded joint will be described in this chapter. Moreover, type of notch's shape also been discussed.

1.2.4   Chapter 4

Investigation about structural performance of non-load-carrying fillet with large gap sizes of welded joint will be discussed. Experimental work was conducted with variable of geometrical parameter and welding condition. Here, semi-automatic CO_2 gas shielded welding was applied to prepare the specimen. Gap size of zero, 20mm and 25mm with different material and welding position will become important criteria in order to discuss their influences. Geometrical parameter of the specimens like toe radius, flank angle and plate thickness was measured in order to confirm the structural performance. Besides, macro observation by stereo microscope was applied in understanding the pattern of surface fracture. Hence, outcome of the study will be the base point of discussion in allowable gap size which applied to CO_2 welding structures.

1.2.5   Chapter 5

Conclusion of overall study for the thesis will be highlighted and summarized in this chapter. Several recommendations work for the future also given for the continuation of the classification code improvement.

1.3 Limitation of the study

Numerical study has been done in 2D in normal condition of environment without considering other type of environment such as corrosive. Such numerical work was consider in plane stress mode since reflect to safety side of numerical calculation in order to published practical formula. In addition, the finite element analysis (FEA) was done only in commercial software of MSC Patran, MSC Marc and MSC Nastran.

The experimental works was also done for non-load-carrying type of semi-automatic CO_2 welded specimen in the normal environment condition with limited gap sizes of zero, 20mm and 25mm which is common in industrial practice. Welding work also perform by a very high skill welder in order to validate the experimental work. Again, the fatigue test was done in three point bending rather than tensile-tensile type test. In this case, both base plate and stiffener was at same thickness. Therefore, the effect of different thickness ratio between base plate and stiffener is not covered.

CHAPTER 2

CHAPTER 2

Literature review: Structural integrity of welded joint

2.1 Background

Welded joint is commonly used for steel structures such as bridges, ships, buildings and others. Since the discovery of the electric arc welding in the 18th century, rapid development of welding technology was established. There are many types of welding processes such as arc welding, oxy-fuel gas welding, resistance welding and solid state welding. Of these, gas metal arc welding has becomes one of the popular methods in the shipbuilding industry. Throughout the years, welding defects are commonly found. Avoid such defects are unavoidable in welding jobs especially at the weld toe. One common example is undercut and uncontrolled weld toe. Some flaws which are introduced at the weld toe may become the stress concentrator and fatigue crack initiation sites (Maddox, 2011).

Many accidents related to structural failure are caused by such factors as overloading, buckling, rupture and fatigue. In fatigue, constant and variable amplitude can initiate crack which will lead to the structural failure. The event may become catastrophic with loss of life and properties. Fricke (2003) stated that welded structures are liable to fatigue failure due to geometrical complexity and metallurgical effect induced by welding works itself. Crack-like defect such as lack of fusion and undercut is an inherent feature of a welded joint. In this case, the crack propagation approach based on linear elastic fracture mechanics (LEFM) is possible in estimating fatigue life. However, in real cases, this kind of defect is often unknown. Therefore, international codes, standards and classification publish the allowable limits for all welding defects as a precaution to failure. Some of the allowable limit which is available in these publications remains the same since it was established. By considering development in welding knowledge, materials technology and many other areas, some of the allowable parameters should be revised.

Nowadays, most construction companies for large structures such as bridges, buildings and ship emphasise on the total cost as a main priority without sacrificing quality and structural integrity. Therefore, welding works are one of the contributing factors which crucially affect the total cost which includes operator and inspector cost as well as

equipment and energy cost. There are examples of a less expensive type of welding method such as shielded metal arc welding and oxy fuel welding. In contrast, the most expensive welding methods are such as electron beam welding and laser beam welding. Due to the high cost, the expensive types of welding methods are normally used for special purposes, especially in high production operation to balance the cost and output.

Japan's shipbuilding companies prefer to use the semi-automatic CO_2 shielded metal arc welding which is identified as cost benefit with high performance. Besides, the type of welding is suitable for constructing welded joint with large gap size. The arc of CO_2 welded joint has better convergence with deep penetration into the base metal. In addition, less slag is generated with low quantities of hydrogen in welding metals and this provides high crack resistance and good mechanical properties.

2.2 Objectives of the study

Structural integrity of welded specimens with defects like undercut and large gap size will be the focus of the study. The study will consist of two parts. The first part will highlight the importance of geometrical parameter in assessing structural performance of butt welded joint with undercut. This will require international standard and codes as references to align with industrial needs. The study will highlight the influence of stress concentration factor and stress gradient in assessing structural performance. Besides, the importance of geometrical parameter such as plate thickness, flank angle, weld bead height and width will be investigated by numerical analysis. This will relate to present construction quality standards, taking into account the plate thickness in specified allowable limit for undercut. Numerical calculation code based on re-tensile plastic zone generation (RPG) stress criterion (Toyosada et. al., 2004) will be applied to calculate the fatigue performance of the study.

The second part of the study is about the effect of large gap size of semi-automatic CO_2 welded joints. The study will highlight the importance of considering the large gap size, which affects the structural integrity of non-load-carrying fillet welded joint. The relationship of both parts will be related to suggest improvement of construction quality standards for shipbuilding especially for JSQS and IACS Rec. 47 based on numerical analysis and experimental work. In addition, other international standards and

6

recommendations were taken into account in this study as major references for the code improvement. There are International Institute of Welding, IIW (2008), American Welding Society (AWS), ISO 5817, DNV, ABS and etc. The experimental work will be conducted based on ISO/TR 14345 (2012), ClasS-NK (2013) and JSME Standard 002 (1984).

2.3 Butt welded joint with undercut

There are many types of defects present in butt welded joints. Such defects normally act as a stress concentrator which will affect the structural integrity. Fig. 2.1 shows the schematic illustration of undercut.
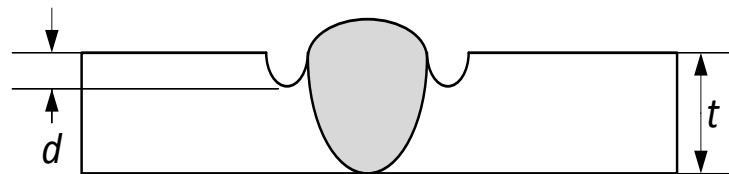
(a) Butt welded joint
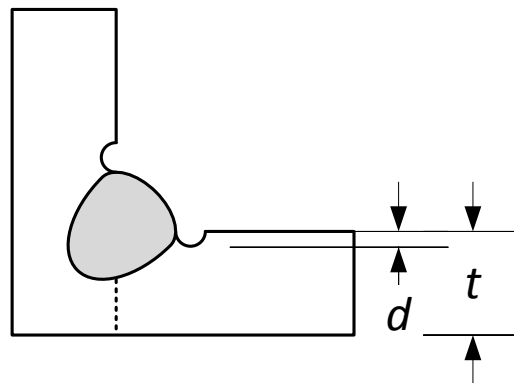
(b) Fillet welded joint

Fig. 2.1 Undercut at welded joint (d = undercut depth, t = thickness)

Undercut was explained by Mashiri et. al. (2001) as a surface depression along the interface between weld and base metal which is caused by welding procedure resulting from missing material. He investigated the effect of undercut depth, width and radius. Throughout the study, he found that the fatigue life of load-carrying-type tee welded joint increases with the increment of undercut radius and width but in contrary with undercut depth. In another study by Yamaguchi et. al (1964), the U-notch specimen illustrates

7

higher fatigue strength compared to the V-notch specimen at the same undercut depth. Their study also revealed that high tensile material with notch illustrates better fatigue performance compared to mild steel. They used specimens with shapes similar to welded joints because their study highlighted on the geometrical effect for fatigue life. Numerical work by Nguyen and Wahab (1996) found that undercut was the significant geometrical effect which affects the fatigue life and fatigue strength with other geometrical defects. Besides, by comparing with the flush ground-welded plate, specimens with undercut reduce the fatigue life twice. They concluded that reducing or eliminating undercut can increase almost 50 % of the welded structure fatigue life. An experimental study on T-joints by Bell et. al. (1989) indicates that fatigue life is significantly reduced by an undercut greater than 0.5 mm. He mentioned that the allowable undercut specified by AWS code of 0.25 mm for cyclic load appears to be on the conservative side. In addition, studies by Tchankov et. al. (1999) under constant amplitude loading showed that fatigue strength becomes smaller with the increase of stress concentration factor. The studies also mention that Miner's damage accumulation rule provides good estimation for welded structure under variable loading.

2.3.1 International standard and classification code related to undercut

In current situations, ship building industries use plate thickness of up to 100 mm. In other words, it is quite conservative to maintain such allowable limits without considering other geometrical parameters. Both JSQS and IACS published allowable limits for undercut depth without considering the plate thickness as mentioned in AWS. Therefore, this study is vital in order to confirm the influence of plate thickness parameters in the limitation of such undercut depth.

Below is a brief explanation of the requirements and allowable limits that were published in international standards and codes.

a)   International Institute of Welding (IIW)

The document was prepared by a group of specialists in the welding field which was chaired by Professor Hobbacher. The objective of this document is to provide a basis for the design and analysis of welded structure and component which is loaded with cyclic load to prevent from fatigue failure. Besides, it will provide more assistance as additional information in establishing and using the other fatigue design code. Steel and aluminium

are the materials which were established in the document. This is because of their common and wide use in the construction field. Fig. 2.2 shows the fatigue design curve for steel as guidance to validate any welded structure performance. Each fatigue design class (FAT) number was taken at 2 million cycles which is referred to nominal stress as X-axis. The slope of the S-N curve is 3 until knee point at 10 million cycles. Then on the basis of shear stresses, the slope becomes 5 from knee point and is assumed to correspond to 100 million cycles.
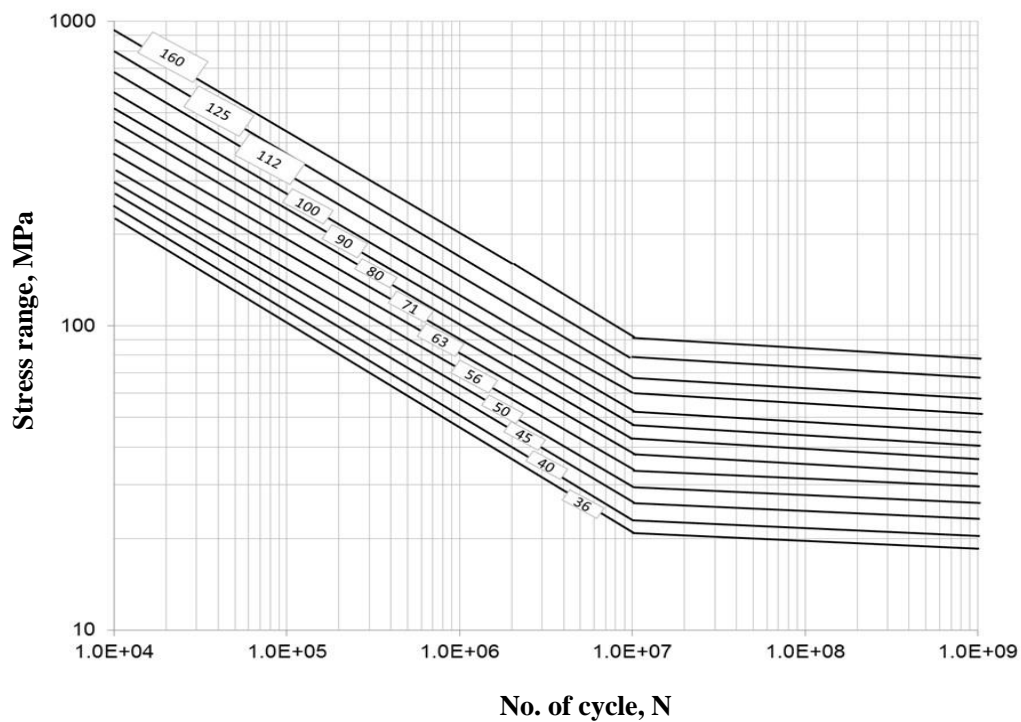
Fig. 2.2 Fatigue resistance S-N curve of nominal stress for steel (IIW, 2008)
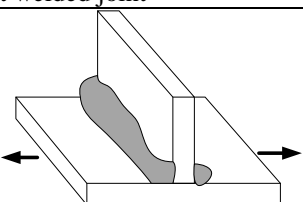
In the recommendation for fatigue design of welded joints and components, there is an allowable limit of undercut specified for steel. However the allowable limit is applicable for the plate thickness of 10 to 20 mm. Besides, undercut deeper than 1 mm is considered as crack-like imperfection. Here, undercut over thickness (*d/t*) ratio is used as the limit. The acceptance level of the limit is related to fatigue class design as described in this chapter and tabulated in Table 2.1.

Table 2.1 Allowable undercut limit by IIW recommendation

Fatigue class	Allowable undercut, d/t	
	Butt joint	Fillet joint
100	0.025	Not applicable
90	0.05	Not applicable
80	0.075	0.05
71	0.1	0.075
63	0.1	0.1
56 or lower	0.1	0.1

The type of welded joint is specified with schematic illustrations as established in IIW documents. Table 2.2 shows some of the examples which is related to the study. The FAT in this study was determined by denoting to FAT St. which satisfies the welding condition. The curve of IIW-FAT80 is applied for as welded joint of the non-load-carrying type of welded joints. However, for toe ground, the category is IIW-FAT100. This is very important during comparison of real structure to fatigue design curve.

Table 2.2 Fatigue design curve (FAT) for steel structure

Structural detail	Description	FAT St.	Remarks
Butt welds, transverse load			
	Transverse loaded butt weld ground to flush, 100% NDT	112	All welds ground flush to surface, grinding parallel to direction of stress
	Transverse butt weld made in shop in flat position, NDT Weld reinforcement <0.1. thickness	90	Weld run on and run off pieces to be used and subsequently removed
	Transverse butt weld not satisfying conditions of above, NDT	80	Same as above. Misalignment <5%
Fillet welded joint			
	Transverse non-load carrying attachment, not thicker than main plate • K-butt weld, toe ground • Two sided fillets, toe ground • Fillet weld(s), as welded • Thicker than main plate	100 100 80 71	Grinding marks normal to weld toe An angular misalignment corresponding to $k_m=1.2$ is already covered

b)   American Welding Society (AWS) - AWS D1.1/D1.1M: 2010

The code mentions about defects in welded joint which is vital to consider in any inspection work or before any structure is put into operation. In general, allowable undercut limit specified in this code shall not exceed 1 mm. Besides, the weld bead height also restricted to not to exceed of 3 mm. In details, the code mentions two kinds of load for non-tubular structures which is statically and cyclically. The allowable undercut for statically load with plate thickness less than 25 mm is 1 mm. However, the exception is for an undercut of less than 2 mm for any accumulated length up to 50 mm in any 300 mm maximum length. In addition, for thickness equal or greater than 25 mm, the undercut shall not exceed 2mm at any length. The most stringent is applicable for the primary member which the weld is transverse to tensile stress under any design condition. For cyclic load, the allowable undercut shall be no more than 0.25 mm and 1 mm for other cases. In this case, the standard makes a clear limit for the undercut depth by introducing the plate thickness as an important variable to state the allowable limit.

c)   British Standard – BS EN ISO 6520-1:1998

This standard defines an undercut as an irregular groove at a toe of a run in the parent metal or in previously deposited weld metal due to welding work. There are many classifications of undercut such as continuous undercut, intermittent undercut and inter run undercut. However, the limitation of undercut depth is not mentioned in this code and is established in ISO 5817.
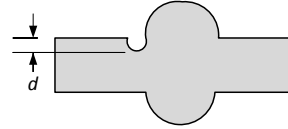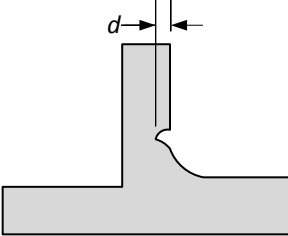
d)   ISO 5817: 2003

There are three quality levels specified in this code. The most stringent quality level is level B, followed by levels C and D. The allowable limit for undercuts under quality level B shall not exceed $0.05t$ (t = thickness) with maximum of 0.5 mm. For quality levels C and D, the undercuts must lower than $0.1t$ and $0.2t$ respectively. The maximum allowable undercut depth for level C is similar to level B but for level D it is 1 mm. This standard emphasised on the relationship of plate thickness and the undercut depth. However, the maximum undercut depth at the lowest quality level still 1 mm.

11

e) **Japan Shipbuilding and Quality Standard (JSQS) and International**

The hull construction quality standards were updated in 2010 by the Japan Society of Naval Architects and Ocean Engineers. The purpose of the standard is to maintain the construction quality of the ship hull by establishing the tolerance limit of construction work. Many revisions have been made since 1964 in order to equivalent the enhancement in construction technology. For undercut defects, Table 2.3 shows the limitation of the undercut depth. For butt welded joint, the undercut depth is limited up to 0.5 mm for continuous welding length of 90 mm. However, for other locations at the welding line, the limit is up to 0.8 mm at any thickness. In fillet welded joint cases, the undercut depth permitted is only up to 0.8 mm at any welding line location. This standard refers mostly to the weld toe site since many undercuts occur at this point of interest.
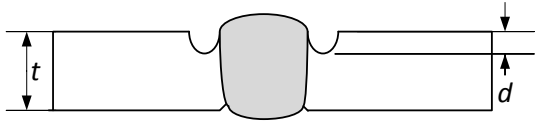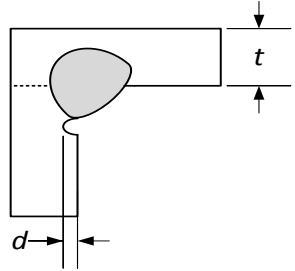
Table 2.3 Limitation of undercut depth of JSQS

Type of joint	Description	Item	Limit	Remarks
Butt welded	Skin plate and face plate between 0.6L	Over 90mm continuous d≤0.5		To be repaired by using fine electrode of CO_2 welding (carefully avoid short bead for higher tensile steels)
	Others	d≤0.8		
Fillet welded		d≤0.8		

f) **International Association of Classification Societies (IACS) Rec. 47**

This hull construction quality standard specifies that the undercut depth for butt welded joints must be lower than 0.5 mm for the strength member and 0.8 mm for other members. The allowable limit is applicable to any plate thickness. Fig. 2.5 presents the schematic diagram for the undercut depth.

Table 2.4 Limitation of undercut depth of IACS (d = undercut depth, t = thickness)

Detail	Limit
Butt weld undercut 	$d \leq 0.5$mm for strength member $d \leq 0.8$mm for other member
Fillet weld undercut 	$d \leq 0.8$mm

g)   Other international standards, codes or reports

Many international codes have established the requirements for welding structure. However, most of the codes refer to AWS D1.1 as reference for detail requirements and allowable limits. Such codes like the API recommended to practise 2A-WSD (RP- 2A-WSD) – 21$^{\text{st}}$ Ed. 2000 while the Offshore Technology report 2001/015 (HSE, UK) makes reference to AWS D1.1. However, in BS-EN 1993 which is formerly known as Eurocode 3-Part 1-9 (2005) for design of steel structures which emphasises on fatigue subject published the method for assessment of fatigue resistance for structural members, joints and connections subjected to fatigue loading was based on the IIW recommendation. Most classification code like ABS and DNV mention about undercut but prefer to ground in order to avoid such stress concentrator.

2.4 Effect of geometrical parameter of butt welded joint

Studies have been conducted since many years ago in order to investigate the influence of geometrical parameters to the structural performance of welded joints. Such geometrical parameters like plate thickness, flank angle, weld bead height and width and weld toe radius have become the subject of interests. Most common of welded joints in built-up structures are butt, fillet and cruciform joints. Besides, many researchers found that by improving the geometrical parameters will extend the structure life. Fig. 2.3 presents the definition of the geometrical parameters.
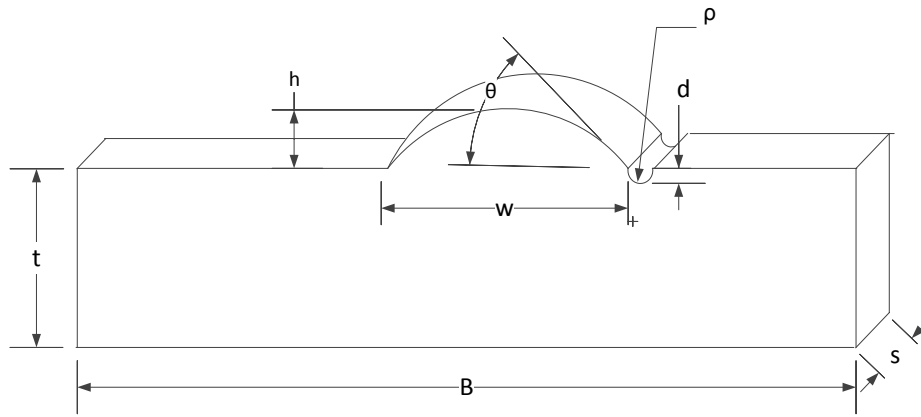
Fig. 2.3 Model configuration of butt welded joint

Here; h = weld bead height, w = weld bead width, d = undercut depth, t = plate thickness,
B = plate width, s = length, Θ = flank angle, ρ = root radius

2.4.1 Thickness

The most influential effect to the fatigue performance is the plate or tube thickness of any welded structure. Many researchers have conducted the fatigue test in order to investigate the thickness effect. Kihl and Sarkani (1997) had conducted over 100 fatigue tests for high strength welded steel cruciform with different thicknesses. The study was performed under both constant and variable amplitude axial loads. Based on experimental and analytical results, thicker plate presents lower fatigue performance.

However, a study by Onozuka and Sugimiya (1989) on non-load-carrying type fillet welded joint with plate thickness from 19 mm to 100 mm found that at plate thickness of 100 mm shows 60 % fatigue life than 19 mm at 2×10^6 cycles. Another numerical study by Mahmud and Sumi (2011) for butt and fillet welded joints shows higher fatigue performance for thicker plate with undercut but the welded joints with no undercut shows poor performance. They also concluded that even though the stress concentration factor plays an important role in determining fatigue performance for thicker plate, a higher stress gradient may reduce the effect after a small amount of crack growth.

2.4.2 Flank angle

The definition of flank angle can be seen in Fig. 2.5. The JSQS and IACS Rec. 47 codes allow a maximum flank angle of 90°. In industrial practice, grinding is normally used to reduce flank angle and undercut radius. However, this will introduce time consumption and increase the construction cost. A study by Lee et. al. (2009) indicates that fatigue life was gradually increased by decreasing the flank angle. He made the study at the same stress range to confirm the effect of the flank angle. Another conclusion by Yamaguchi et. al. (1964) was that the magnitude of the flank angle is a dominant factor which governs the fatigue strength of welded joints.

2.4.3 Weld bead height and width

Some researchers believe that weld bead reinforcement height and width may contribute to the mechanical performance of the structures. Experimental results from William et. al. (1970) stated that the increase of width and height of weld bead resulted in decrease of fatigue resistance of the material. However, their reports show the effects of the metallurgical notches and the micro-geometry from the welding process play higher possibilities in contributing to fatigue performance than the geometrical profile. Experimental work was also performed by Yamaguchi et. al. (1964) for cruciform and butt welded joint in order to confirm the effect of the notches and welding geometry on fatigue strength. The study shows there is no significant effect of weld bead width compares to weld bead height. Fatigue results of the welded specimen shows poor performance for higher weld bead reinforcement height. In this case, there is a common relationship between the weld bead reinforcement height and the flank angle where both are increased linearly. Again, welded specimens with no weld bead or fully ground presented higher fatigue strength compared to the others.

2.4.4 Weld toe radius

There is no specification of allowable limit for the weld toe radius (Fig. 2.5) specified in any standards and codes because of the difficulty of measurement in the industrial point of view. However, most researchers believe that increasing the weld toe radius can increase the fatigue performance of welded structures. Experimental work conducted by Lee et. al.

(2009) found the fatigue life increase with the increase of the weld toe radius. He made arrangements to study the weld toe radius from 0.56 to 2.11 mm. In industrial practice, enlarging the weld toe radius can be simulated as grinding work of TIG dressing. Many standards and codes put emphasis on surface finishing work like grinding after performing a welding job in order to reduce the stress concentration point at sharp edges and improve fatigue performance.

An experimental work and finite element analysis performed by Pang (1993) on cruciform welded joints present a wide combination of weld toe radius and flank angle. His study found the stress concentration factor, K_t for the bluntest and sharpest of weld toe profiles were 2.2 and 12 respectively. Moreover, he suggested for more realistic value of $K_t = 5.0$ for a toe radius of 0.1mm and flank angle of 45° even though the experimental result through extrapolation showed $K_t = 1.85$. The study shows the relationship between the toe radius and the stress concentration factor for welded joint.

2.5 Fillet welded joint with large gap size

The study of structural integrity and fatigue performance related to large gap on fillet welded joint is currently not available. This is due to the belief by most designers, engineers and inspectors that welded joint with zero gap will give better performance to fatigue life. However, based on a previous study by Miki et. al. (1993) it shown that welded joint with zero gap presents lower fatigue strength compared to 2 mm and 3 mm root gap size. He found an unfused portion after a micro-etch test and photomicrograph for a zero gap specimen very sharp with crack-like shape. The study gives an overview on the penetration of weld metal into the root section which becomes deeper and gives better performance of fatigue life.

In industrial practice, defects or flaw detectable in welded joint may reduce fatigue life. However, Maddox (2011) claimed that most of the fabricator has changed their reaction to any kind of defects. The design philosophy of 'fit for purpose' becomes the main focus in considering any defect, whether it will bring premature failure of the structure. Hence, detectable defects in welded joints depend on the sensitivity of non-destructive testing equipment. Such repair work may be very expensive and unnecessary

since it may introduce more harmful defects. In addition, cracks may arise during repair work which has undergone difficult conditions.
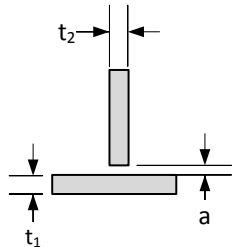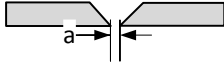
2.5.1   International standards and classification codes related to the gap size

There are some standards and classification codes that give allowable limit to the gap size of welded joint.

a) JSQS

The allowable gap size as specified in this standard should not exceed 2 mm for standard and 3 mm for maximum tolerance.
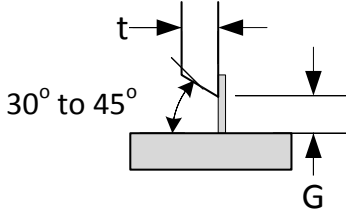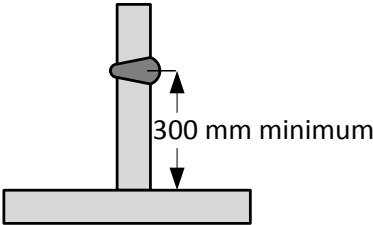
Table 2.5 Limitation of welding gap size in JSQS

Sub section	Item	Standard range	Tolerance limits	Remarks
Gap before welding	Fillet weld	$a \le 2$	$a \le 3$	$3 \le a \le 5$ Increased leg length Rule leg + (a-2) $5 \le a \le 16$ Welding with bevel preparation or liner treatment
	Butt weld (manual welding)	Manual welding $2 \le a \le 3.5$ CO_2 welding $0 \le a \le 3.5$	$a \le 5$	$5 \le a \le 16$ Attached the backing material and after welding remove it. Then the opposite side only defective parts $16 \le a \le 25$ Welding up with edge preparation of partial renew $a > 25$ Partial renew

b) IACS

The standard gives a formula for allowable gap size. However, the maximum gap size is 5 mm and is reduced after consideration of leg length. Table 2.6 shows details about the allowable limit of the gap size.

Table 2.6 Allowable limit of welding gap size in IACS

Detail	Remedial standard
Tee fillet	3mm < G ≤ 5mm – leg length increased to Rule leg + (G-2)
	5mm < G ≤ 16mm or G ≤ 1.5t – chamfer by 30º to 40º build up with welding, on one side, with backing strip if necessary, grind and weld t 30º to 45º G
	G > 16mm or G > 1.5t use insert plate of minimum width 300mm 300 mm minimum

c) BS EN 1011-2:2001

The standard suggests for fillet welded joints to have close contact between the plates because the existence of gap will resulted of risk of cracking. However, the standard allows a maximum of 3 mm of gap. Besides, consideration for large gap sizes shall be made by increasing the throat size of the fillet weld.

d) Other international standards, codes and classification

International standards related to welding structure such as AWS, Eurocode 3 and UK-HSE and classification society, ABS, DNV, ClasS-NK-Common Structure Rules (CSR) are found not much critical in specifying any allowable limit to the gap size of welded joints. Most of the standards and codes keep silent in establishing allowable gap sizes for the welded joint.

2.6 Type of stress

In welded structures, geometrical conditions and complexity can cause uneven stress distribution and concentration along the weld toe towards the plate thickness. There are three types of stresses commonly used in the calculation for fatigue assessment. The kinds of stresses are defined in Section 2.6.2 to 2.6.4. Furthermore, IIW fatigue recommendations established the methods to assess the fatigue performance of welded structures. The IIW fatigue design S-N curves were established based on nominal stress. Besides, UK-HSE basic design curve becomes as references in order to compare the calculation of hot spot stress approach. The different approaches based on the combination of S-N curves with the linear cumulative damage law for the fatigue assessment are nominal stress, hot spot stress and effective notch stress as the reference stress.

2.6.1 UK-HSE basic design curve

The fatigue design curve was established in IACS Rec. 56 Fatigue assessment of ship structures (1999). The type of stresses which was defined in equation 2.6 can be applied to the nominal stress, hot spot stress and effective notch stress approach depends on the kind of stresses used in the calculation. In this study, the tee fillet welded specimen falls under Curve C which is defined by UK-HSE basic design S-N curve in Fig. 2.4 and Tables 2.7 and 2.8. For ship structural details, the S-N curve is presented by the following formula:

$$S^m N = K \tag{2.1}$$

Here: S = stress range as defined in Section 2.6.2 – 2.6.4, N = number of cycle to failure, m, K = constant depending on material and weld type, type of loading, geometrical configuration and environmental condition
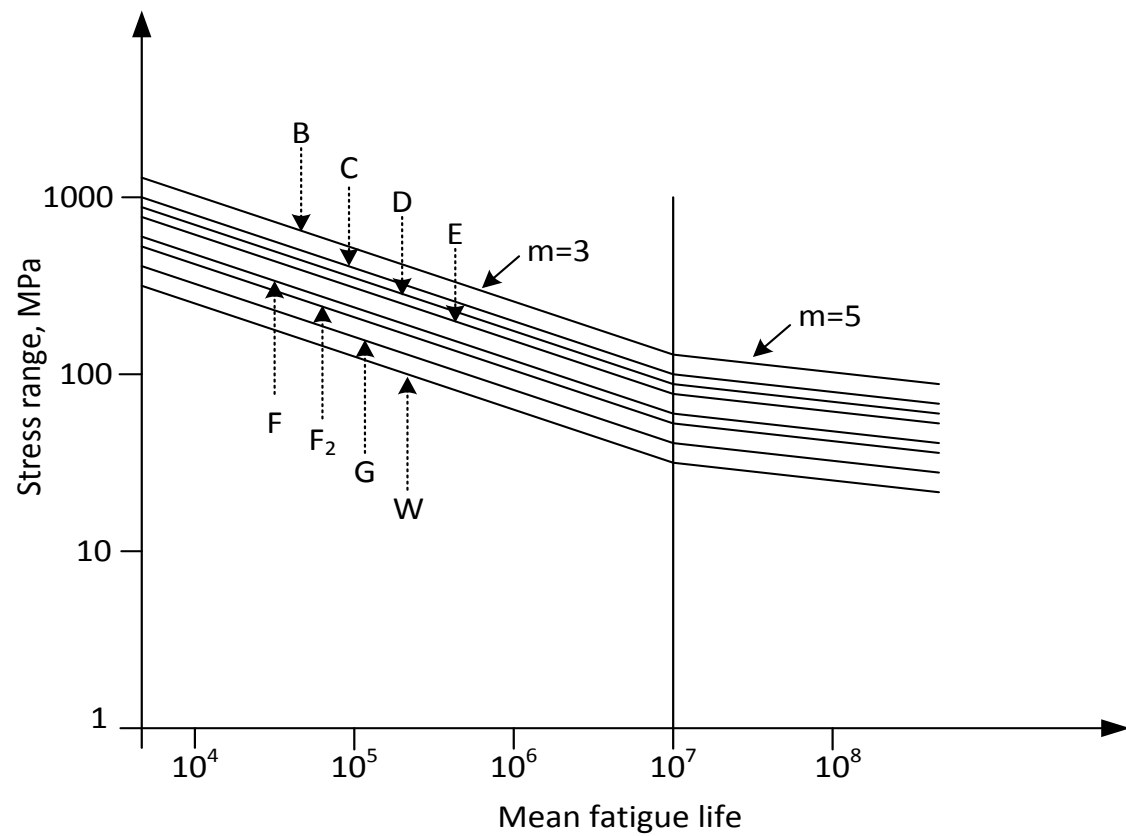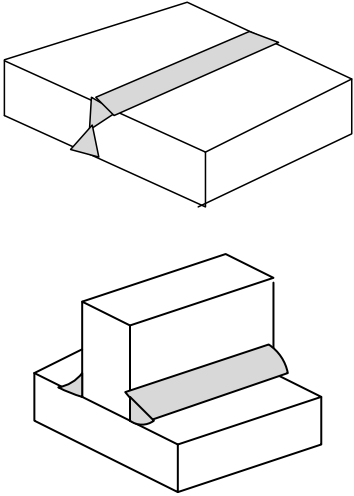
Fig. 2.4 UK-HSE basic design S-N curve

Table 2.7 New HSE basic design S-N curve

Class	K		Classification Factor
	$N \leq 10^7$ (m=3)	$N \geq 10^7$ (m=3)	
B	5800×10^{12}	4034×10^{16}	0.64
C	3464×10^{12}	1708×10^{16}	076
D	1520×10^{12}	4329×10^{15}	1
E	1026×10^{12}	2249×10^{15}	1.14
F	6319×10^{11}	1002×10^{15}	1.34
F2	4330×10^{11}	5339×10^{14}	1.52
G	2481×10^{11}	2110×10^{14}	1.83
W	9279×10^{10}	4097×10^{13}	2.13

Table 2.8 Category for welded joint classification

Joint classification	Description	Examples
Category 2		
B	Full penetration welds with the weld cap ground flush with the surface and with the weld proved to be free from defects by NDT	
C	Butt of fillet welds made by an automatic submerged or open arc process and with no start stop positions within their length	
D	As (C) but with stop-start position within the length	

2.6.2 Nominal stress

Nominal stress is a kind of stress distribution in welded connection without consideration of any structural configuration. Normally, most S-N curves are based on nominal stress. In general, it can be defined by integral load parameters and sectional properties which allow it determination also in section at the fatigue critical point. As mentioned in the IIW recommendation, the measurement of nominal stress must exclude the stress or strain concentrator due to correspond to the discontinuity of structural component. Besides, strain gauges used in experimental work should be placed outside the stress concentrator field of the welded joint. In this study, common formulae based on the strength of material have been used in order to determine the stress range.

2.6.3 Hot spot stress

The structural hot spot stress is calculated based on the finite element analysis. The stress includes all stress raising effects of a structural detail excluding that due to the local weld profile itself. However, non-linear peak stress caused by the local notch like the weld toe is excluded from the structural stress. This approach is normally used where there is no clearly defined nominal stress due to complicated geometric effects or where the structural discontinuity is not comparable to a classified structural detail. Based on the finite element analysis, hot spot stress can determine by reference points with extrapolation to the weld toe under consideration from stresses at the reference point.
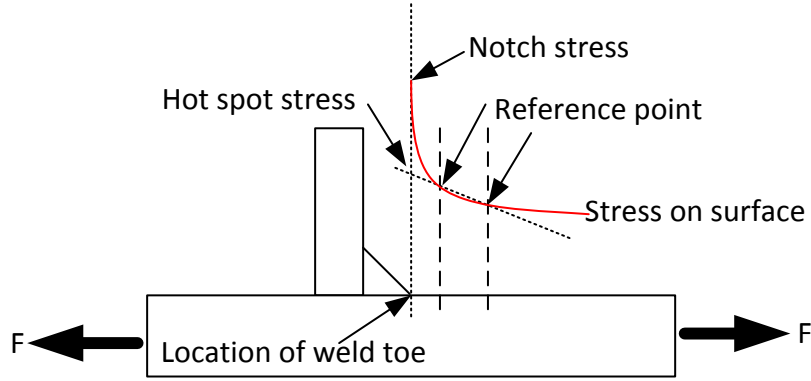
Fig. 2.5 Definition of hot spot stress (IIW, 2008)

As can be seen in Fig. 2.5, the hot spot stress was calculated by using reference point by surface extrapolation to the weld toe under consideration from stresses at the reference point. Normally the finite element analysis is carried out to calculate the hot spot stress. All of the formulas are based on plate thickness, t. Below are the extrapolation equations of type 'a' hot spot as shown in Fig. 2.6:
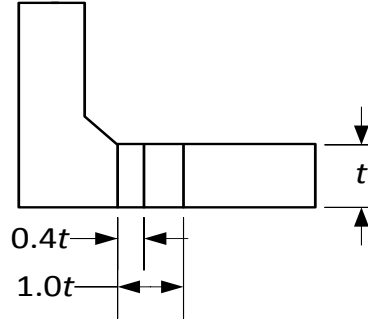
Fig. 2.6 Hot spot type 'a'

a) For the fine mesh with element length not more than $0.4t$ at the hot spot:

$$\sigma_{hs} = 1.67 \cdot \sigma_{0.4t} - 0.67 \cdot \sigma_{1.0t} \tag{2.2}$$

b) For evaluation based on three references point at $0.4t$, $0.9t$ and $1.4t$:

$$\sigma_{hs} = 2.52 \cdot \sigma_{0.4t} - 2.24 \cdot \sigma_{0.9t} + 0.72 \cdot \sigma_{1.4t} \tag{2.3}$$

c) Coarse mesh with higher order elements having length equal to plate thickness at the hot spot:

$$\sigma_{hs} = 1.5 \cdot \sigma_{0.5t} - 0.5 \cdot \sigma_{1.5t} \tag{2.4}$$

22

For type 'b' hot spot calculation which is independent of plate thickness as shown in Fig. 2.7, the equations below should be applied:
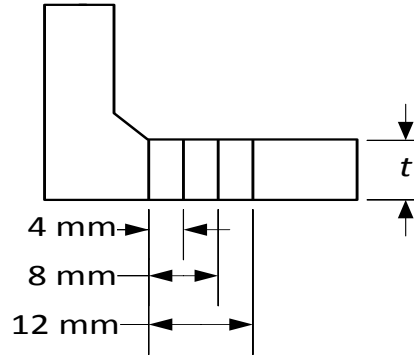
Fig. 2.7 Hot spot type 'b'

a) Fine mesh with element length of not more than 4 mm at the hot spot based on three locations at 4 mm, 8 mm and 12 mm.

$$\sigma_{hs} = 3.\, \sigma_{4mm} - 3\,.\, \sigma_{8mm} + \sigma_{12mm} \qquad (2.5)$$

b) Coarse mesh with higher order elements having length of 10mm at the hot spot:

$$\sigma_{hs} = 1.5.\, \sigma_{5mm} - 0.5\,.\, \sigma_{15mm} \qquad (2.6)$$

2.6.4 Effective notch stress

The definition is the total stress at the root of notch as can be seen in Fig. 2.5 by assuming linear-elastic material behaviour. Radaj et. al. (2009) mentioned that the stresses can be calculated for sharp or mild notches at the weld toe, weld root or nugget edge where the structural stresses have been defined. The elastic notch stress concepts were originally restricted to the high-cycle fatigue range. Even though the present study does not consider the effective notch stress, the calculation can be made by parametric formula or by FEA. The calculation method is valid for plate thickness more or equal to 5 mm. At weld toes, effective notch stress may be assumed to be of 1.6 times than that of the structural hot spot stress.

23

2.7 Fatigue test

In order to evaluate the welded specimens under cyclic load, such fatigue test will be conducted. The most common load applied during the test is tension-tension and three point bending load. Below are the guidance provided by the technical report or international standards in order to conduct the fatigue test. Besides, it is important to refer to this code to confirm the reliability of the test results.

The technical report, ISO/TR 14345 (2012) covered the method of fatigue testing of welded component under constant and variable amplitude loading. The guidance is limited to medium and high cycle, which is nominal stress that does not exceed the yield strength of the welded structure. However, there is no coverage for low cycle fatigue, corrosion and high temperature fatigue test in this guidance. In addition, the method for specimen preparation and the evaluation of the test result is explained.

As seen in figure 2.8, a minimum distance of load action for the three point bending fatigue test is recommended by the guidance. It is common to have a normal distribution for load action at different plate thickness.
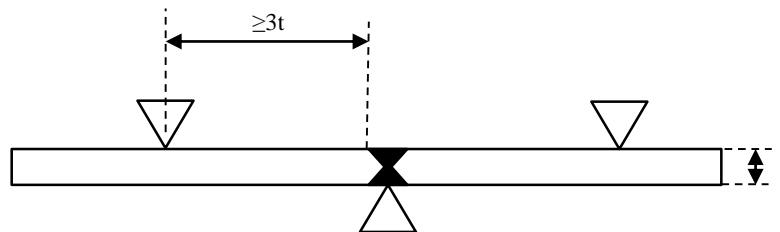
Fig. 2.8 Distance recommended by ISO/TR 14345:2012

2.8 Mechanical test

All mechanical tests for experimental work in this research were evaluated according to ClasS-NK (2013) which placed emphasis on butt and fillet welded joints. The code gives the requirements for qualification tests of welding procedures for steel in the hull construction and marine structures. For fillet weld type, the tests and examinations below must be done:

a) Visual test – 100%

b) Surface crack detection – 100% by dye penetrant testing or magnetic particle testing

c) Macro examination

- The specimen will be prepared by etching one side of the surface to clearly reveal the weld metal, fusion line, root penetration and the heat affected zone

d) Hardness test

- The test is required for steel with minimum yield strength of 355 MPa. Normally Vickers method of HV10 is used. The results of the hardness test shall not exceed 350HV10 for yield strength less or equal to 420MPa and 420HV10 for yield strength between 420MPa to 690MPa.

e) Fracture test

- The test can be done by folding the stiffener plate onto the base plate. The stiffener plate can be bent from 45° to 90° in order to reveal any cracks, porosity and pores, inclusion, lack of fusion and incomplete penetration.

CHAPTER 3

CHAPTER 3

Numerical Investigation of Butt Welded Joint with Undercut

3.1 Introduction

It is common practice to refer to international standards or codes before start to produce any product or structural construction. In every country in the world, there are different requirements in international and national standards based on industrial local practices and legislations. However, most of the countries make reference to international standards and codes which are worldwide accepted such as ASME, AWS, BS, ISO and JIS especially for business and trading activity. Such benefits through international standard compliance refer to the safety, reliability and quality level of services or products which cannot compromise. Inspection job is the most critical task before any structure put into service. Again, periodically maintenance also acquires engineers to perform thorough inspection to ensure safety and structural integrity. For welded structures in shipbuilding industries, inspectors or engineers often make reference to international code of standard such as IACS Rec. 47 and JSQS. Welded joint defect such as undercut commonly found during the inspection. Even though there is improvement in welding technology, those defect commonly occurred due to several factors such as welder's skill, lack of structural design consideration and insufficient setting of welding condition.

Defects such as undercut, porosity and lack of fusion at the welding structures cannot be avoided completely. Even though there are many techniques suggested by international code and standards, such defect still occurred. In order to allow the occurrence, most of requirements with regard to welding give certain parameters as a guide. Table 3.1 shows the codes and report which are referring to the welding requirements in this study. In this table, some code was considering thickness and undercut depth but some other codes only consider undercut depth. Again, the study is important to confirm the influence of many geometrical for establishing allowable limit for welded structure.

26

Table 3.1 Available standard for welded structure with undercut

No.	Standard	For Strength Member	Other Member
1.	American Welding Society, AWS D1.1/D1.1M:2006	$d \leq 0.25$ mm $d \leq 1$ mm – other cases	If thickness (t) ≤ 25mm, $d \leq 1$ mm
			If thickness (t) > 25mm, d ≤ 2 mm
2.	JSQS / IACS	$d \leq 0.5$ mm	$d \leq 0.8$ mm
3.	ISO 5817 :2003	If thickness (t) : 0.5 to 3mm – Undercut, d is not permitted If thickness (t) > 3mm, undercut, $d \leq 0.05$t or maximum of 0.5mm	

3.2 Theoretical background

The following theories are applied in the numerical works in this chapter.

3.2.1 *Stress concentration factor*

This study is focusing on the undercut effect of welded structure which causing inhomogeneous stress distribution with applied load. Stress concentration factor (SCF) is defined as the ratio of maximum stress and nominal stress at undercut root. SCF expressed by $K_{t(net)}$ indicate how stress amplified at undercut root net ligament area and is calculated based following definition:

$$K_{t(net)} = \sigma_{max} / \sigma_{nominal} \tag{3.1}$$

For tension cases;

$$\sigma_{nominal} = F / a \tag{3.2}$$

For bending cases;

$$\sigma_{nominal} = 6M / a^2 \tag{3.3}$$

here; a = s(t-d); P = load; M =moment; s = plate width; a = net area thickness; t = plate thickness; d = undercut depth

Neuber's trigonometric formula for SCF is defined as follows:

$$K_{tN} = \frac{(K_{ts}-1)(K_{td}-1)}{\sqrt{(K_{ts}-1)^2(K_{td}-1)^2}} + 1 \tag{3.4}$$

$$K_{ts} = 1 + 2\sqrt{t/\rho} \tag{3.5}$$

For pure tension;

$$K_{td} = \frac{\beta_1 - 2c}{1 - c/\sqrt{e/\rho + 1}} \tag{3.6}$$

In plane bending;

$$K_{td} = \frac{2(e/\rho + 1) - \beta_1\sqrt{e/\rho + 1}}{4/\beta_2(e/\rho + 1) - 3\beta_1} \tag{3.7}$$

here; K_{ts} is SCF for shallow, K_{td} for deep notches, ρ is an undercut radius, e is a distance from undercut root towards plate thickness (t-d), $\beta_1 = \dfrac{2(e/\rho + 1)\sqrt{(e/\rho)}}{(e/\rho + 1)\tan^{-1}\sqrt{(e/\rho)} + \sqrt{e/\rho}}$,

$\beta_2 = \dfrac{4\sqrt{(e/\rho)}^{3/2}}{3\left\{\sqrt{e/\rho} + (e/\rho - 1)\tan^{-1}\sqrt{(e/\rho)}\right\}}$ and $c = \dfrac{\beta_1 - \sqrt{(e/\rho + 1)}}{4/\beta_2\sqrt{(e/\rho + 1)} - 1}$.

3.2.2   Stress gradient

Stress gradient can be simply described as how fast the stress decreases along the extension of the undercut. The stress gradient at the notch root gives an indication of the volume of highly stressed material which is significant for the geometrical effect on fatigue limit (Fillippini, 2000). In other words, how fast the decrement of stress from undercut root gives an important indicator on the fatigue performance. Below is the definition of stress gradient, ϕ:
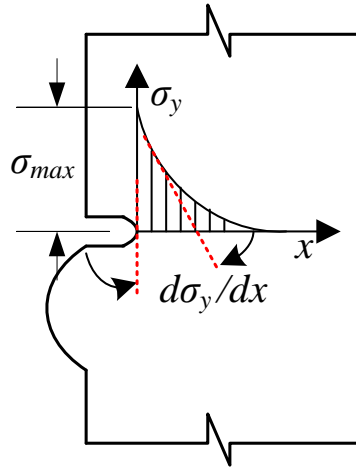
Fig. 3.1 Definition of stress gradient, ϕ (Fillippini, 2000)

$$\sigma_y(x) = \sigma_{max} + \phi x \qquad (3.8)$$

Stress gradient;

$$\phi \equiv \left(\frac{d\sigma_y}{dx}\right)_{x=0} \qquad (3.9)$$

3.2.3 Residual stress

The inherent stress method is used to estimate the residual stress distribution for the butt welded joint. In this study, the following equation established by Matsuoka et. al (1991) is used in order to calculate the residual stress for the butt welded joint:

$$\sigma_1(x, y: T) = \alpha\sigma_Y \exp(-\pi(x/B)^2) f(y; T) \qquad (3.10)$$

Where; $f(y; T) = \sum_{n=0}^{\infty} \exp(-\pi(\lambda y_n/B)^2)$, $y_n = |y + \{(-1)^n(n + 0.5) - 0.5\}T|$, $B = \beta(F/\sigma_y)$, $F = \gamma Q$

Here; Heat input, Q (J/mm), T=plate thickness (mm), non-dimensional coefficient, β=1.357, γ=0.16, α=1.942 and λ=1.788, σ_Y= yield strength of parent plate

29

3.2.4 RPG stress criterion

Paris Law is the base for the study. The law relates the stress intensity factor range to sub-critical crack growth under a fatigue stress regime.

$$\text{da/dN} = C\Delta K^{m} \tag{3.11}$$

Where: a = the crack length

           N = the number of load cycles

           C,m = material constants

           ΔK = the range of the stress intensity factor

Paris' law proposed by Paris and Erdogan (1963) is a fatigue crack propagation equation. Life prediction for fatigue cracks was made very much easier and far more quantitative, when Paris postulated that the range of stress intensity factor might characterize sub-critical crack growth under fatigue loading in the same way that K characterized critical or fast fracture. He examined a number of alloys and realized that plots of crack growth rate against range of stress intensity factor gave straight lines on log-log scales. At that time most researchers were believing that a fatigue crack opens during cyclic loading, because according to the Dugdale (1960) model calculation results of the crack opening displacement at the minimum load (P_{min}) following the maximum load show that the crack opens. Then Elber (1971) pointed out that fatigue cracks remained closed during a part of load cycles because the fatigue crack propagated in the residual tensile plastic deformed zone ahead of the crack tip. He proposed an effective stress intensity factor range in the replacement of the stress intensity factor range in Paris' law to be used as the fatigue crack propagation parameter.

$$\text{da/dN} = C\ (\Delta K_{eff})^{m} \tag{3.12}$$

where;   da/dN = fatigue crack propagation rate

           ΔK_{eff} = effective stress intensity factor range

           C,m = material constant

Toyosada (1994) established important criteria to evaluate fatigue crack growth together with RPG criterion is calculated by numerical method. He developed a fatigue crack opening and closing simulation model for a through thickness crack under an arbitrary stress distribution. The program simulates fatigue crack growth by considering strain hardening of work material which was developed based on re-tensile plastic zone generated load (P_{RPG}). In his study, stress at the crack tip increases rapidly after the loading process due to very large stress concentration factor. Then, stress level at crack tip reaches the value of material yield stress. Finally, more applied loading will develop the tensile plastic zone ahead of a crack tip. Fatigue crack propagation developed by following expressed equation:

$$da/dN = C \, (\Delta K_{RP})^m \tag{3.13}$$

Where: da/dN = fatigue crack propagation rate

ΔK_{RP} = effective stress intensity factor range based on RPG load

$\Delta K_{RP} = (P_{max} - P_{RPG}) \sqrt{\pi a f}$

P_{max} = maximum load

P_{RPG} = RPG load

f = magnification factor

a = crack length

C, m = material constant

3.3 Finite Element Analysis (FEA)

3.3.1 FEA Modeling

In order to evaluate fatigue strength of butt welded joint, Fig. 3.2 illustrates a schematic model which is analysed by commercial finite element software, Patran/MD Nastran 2011. The analysed plate thickness (t) varies from 10 mm, 25 mm and 30 mm with different weld bead height (h) and flank angle (θ). All model parameters such as undercut (d) are tabulated in Table 3.2. The model can be treated as plane stress. To study the effect of variable geometrical parameter with undercut to butt welded joint, all parameters such as

plate width (*B*), weld bead width (*w*), root radius (*ρ*), load (*F*) and moment (*M*) are remaining constant. The model was design according to allowable limit by AWS, JSQS and IACS Rec. 47. The codes specified that undercut for butt welded joint is not more than 0.5 mm and 0.8 mm for strength member and other member respectively. Table 3.1 will explain briefly about the allowable limit that requires in the several codes. In addition, the JSQS and IACS Rec. 47 specified weld bead height must less or equal to 6 mm for maximum flank angle of 60º.

For both tension and bending cases, boundary conditions with uniform distributed load (*F*) and moment (*M*) are applied at one edge and fixed at another edge. σ_o in this case is defined as applied stress. As seen in Fig. 3.3, fine mesh size is defined near to undercut root in order to increase accuracy, especially considering the inherent high stress and strain gradient. This result is vital in order to obtain stress distribution along undercut root. Mesh division is made in 4-node quadrilateral element type. For this study, minimum mesh size is 0.05mm x 0.05mm nearly at undercut area and 0.5 mm x 0.5 mm at another area of infinite plate. In addition, mechanical properties for the model such as modulus of elasticity, *E* are set for 2.1 x 10^5 MPa and Poisson's ratio, *v* is 0.3.
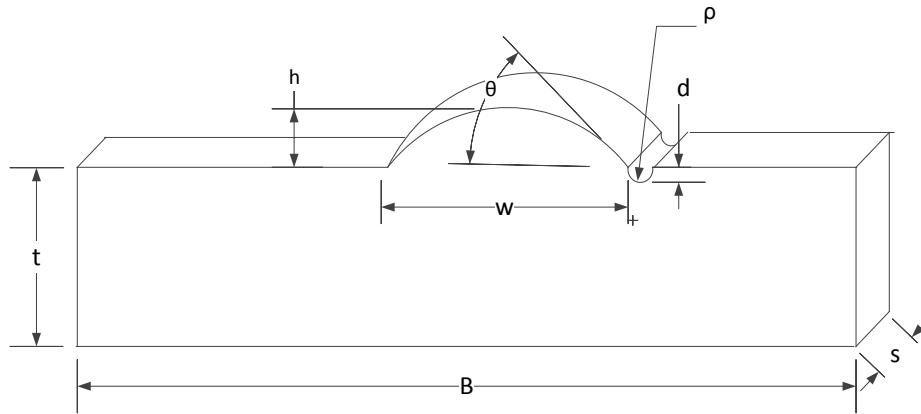
Fig. 3.2 Model configuration of butt welded joint

Here; h = weld bead height, w = weld bead width, d = undercut depth, t = plate thickness, B = plate width, s = length, Θ = flank angle, ρ = root radius

32
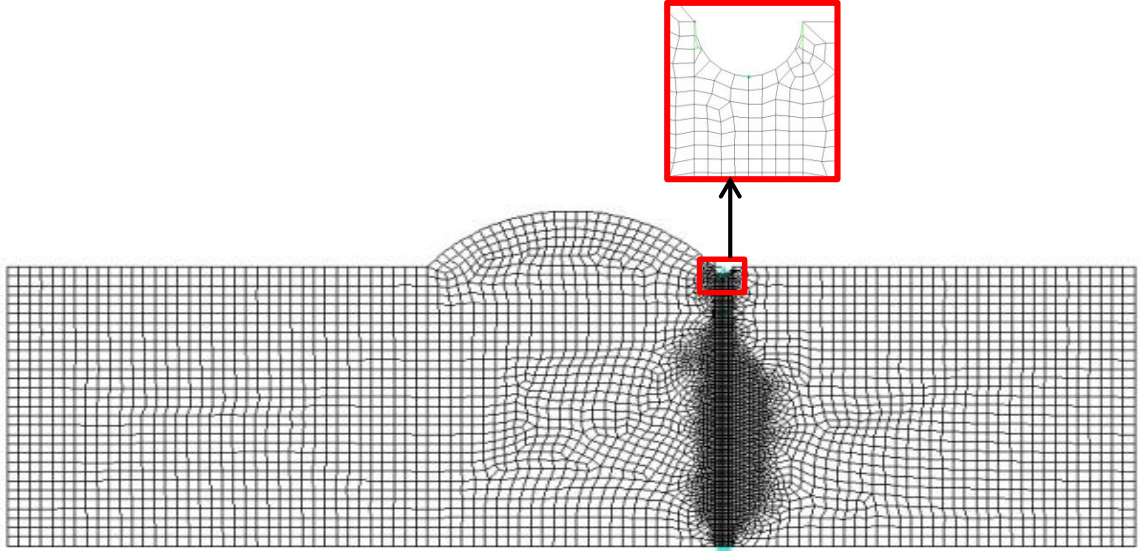
Fig. 3.3 Meshing elements

3.3.2 Effect of plate thickness with undercut in comparison to international code

The study will consist of FEA modelling based on the allowable limit which is established in AWS and JSQS. Both codes were mentioning the allowable limit for undercut depth. However, JSQS classification code did not consider plate thickness as the parameter in assessing the welded structure defect. In this case, the role of stress concentration factor will be highlighted in order to access the structural integrity of butt welded joint specimens. Table 3.2 presents geometrical condition for this study. Here, the plate thickness, t and undercut, d will be highlighted of the study. The ratio of d/t was established in order to confirm and suggest new allowable limit to be consider in JSQS.

Table 3.2 Geometrical condition for modelling

Model name	Plate thickness, t (mm)	Flank angle, θ	Weld bead height, h (mm)	Undercut depth, d (mm)	d/t
AWS10	10	0	0	1	0.1
JSQS10				0.8	0.08
AWS25	25			1	0.04
JSQS25				0.8	0.032
AWS30	30			2	0.067
JSQS30				0.8	0.027
AWS10	10	8.1	1	1	0.1
JSQS10				0.8	0.08
AWS25	25			1	0.04
JSQS25				0.8	0.032
AWS30	30			2	0.067
JSQS30				0.8	0.027
AWS10	10	23.42	3	1	0.1
JSQS10				0.8	0.08
AWS25	25			1	0.04
JSQS25				0.8	0.032
AWS30	30			2	0.067
JSQS30				0.8	0.027
AWS10	10	46.75	6	1	0.1
JSQS10				0.8	0.08
AWS25	25			1	0.04
JSQS25				0.8	0.032
AWS30	30			2	0.067
JSQS30				0.8	0.027
AWS10	10	66.35	9	1	0.1
JSQS10				0.8	0.08
AWS25	25			1	0.04
JSQS25				0.8	0.032
AWS30	30			2	0.067
JSQS30				0.8	0.027

3.3.2.1   Result and discussion

Stress concentration factor will highlight in this study. Table 3.3 present all results which was analysed by FEA and calculated with above equations. The result shows the influence of *d/t* ratio in contributing to stress concentration factors.

Table 3.3 Stress concentration factor at different flank angle and *d/t* ratio

Flank angle, θ	Model name	Plate thickness (mm)	Undercut depth, *d* (mm)	σ_{max}/σ_o	*d/t*	$K_{t(net)}$
0	AWS10	10	1	3.17	0.10	2.85
	JSQS10		0.8	3.07	0.08	2.83
	AWS25	25	1	2.98	0.04	2.86
	JSQS25		0.8	2.9	0.032	2.81
	AWS30	30	2	2.98	0.067	2.78
	JSQS30		0.8	2.88	0.027	2.81
8.1	AWS10	10	1	3.23	0.10	2.90
	JSQS10		0.8	3.16	0.08	2.91
	AWS25	25	1	3.16	0.04	3.03
	JSQS25		0.8	3.17	0.032	3.06
	AWS30	30	2	3.13	0.067	2.92
	JSQS30		0.8	3.18	0.027	3.10
23.42	AWS10	10	1	3.28	0.10	2.95
	JSQS10		0.8	3.25	0.08	2.99
	AWS25	25	1	3.36	0.04	3.22
	JSQS25		0.8	3.41	0.032	3.30
	AWS30	30	2	3.57	0.067	3.01
	JSQS30		0.8	3.48	0.027	3.38
46.75	AWS10	10	1	3.29	0.10	2.96
	JSQS10		0.8	3.28	0.08	3.01
	AWS25	25	1	3.46	0.04	3.32
	JSQS25		0.8	3.58	0.032	3.47
	AWS30	30	2	3.34	0.067	3.12
	JSQS30		0.8	3.71	0.027	3.61
66.35	AWS10	10	1	3.30	0.10	2.97
	JSQS10		0.8	3.21	0.08	2.95
	AWS25	25	1	3.53	0.04	3.39
	JSQS25		0.8	3.52	0.032	3.41
	AWS30	30	2	3.36	0.067	3.14
	JSQS30		0.8	3.66	0.027	3.56

3.3.2.2   Stress distribution

Figs. 3.4 to 3.8 show the stress distribution along a-direction for all models at different flank angle. In all figures, maximum stress occurred at the tip of undercut root. In this case, maximum stress is $\sigma_{max}/\sigma_o = 3.71$ at a plate thickness of 30 mm at flank angle of 46.75° (Table 3.3). Though, ratio of undercut depth (*d*) over plate thickness (*t*), *d/t*, have

significant effect on stress concentration at notch root. The welded specimen with weld bead shows higher stress ratio compare to the welded specimen with no weld bead. As can be seen in Table 3.3, higher maximum stress ratio, σ_{max}/σ_o was found at higher flank angle. Moreover, the results of welded specimen with weld bead found higher stress concentration for higher *d/t* ratio. For the same model, at *d/t* ratio = 0.1, flank angle of 0° and plate thickness of 10 mm, the maximum stress concentration is 3.17 and at d/t ratio = 0.08, maximum stress concentration is 3.07. The results show a stress concentration at undercut root is proportional to *d/t* ratio. Again, maximum stress distribution slightly higher at thicker plate thickness for welded specimen with weld bead but in contrary for welded specimen without weld bead.

The effect of weld bead height on stress concentration factor is shown in Fig. 3.9. The results shows stress concentration factor, $K_{t(net)}$ increase by increment of weld bead height. However the increment occurred up to 6mm and decrease at 9 mm of weld bead height. The results found higher stress concentration factor at JSQS model for thickness of 25 and 30 mm. AWS and JSQS model with thickness of 10mm shows similar pattern on $K_{t(net)}$. The graph also found higher stress concentration, $K_{t(net)}$ at thicker plate as shown by AWS model and JSQS model at plate thickness of 30 mm compare to 25 mm and 10 mm.
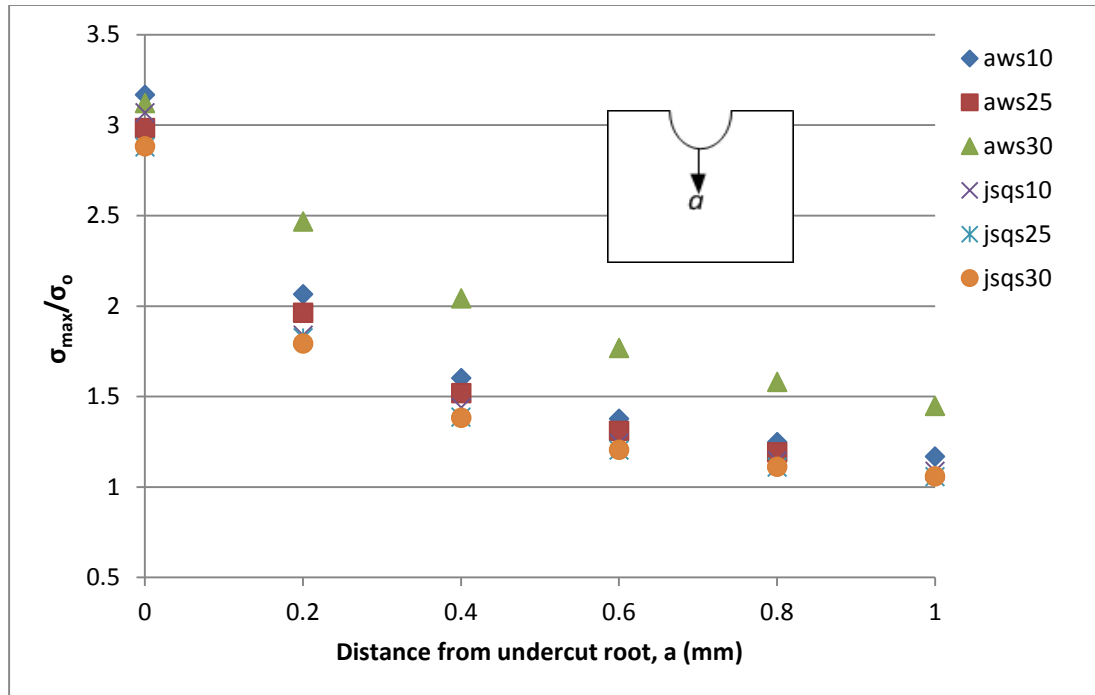
Fig. 3.4 Stress distribution at flank angle, $\theta = 0^o$ up to 1 mm distance from root
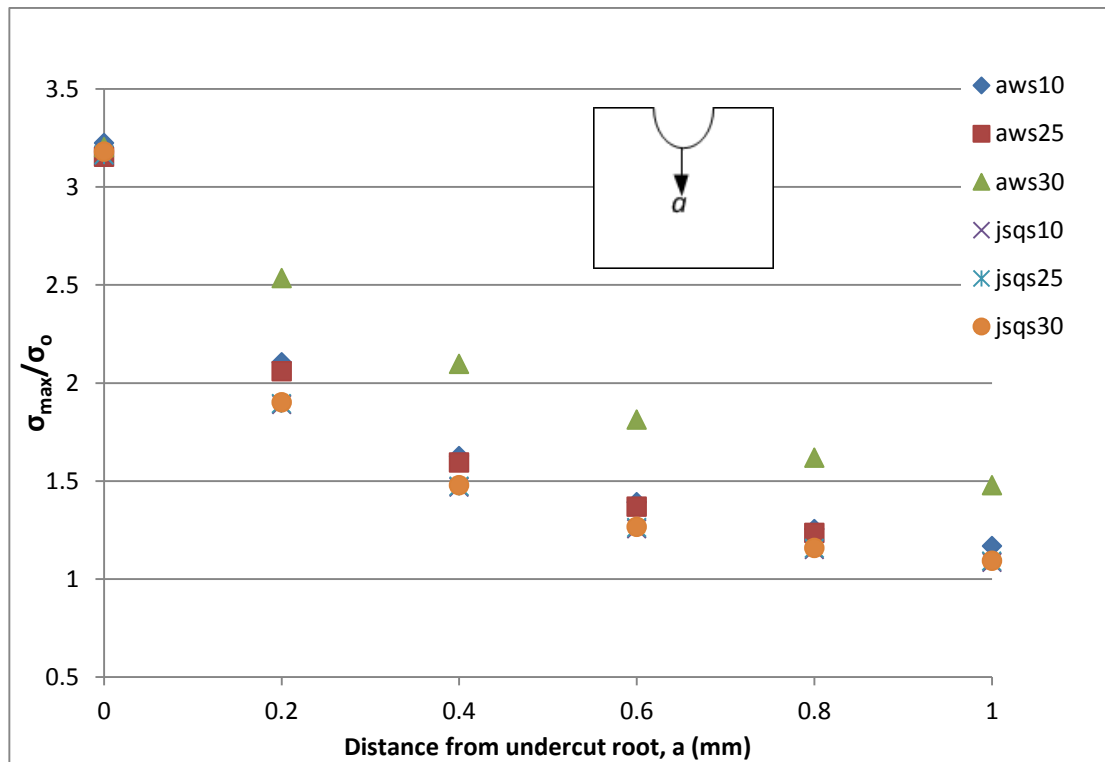
Fig. 3.5 Stress distribution at flank angle, θ = 8.1° up to 1 mm distance from root
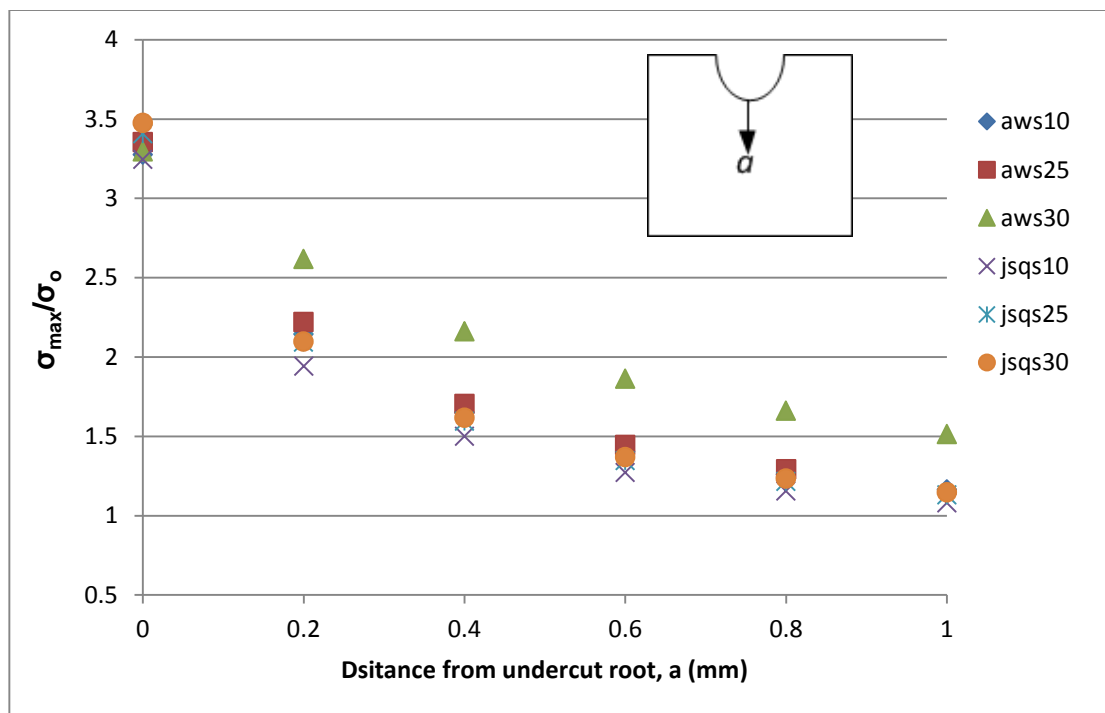
Fig. 3.6 Stress distribution at flank angle, θ = 23.42° up to 1 mm distance from root
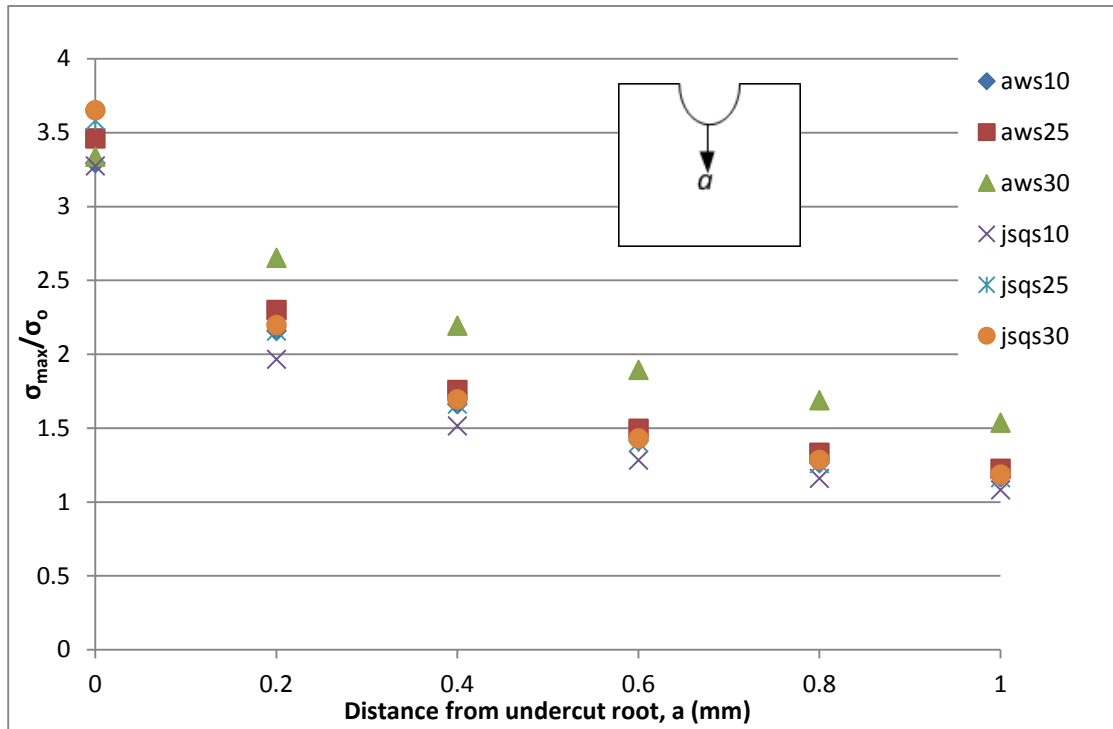
Fig. 3.7 Stress distribution at flank angle, $\theta = 46.75^o$ up to 1mm distance from root
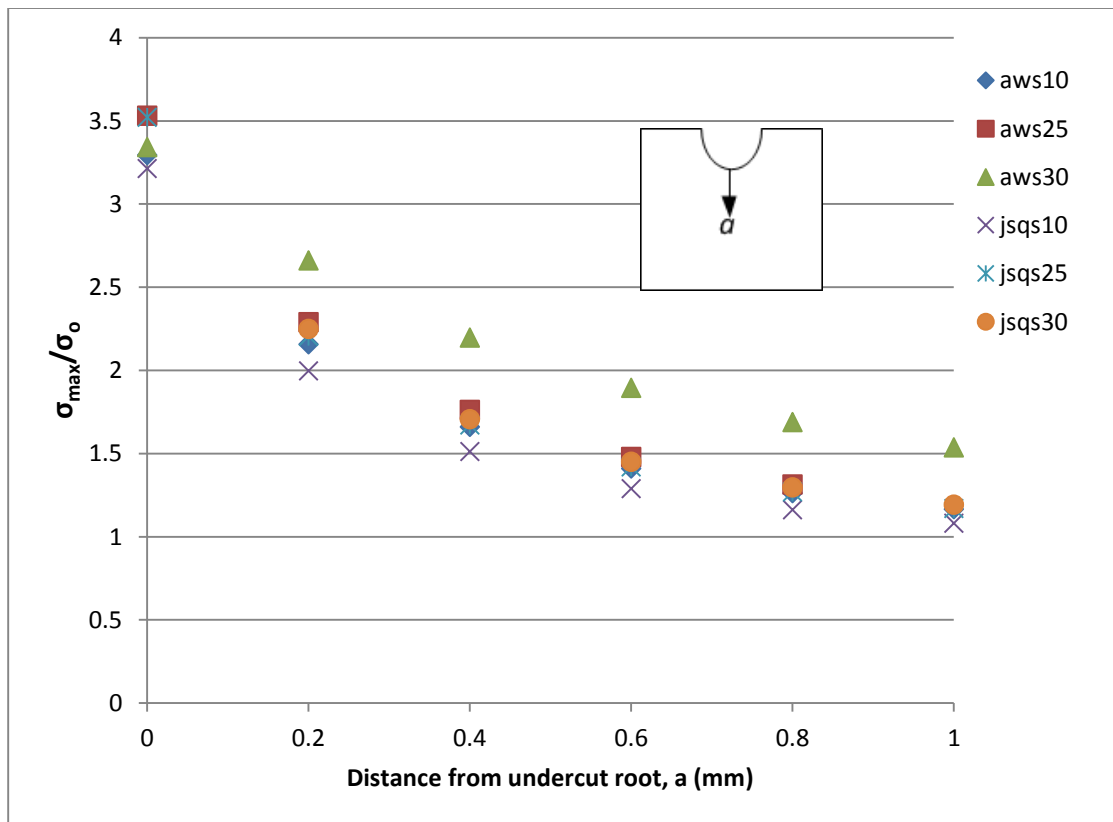
Fig. 3.8 Stress distribution at flank angle, $\theta = 66.35^o$ up to 1mm distance from root
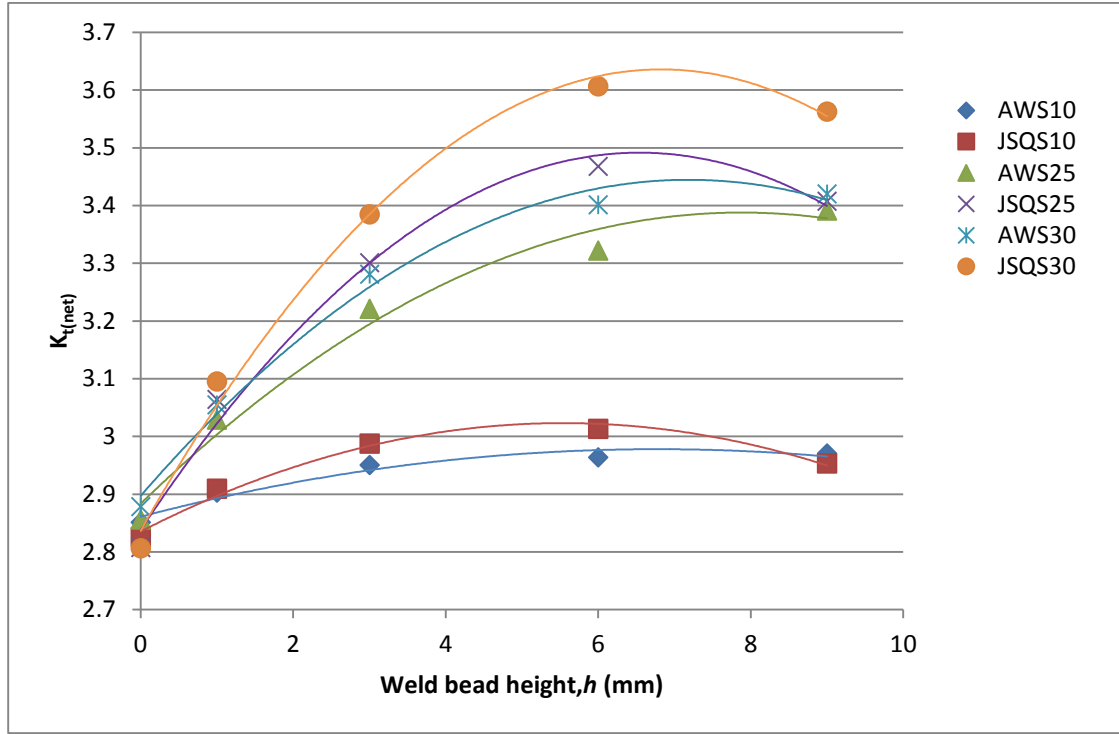
Fig. 3.9 $K_{t(net)}$ at different weld bead height

3.3.2.3   Stress concentration factor, K_t

In the evaluation of structural integrity, stress concentration factor is one of the main factors to be considered. As mention earlier in Chapter 2, many researchers found any location with higher stress concentration may consequence of crack initiation. Figs. 3.10 and 3.11 display stress concentration factor of gross and net stresses respectively which is obtained through empirical formula (eq. 3.1). $K_{t(net)}$ is obtained from net area, $s(t-d)$ but $K_{t(gross)}$ from gross area. Flank angle as shown in Fig. 3.2 is obtained from the measurement of analyzing the model. Undercut depth and thickness ratio, d/t is mainly vital for the purpose of this study.

Fig. 3.10 shows value of stress concentration factor growth with the increment of d/t ratio without excess weld bead. However, model with excess weld bead, which flank angle from 8.1º to 66.35º shows decreases of $K_{t(net)}$ value with increment of d/t ratio. In addition, the trend line of $K_{t(net)}$ flank angle of 46.75º and 66.35º is almost similar even the flank angle differences are about 20º. The results indicate the stress concentration factor keep remain after weld bead height of 6 mm. The trend line in Figs. 3.10 and 3.11

shows the influence of geometrical shape factor in order to estimate the stress concentration factor. It also corresponds to stress distribution along undercut root.
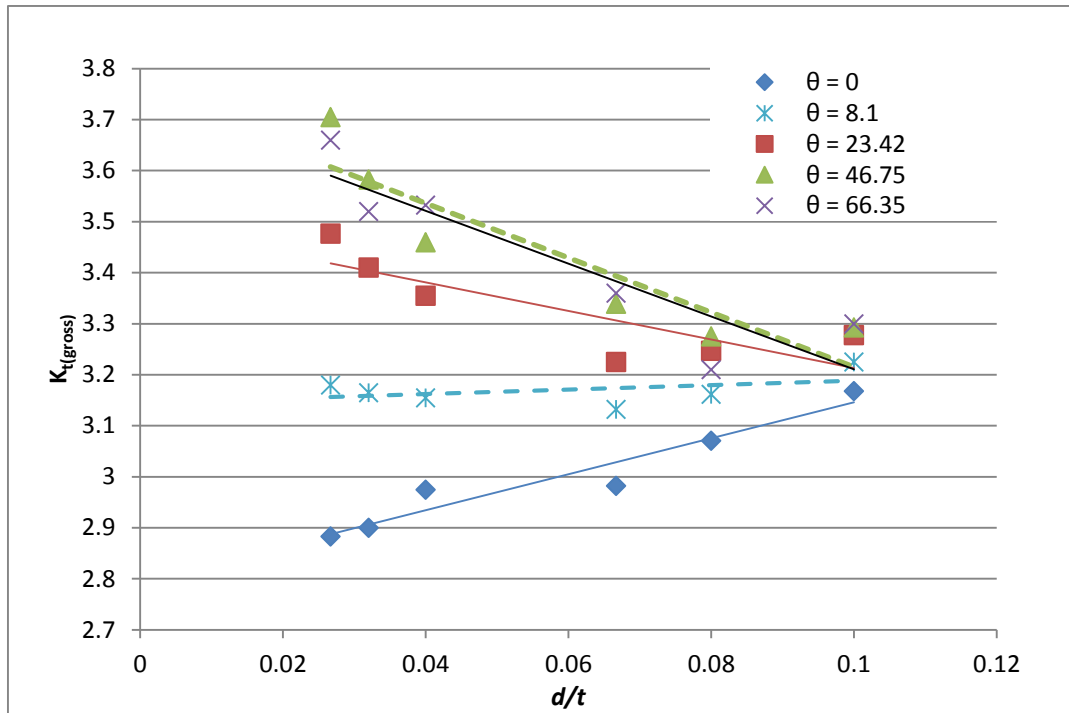
Fig. 3.10 $K_{t(gross)}$ for different weld bead height, h
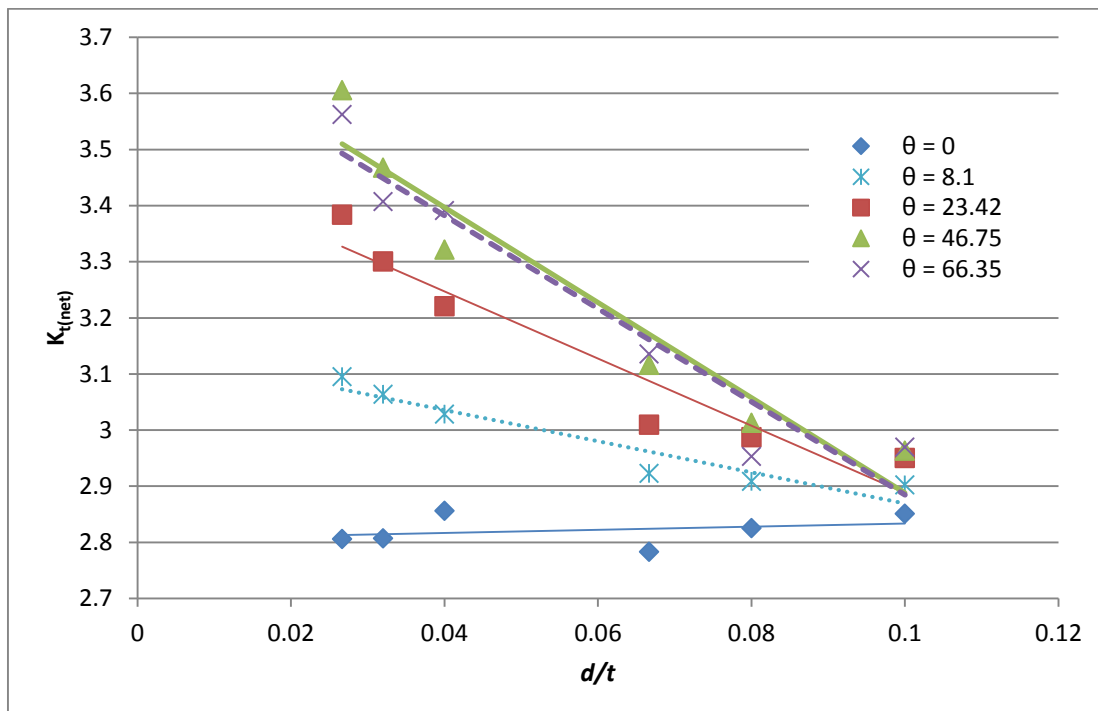
Fig. 3.11 $K_{t(net)}$ for different weld bead height, h

3.3.2.4   Stress gradient, *Φ*

Referring to Fig. 3.12, it shows stress gradients rise with increasing of undercut depth (*d*) over thickness (*t*) ratio. In this case, all models vary in term of undercut and thickness ratio. The figure also shows that stress gradient increase with the increasing of weld bead height. The result plays similar role for flank angle. In details, stress gradients increase with increment of *d/t* ratio. It shows at *d/t* ratio of 0.027, the stress gradient is range from 2.17 to 3.18 but for *d/t* ratio of 0.1, stress gradient range from 7.8 to 8.6. This result reveal at higher *d/t* ratio gives higher stress gradient. Stress gradients will show how steep stress distribution curve which will explained how fast stress decreases from undercut root. In other words, it becomes one of important factor to consider in calculating fatigue life for any structures.
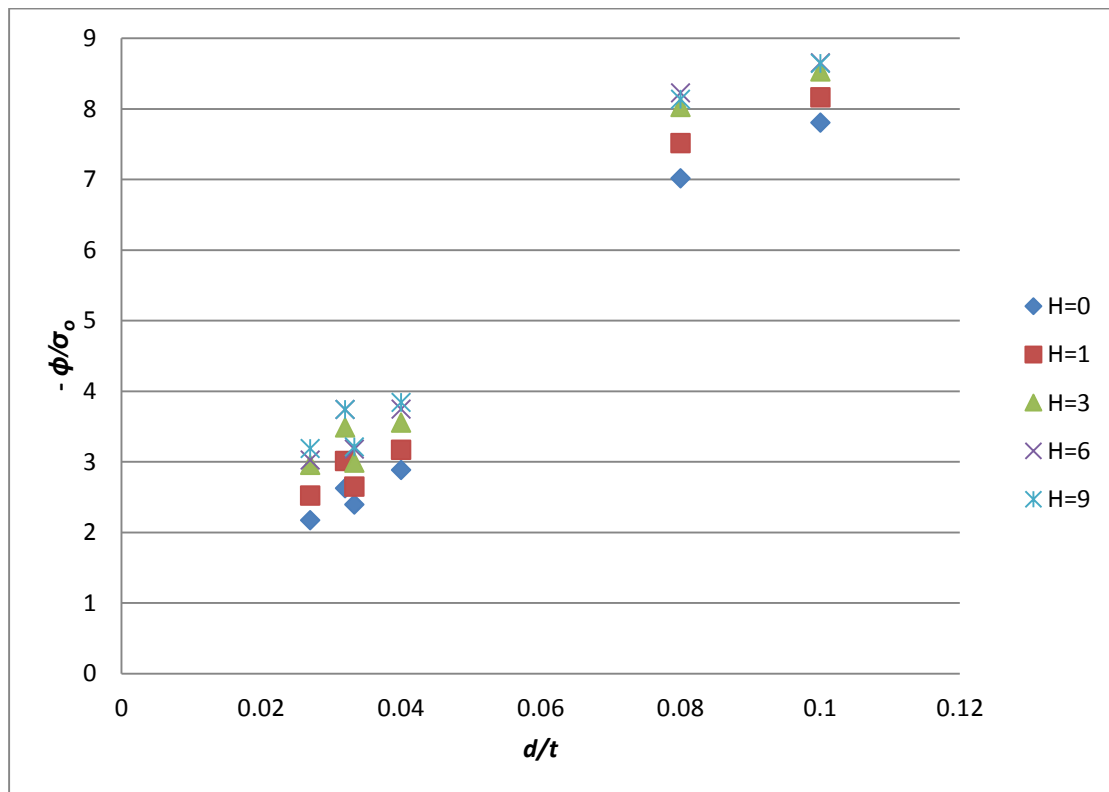
Fig. 3.12 Stress gradient at different weld bead height, *h*

3.3.2.5 Fatigue crack growth calculation

The following results are obtained from numerical code based on the RPG criterion and crack closure model by Toyosada et. al (2004). In this case, initial crack size is assumed to be 0.05mm and final crack size is the maximum plate thickness. In fatigue life estimation of butt joints, stress distribution data obtained by finite element analysis is used as input into the numerical code. As seen at Fig. 3.13, more fatigue life observed for higher stress ratio. In this figure, the stress ratio was calculated based on maximum stress with different stress range. Figs. 3.14 to 3.18 show the undercut and plate thickness effect with different flank angle to fatigue life. With different configuration, JSQS model gives higher fatigue life compare to AWS model. However, AWS model gives slightly higher fatigue life than JSQS model for plate thickness of 25 mm. Undercut and thickness ratio for both models at same plate thickness is 0.04 and 0.032 respectively. The d/t ratio almost closed and gives similar curves pattern as Figs. 3.14 to 3.18.

Next, Figs. 3.19 to 3.21 are the plot at plate thickness based with different of flank angle and d/t ratio. Plate thickness of 10 mm shows wide differences of fatigue life given by AWS and JSQS model. In this case, model JSQS gives more fatigue life compare to AWS model. As seen in the figures, at same plate thickness of 10 mm and 30 mm respectively, with different flank angle and d/t ratio, JSQS model indicate more fatigue life compare to AWS model. However, fatigue life of AWS and JSQS at plate thickness of 25 mm (Fig.3.17) shows similarity except for flank angle of 8.1° at $d/t = 0.032$.
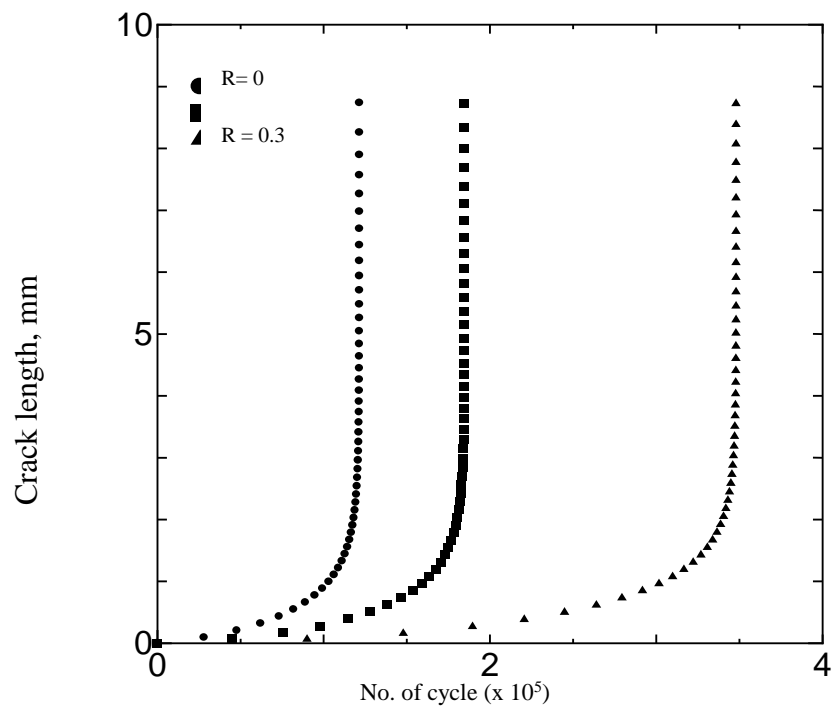
Fig.3 13 Crack growth curve for model AWS10h0 at different stress ratio
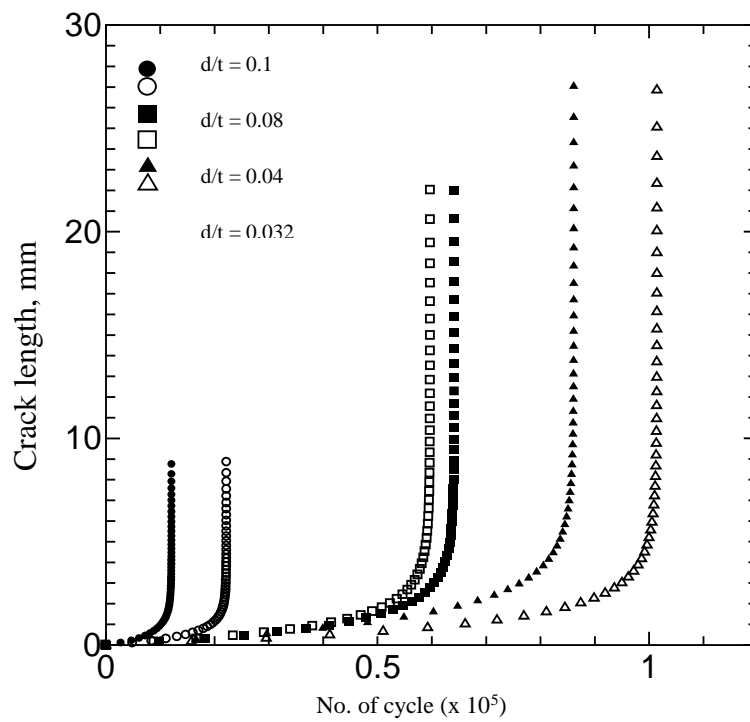
Fig. 3.14 Fatigue crack growth at flank angle of 0°
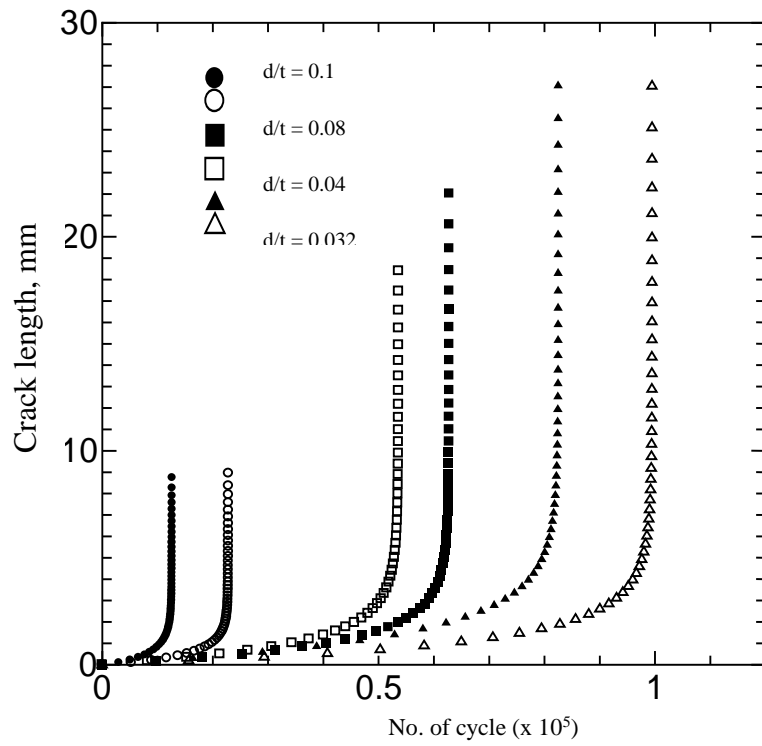
Fig. 3.15 Fatigue crack growth at flank angle of 8.1°
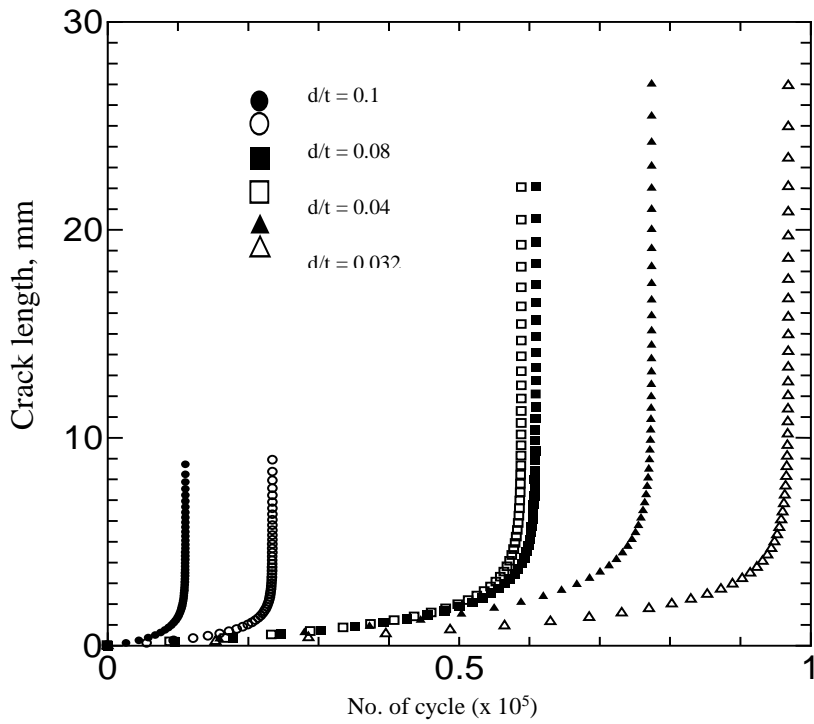
Fig. 3.16 Fatigue crack growth at flank angle of 23.42°

44
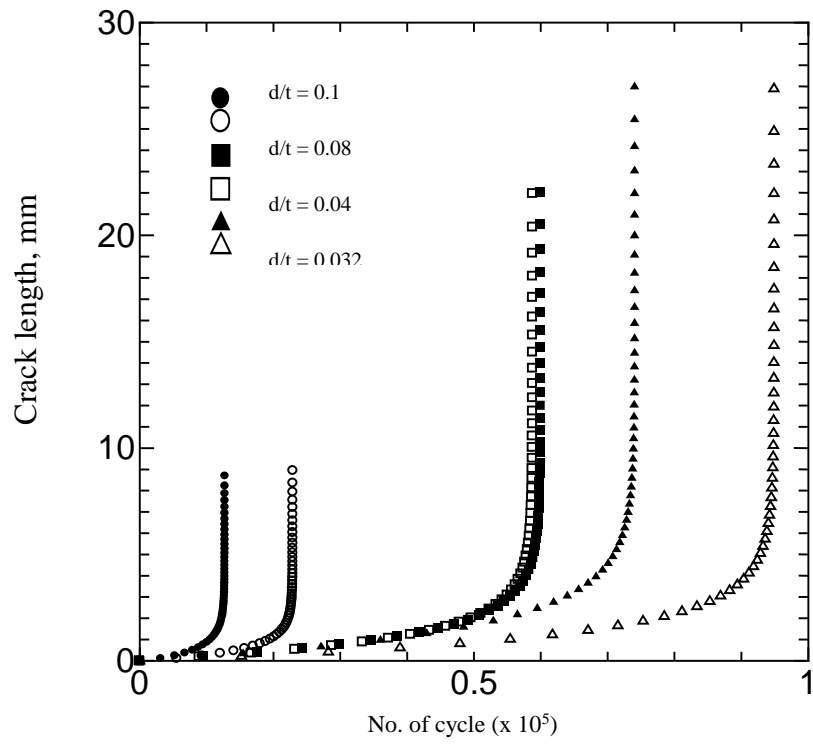
Fig. 3.17 Fatigue crack growth at flank angle of 46.75°
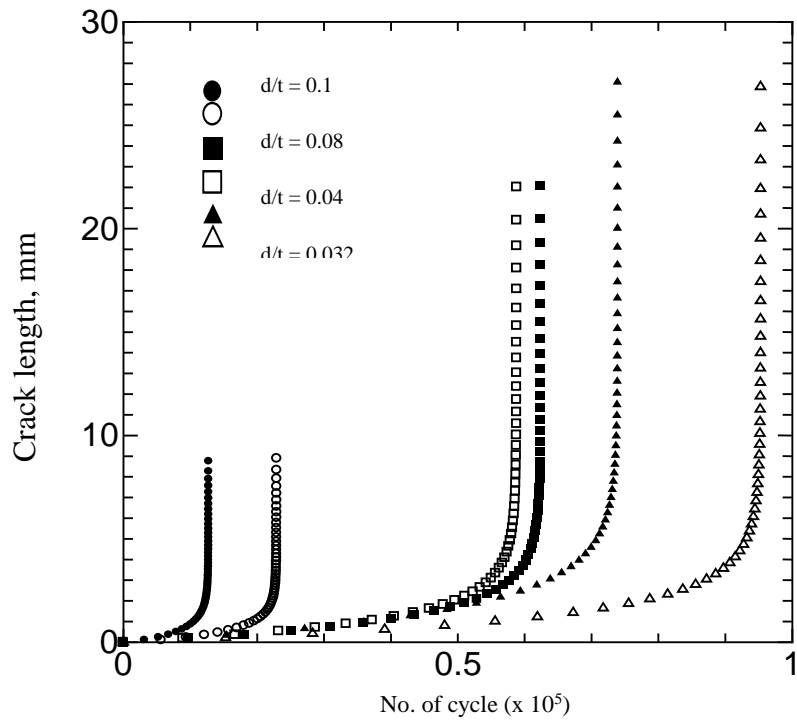
Fig.3.18 Fatigue crack growth at flank angle of 66.35°

45
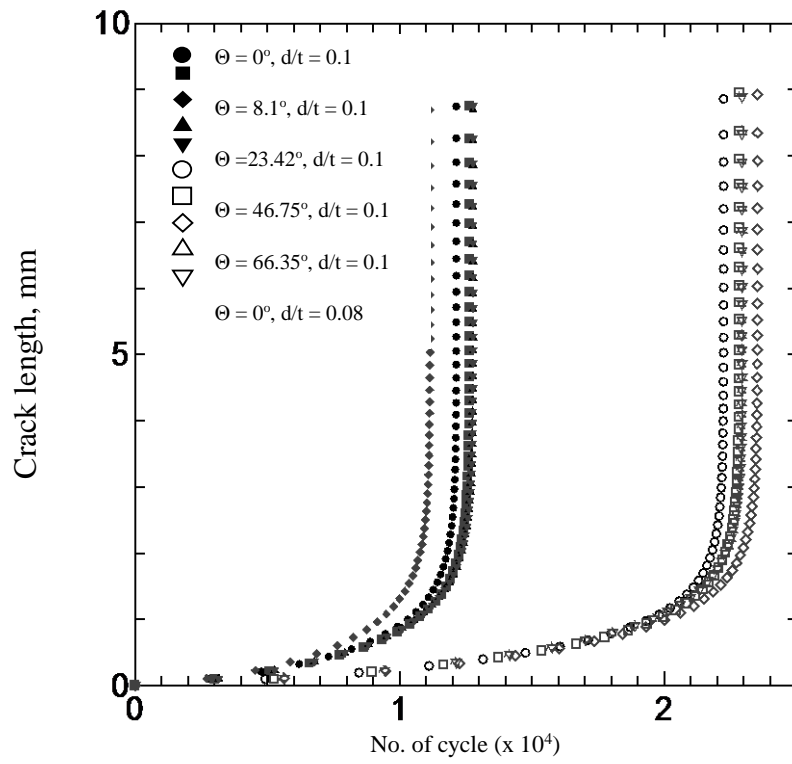
Fig. 3.19 Fatigue crack growth at thickness of 10 mm
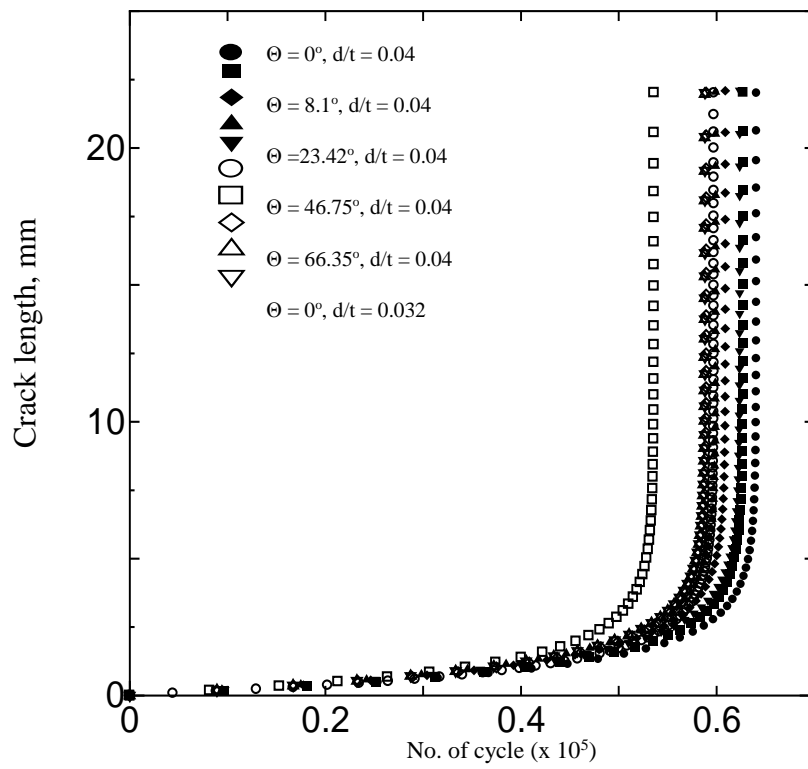
Fig. 3.20 Fatigue crack growth at thickness of 25 mm
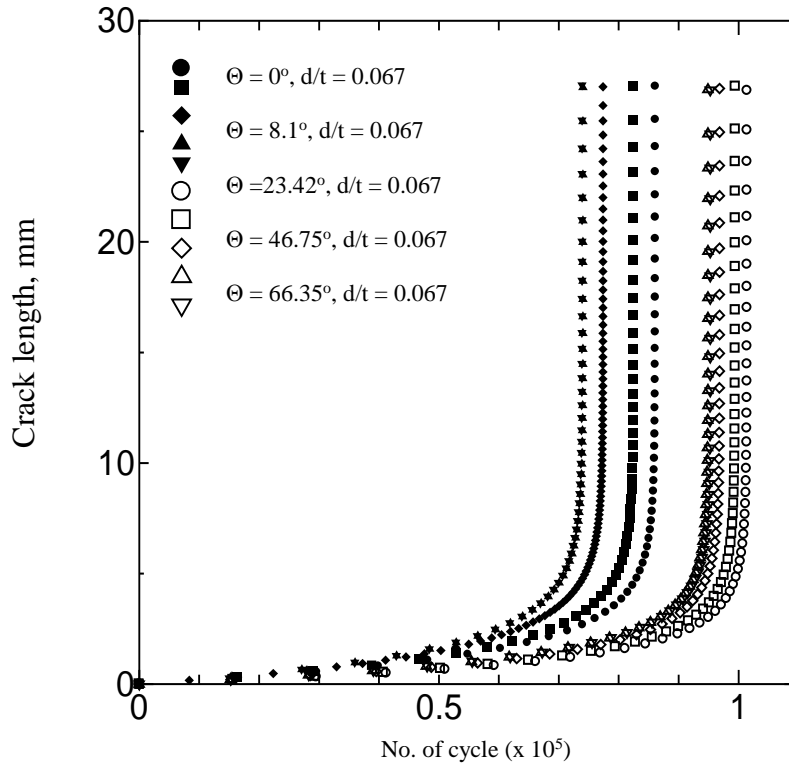
Fig. 3.21 Fatigue crack growth at thickness of 30 mm

3.3.3 *Effect of geometrical parameter of butt welded joint*

3.3.3.1 **Stress concentration factor, K_t**

In order to investigate the influence of geometrical parameter in butt welded joint, the numerical study with different setup as can be seen in Table 3.4 will be performed. The importance of stress concentration factor, $K_{t\,(net)}$ on butt welded joint with variable weld bead height (*h*) and undercut depth (*d*) will be highlighted. The study will focus on undercut with one single root radius (ρ = 0.25 mm) where undercut breadth is 2ρ at variable geometrical parameter. At industrial point of view, it is not practical to obtain undercut root radius by considering difficulties of measuring it. There are 3 types of undercut as mention by Nguyen and Wahab (1996). The types of undercut are curve, crack-like and micro-flaw, see Fig. 3.22. Therefore, the study will focus on crack-like undercut (type 2) which is found relatively large number at welded joint. Practical formula will be established for evaluation of structural integrity at the end of this study.

47

Table 3.4 Model's dimension

Plate thickness, t (mm)	10	25	30		
Flank angle, θ	0	8.1	23.42	46.75	66.35
Weld bead height, h (mm)	0	1	3	6	9
Undercut depth, d (mm)	0.25	0.5	1		

Type 1: curved

Type 2: crack-like

Type 3: micro flaw
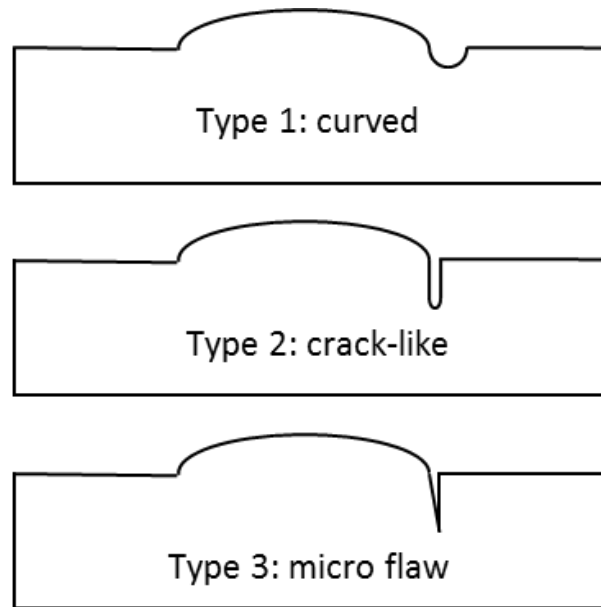
Fig.3.22 Types of undercut

3.3.3.2 Selection of the cases

a) Tension cases

There are 45 models analysed with different model configuration. Geometrical conditions can refer to Table 3.4 which contains the variation of configurations of plate thickness (t), flank angle (θ), weld bead height (h) and undercut depth (d). Such model was analysed and resulted of stress distribution along undercut root. Stress distribution along undercut root is obtained from finite element analysis results. Some of the model treated as plane strain to compare with plane stress results. The comparison shows plane stress gives higher tendency compare to plain strain. As shown in Fig. 3.23, maximum stress occurred at the

48

tip of undercut root. In this case, for plate thickness of 25 mm and undercut depth of 0.25 mm, dimensionless maximum stress, σ_{max}/σ_o is 3.88 at weld bead height over thickness ratio (h/t) of 0.36.

As can be seen, higher h/t ratio illustrate higher of stress value at undercut root compare to others. Therefore, the height of weld bead plays important role in influencing stress for the butt welded joint. In addition, Fig. 3.24 shows the stress distribution for same plate thickness at weld bead height (h) of 9mm. It clearly shows that the model with higher undercut over plate thickness ratio, d/t illustrates higher stress at undercut root with σ_{max}/σ_o = 5.48 while for d/t = 0.01 and 0.02 is 3.89 and 4.59 respectively. Next, Fig. 3.25 presents stress distribution at different plate thickness at same undercut (d = 0.25 mm) and weld bead height (h = 9 mm). Results shows σ_{max}/σ_o = 4.05 at plate thickness of 30 mm while for plate of 25 mm and 10 mm gives 3.89 and 3.12 respectively. Therefore, maximum stress at undercut root found higher at a thicker plate thickness.
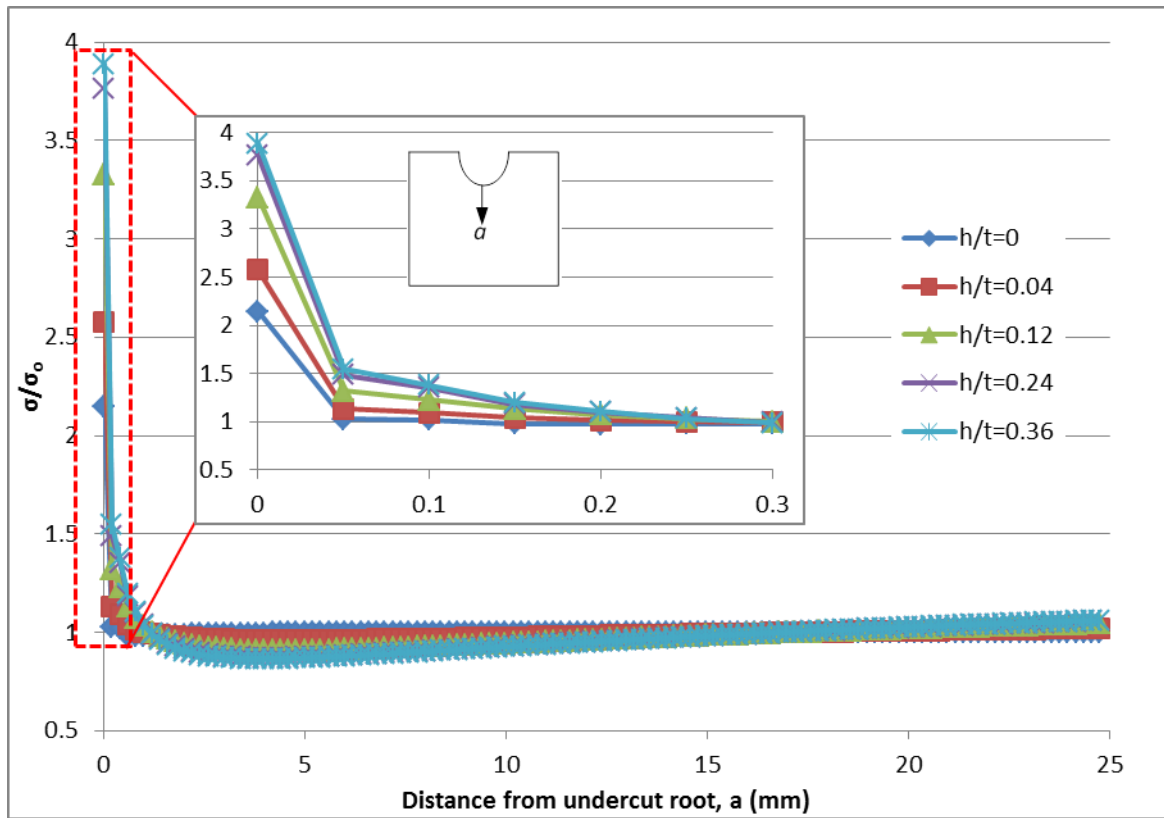
Fig. 3.23 Stress distribution at t=25 mm and d=0.25 mm

49
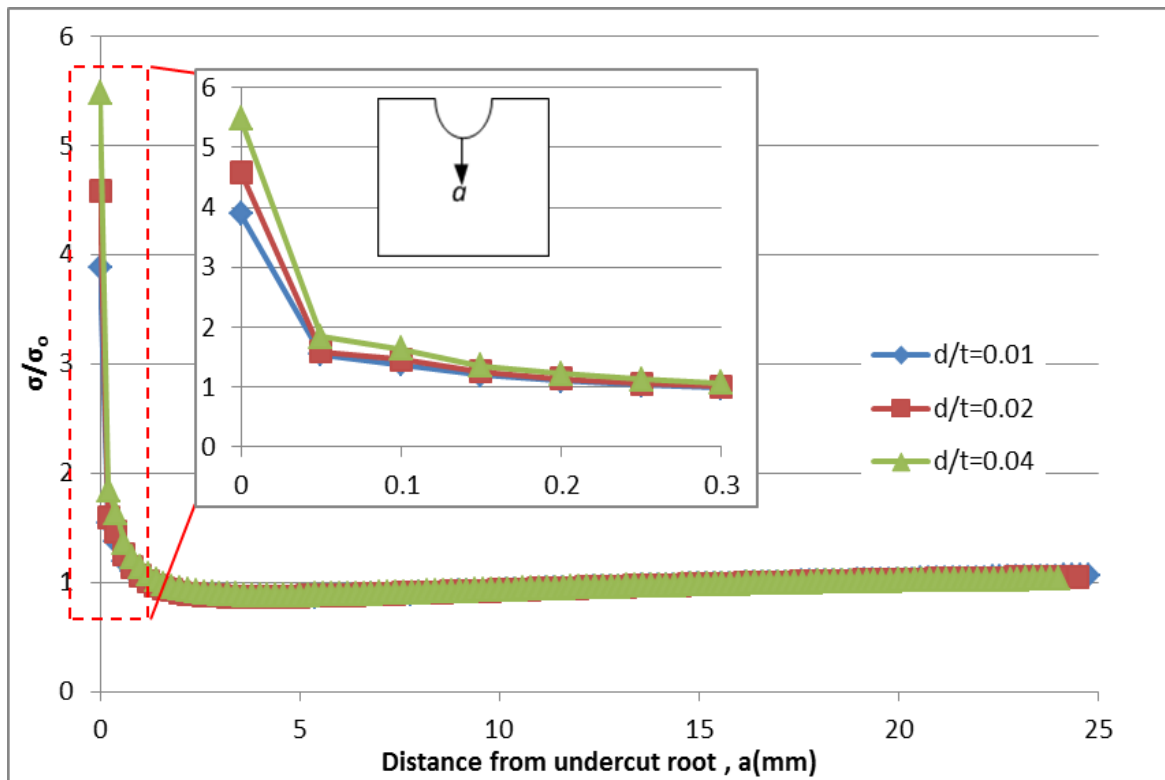
Fig. 3.24 Stress distribution at *t*=25 mm and *h*=9 mm
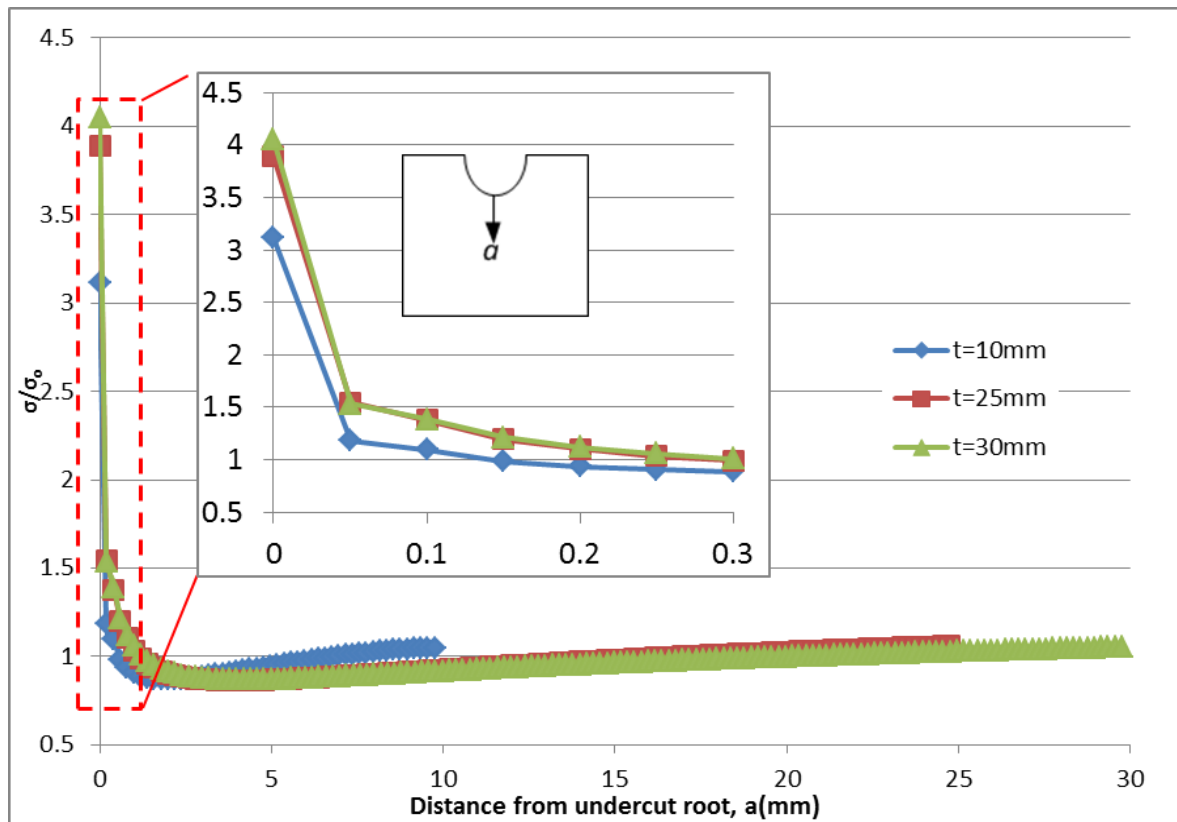
Fig. 3.25 Stress distribution at *d*= 0.25 mm, *h*=9 mm

50

Fig. 3.26 illustrates the stress concentration factor with the effect of weld bead height over thickness ratio (h/t) with different of undercut over plate thickness ratio (d/t) at plate thickness of 25 mm. It was found by the increase of h/t gives increments to SCF at undercut root. The figure found SCF increase from $h/t = 0$ to $h/t = 0.36$ at same d/t ratio. In this case for $d/t = 0.04$, SCF for $h/t = 0$ and $h/t = 0.36$ is 4.11 and 5.25. The result also shows at the same weld bead height, SCF increase by increments of d/t ratio. In addition, at plate thickness of 25 mm, increments of undercut depth over plate thickness ratio (d/t) give increments of SCF value. For $h/t = 0.36$ and at $d/t = 0.01$ the maximum SCF is 5.25 while at $d/t = 0.02$ and 0.04, SCF is 3.85 and 4.49 respectively. The results show a stress concentration at undercut root is proportional to d/t ratio.
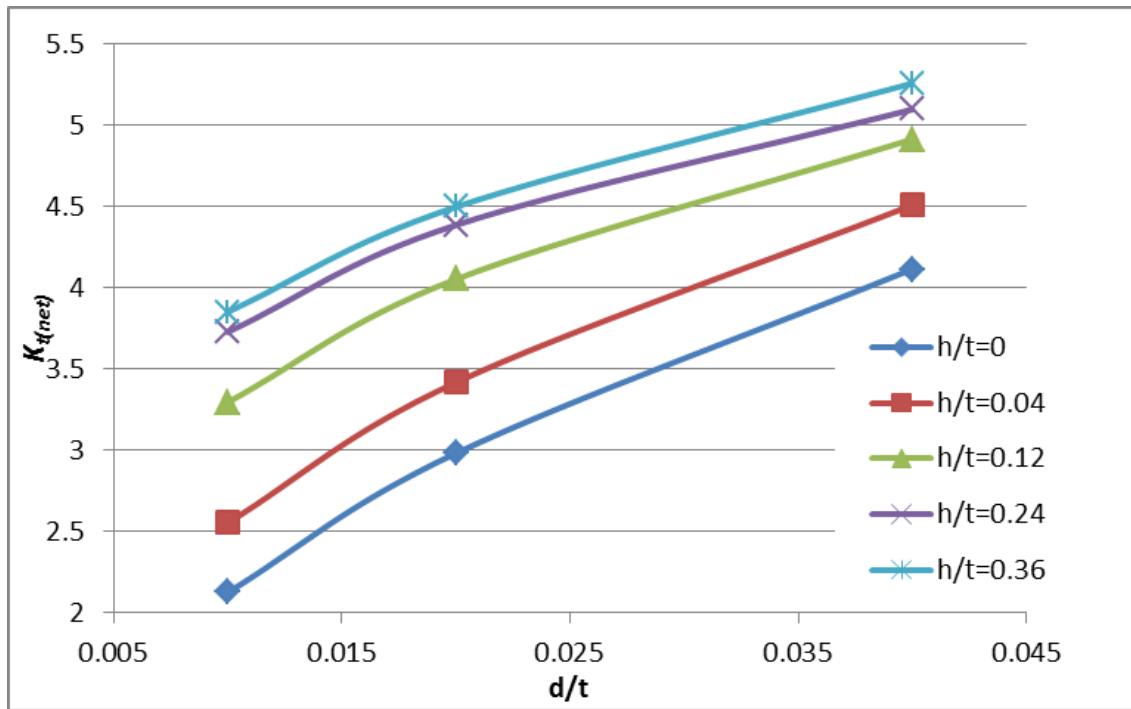
Fig. 3.26 SCF at plate thickness of 25 mm (tension)

b) Bending cases

In bending cases, the same model was used with moment acting at the edge of the plate. Stress distribution for plate under bending moment is illustrated in Fig. 3.27. Its shows stress distribution rapidly decreases away from the undercut root (ρ) and at approximately $\sqrt{\rho}$ distance or 0.5 mm from undercut root, the stress linearly decreases until at the middle

of the plate thickness. Fig. 3.27 also shows higher stress value occurred at *h/t* of 0.36 with $\sigma_{max}/\sigma_o = 5.97$ compared with other *h/t* of 0.24, 0.12, 0.04 and 0 which gives $\sigma_{max}/\sigma_o = 5.64$, 5.22, 4.57 and 4.05 respectively.
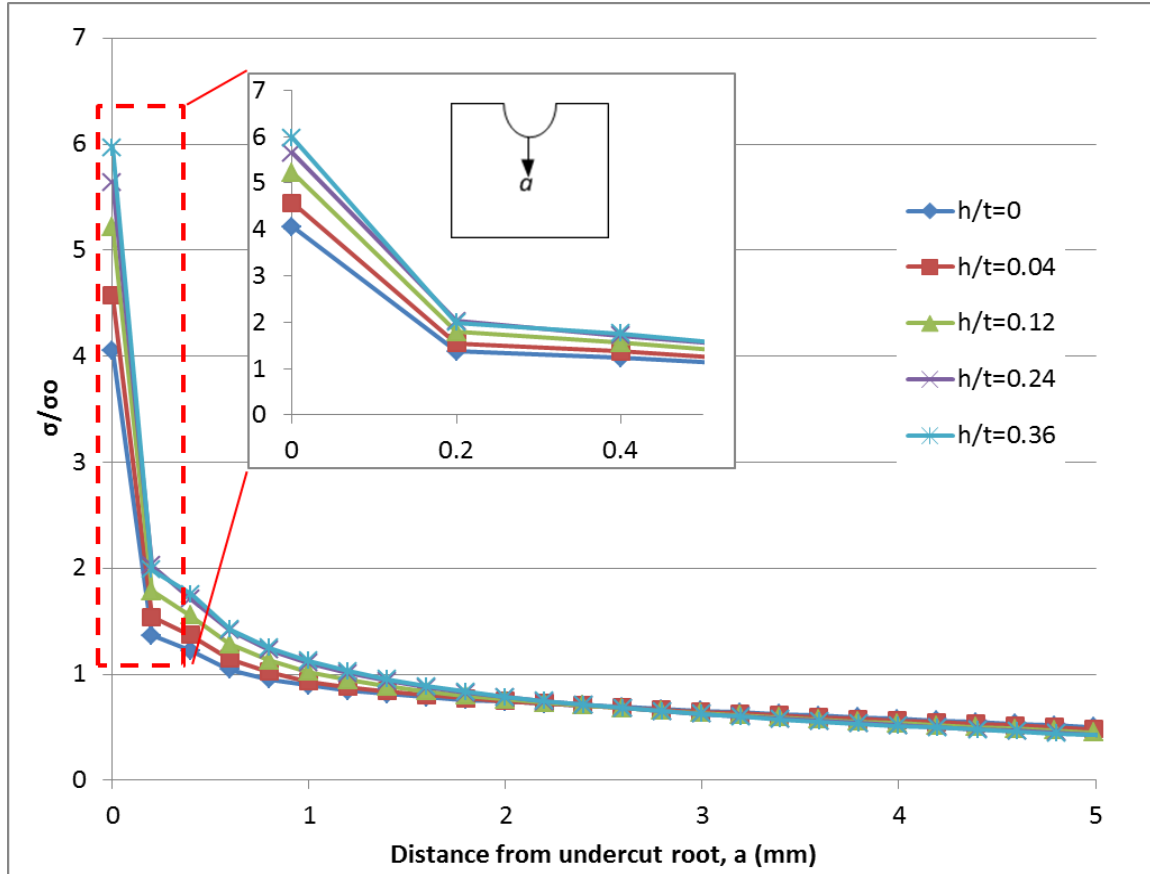
Fig. 3.27 Stress distribution at *t* = 25 mm and *d/t* = 0.04
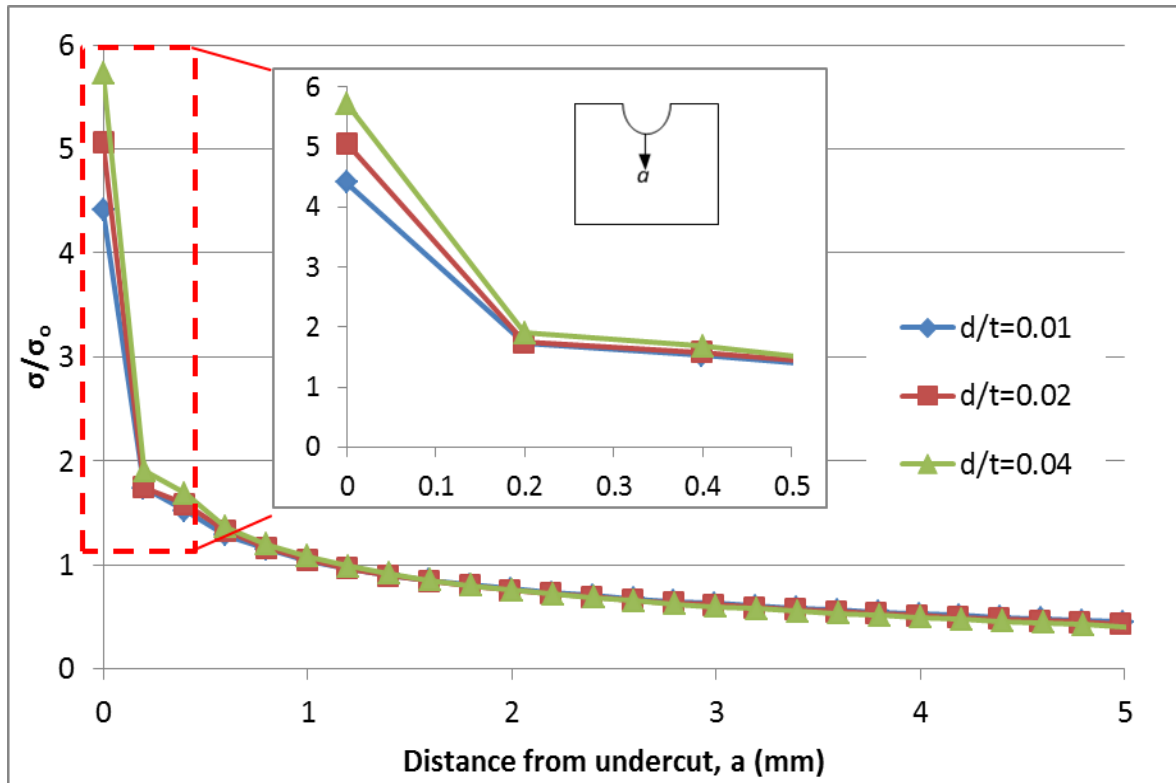
Fig. 3.28 Stress distribution at $t = 25$ mm and $h/t = 0.36$
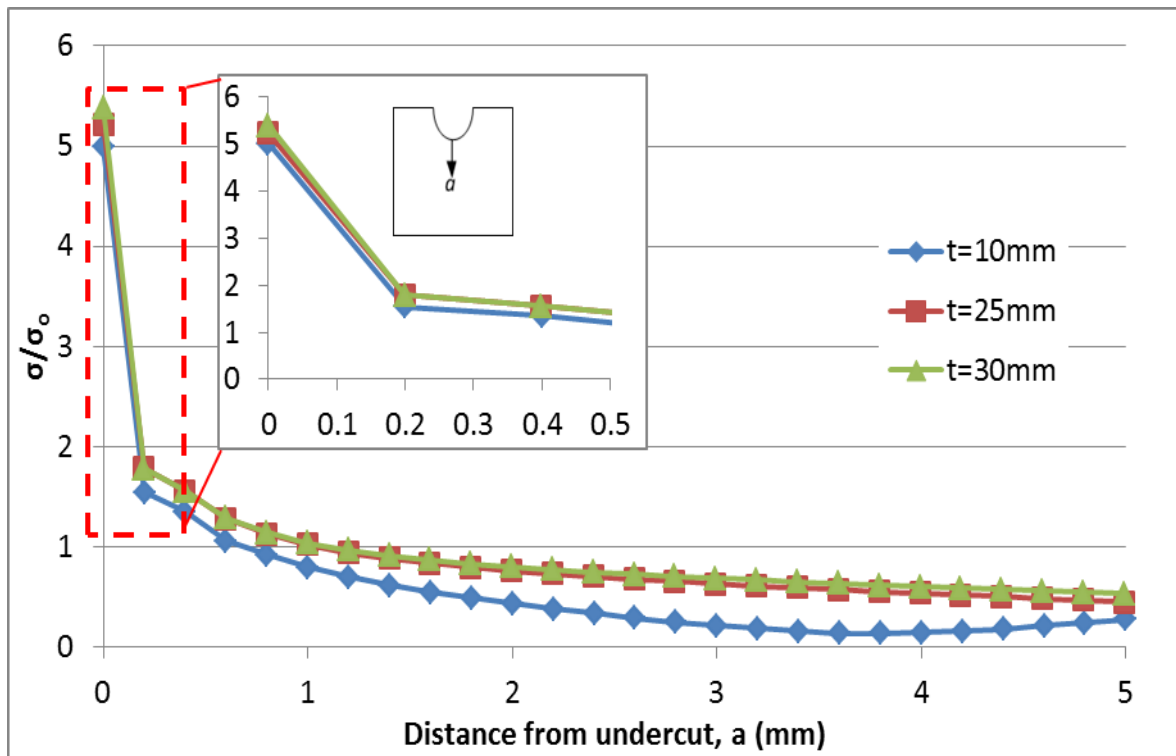
Fig. 3.29 Stress distribution at $d= 1$ mm, $h = 3$ mm

53

Fig. 3.28 illustrates stress distribution at different undercut depth over plate thickness ratio, d/t. In this case, maximum stress found higher at d/t of 0.04 with $\sigma_{max}/\sigma_o = 5.73$ while at d/t of 0.02 and 0.01 with $\sigma_{max}/\sigma_o = 5.06$ and 4.41 respectively. Again the results indicate at higher of σ_{max}/σ_o occurred at higher d/t ratio for both bending and tension cases. Similarly results found higher σ_{max}/σ_o at thicker plate as shown in Fig. 3.29. Futhermore, σ_{max}/σ_o value found higher at bending cases compare to tension cases for same geometrical parameter.
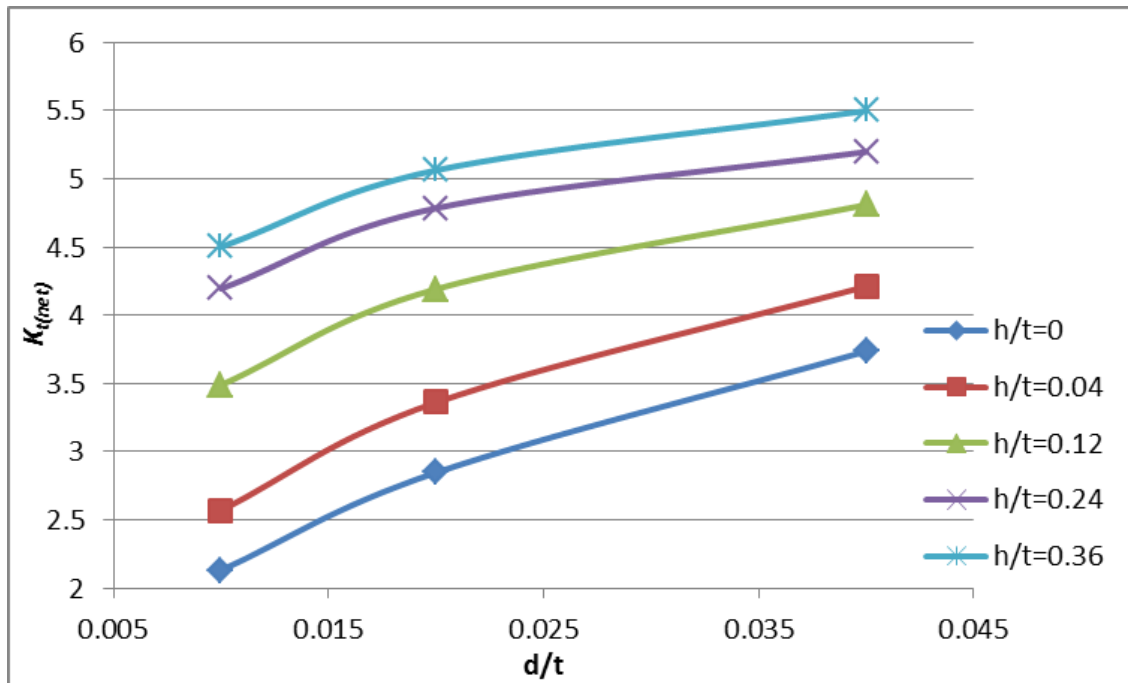
Fig. 3.30 SCF at plate thickness of 25mm (bending)

Fig.3.30 illustrates SCF increase with the increment of d/t ratio for same plate thickness of 25 mm. For no excess weld ($h=0$), higher SCF found at d/t of 0.01 with 3.74 while lower SCF with value of 2.13 shows at d/t of 0.04. SCF also found increase with the effect of h/t ratio. At the same d/t ratio of 0.04, SCF at $h/t = 0$ is 3.74 while at h/t of 0.36 is 5.5. The result shows SCF increase by increment of h/t ratio.

54

3.3.4 Practical formulas

Several factors have significant influence to stress concentration factor. Based on Neuber's equations, SCF can be approximated as:

$$K_{t(net)} = 1 + A\left(\frac{d}{t}\right)^{\alpha} + B\left(\frac{h}{t}\right)^{\beta} \tag{3.14}$$

Least square fitting is used in order to obtain unknown coefficients of A, B, α and β as shown in Tables 3.5 and 3.6. Proposed equation (3.12) simply can be used by referring to plate thickness with the range of h/t ratio.

Table 3.5 Variable constant for tension cases

Thickness	h/t	A	B	α	β
10mm	0-0.3	14.11	1.52	0.66	0.94
	0.3-0.9	9.54	0.56	0.51	0.22
25mm	0-0.12	25.12	5.63	0.65	0.81
	0.12-0.36	12.74	1.75	0.42	0.52
30mm	0-0.1	28.36	7.03	0.65	0.8
	0.1-0.3	18.27	2.59	0.56	0.36

Table 3.6 Variable constant for bending cases

Thickness	h/t	A	B	α	β
10mm	0-0.3	6.73	2.98	0.49	0.96
	0.3-0.9	4.26	1.09	0.12	18.8
25mm	0-0.12	17.32	8.3	0.58	0.89
	0.12-0.36	7.65	2.59	0.22	1.2
30mm	0-0.1	21.24	9.48	0.6	0.85
	0.1-0.3	8.59	14.83	0.2	3.17

3.3.4.1 Allowable limit based on JSQS and IACS Rec. 47

Referring to the allowable limit by JSQS and IACS Rec. 47, Tables 3.7 and 3.8 is established to present allowable limit available through this study. Below table represents allowable SCF for strength member and other member as specified by the code. As can be seen, allowable SCF found higher at thicker plate with h/t consideration for both tension and bending cases. However, another important criterion to be considered is stress gradient,

ϕ in the evaluation of fatigue strength. This phenomenon can be explained by referring to Fig. 3.31 where curve A shows higher of maximum stress value compare to curve B at a point of undercut root radius. However, the stress value of the curve A, σ_A is lower than curve B, σ_B at the same distance of δx. So, this shows how important the role of stress gradient, ϕ to assess fatigue strength.

Table 3.7 Allowable limit for strength member

		Tension cases	Bending cases
Thickness	h/t	$K_{t(net)}$	$K_{t(net)}$
10mm	0-0.3	3.44	3.49
	0.3-0.9	3.62	4.12
25mm	0-0.12	3.99	4.05
	0.12-0.36	4.49	4.99
30mm	0-0.1	4.09	4.16
	0.1-0.3	4.53	5.12

Table 3.8 Allowable limit for other member

		Tension cases	Bending cases
Thickness	h/t	$K_{t(net)}$	$K_{t(net)}$
10mm	0-0.3	4.15	3.89
	0.3-0.9	4.18	4.3
25mm	0-0.12	4.69	4.61
	0.12-0.36	5.03	5.35
30mm	0-0.1	4.81	4.75
	0.1-0.3	5.08	5.48
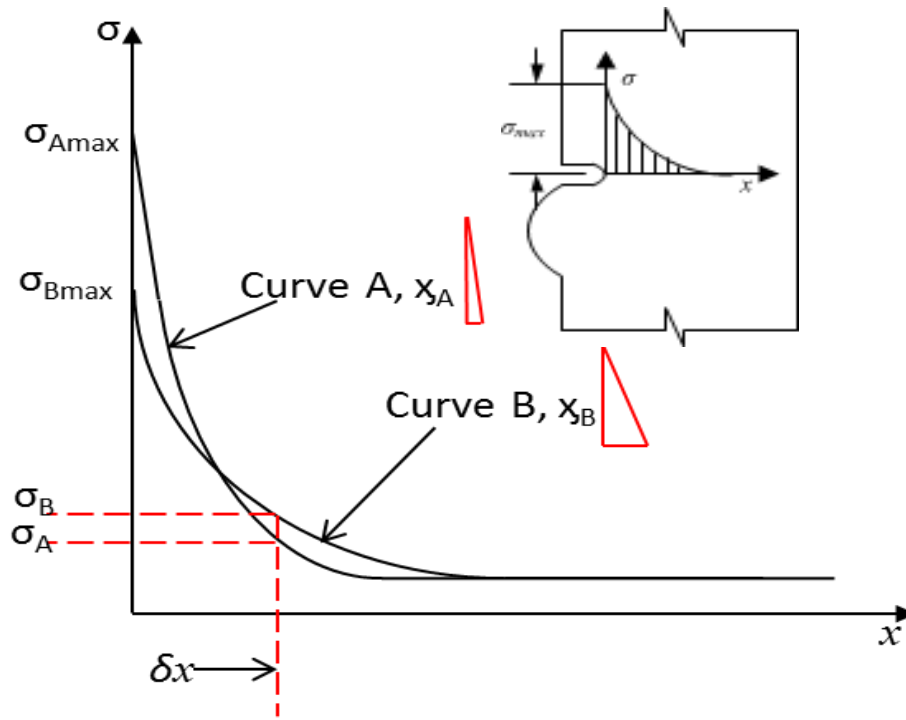
Fig. 3.31 Stress gradient illustration

3.3.4.2 Stress gradient

Another important geometrical parameter to evaluate the welded structures is the stress gradient. As can be seen in Fig. 3.31, crack will propagate further of plate thickness direction with lower stress gradient. This is because the decreasing of maximum stress from crack initiation is less compare to higher stress gradient.

3.3.5 Effect of undercut shape

This study will focused on the importance of stress gradient in the evaluation of fatigue strength. Shape factor also include in this study in order to establish practical evaluation of butt welded joint. In this case, U and V-notch undercut type is applied for the analysis (Fig. 3.32). In order to evaluate the shape factor, both shapes are constraint in a box with dimension of width, b and depth, d. The study is limited to undercut depth, $d = 0.5$ mm with variable of width, b. In addition, the concept by limiting U and V-notch in b/d ratio is more practical. In-service situations, measuring width and depth are more realistic compare to identifying the type of notch. Results of the study will give an overview the important of stress gradient and similarly shape factor consideration in evaluation of fatigue strength.

a)   U-notch   b)   V-notch
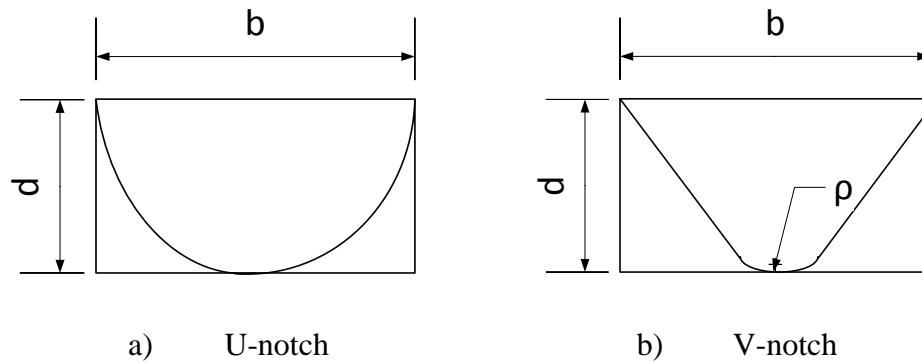
Fig. 3.32 Type of notch shape

Table 3.9 Model dimension – without undercut

Weld bead height, h (mm)	0	2.5	5	7.5	10
Flank angle, θ (deg)	0	75	90		
Weld bead width, $2\,Bw$ (mm)	10	16	20		
Root radius, ρ (mm)	0				
Undercut depth, d (mm)	0				
Shape ratio b/d	2	3	4		

Table 3.10 Model dimension – with undercut

Weld bead height, h (mm)	0	2.5	5	7.5	10
Flank angle, θ (deg.)	0	75	90		
Weld bead width, $2Bw$ (mm)	10	16	20		
Root radius, ρ (mm)	0.25	5			
Undercut depth, d (mm)	0.5				
Shape ratio b/d	2	3	4		

3.3.5.1   Results and discussion

Figs.3.33 (a) and (b) shows numerical simulation results of the fatigue life for the model with weld bead height, $h = 0$ as stated in Tables 3.10. As can be seen, all V-notch model show higher fatigue life compare to all U-notch model. This can be explained by referring to the stress distribution for each model. Fig. 3.34 presents stress distribution for U-notch model. In this case, lower shape ratio (b/d) gives higher stress concentration factor.

However, by considering stress gradient, U-notch model with higher shape ratio (b/d) gives low stress gradient (Fig. 3.36). Again at Fig. 3.34 shows at about 0.13 mm from undercut root, stress distribution for U-notch model at shape ratio b/d =2 start to decrease compare to b/d of 3 and 4. The results illustrate the influence of shape ratio b/d in affecting *SCF* and stress gradient. Based on this, lower b/d ratio gives higher fatigue life compare to others. Next, Fig. 3.35 presents stress distribution for V-notch model with different shape ratio, b/d. Based on this figure, even though V-notch model with higher ratio b/d gives lower *SCF* but there is no significant effect to stress gradient. By referring back to Figs. 3.33(a) and (b), there are no significant differences to fatigue life for V-notch model with different shape ratio, b/d.
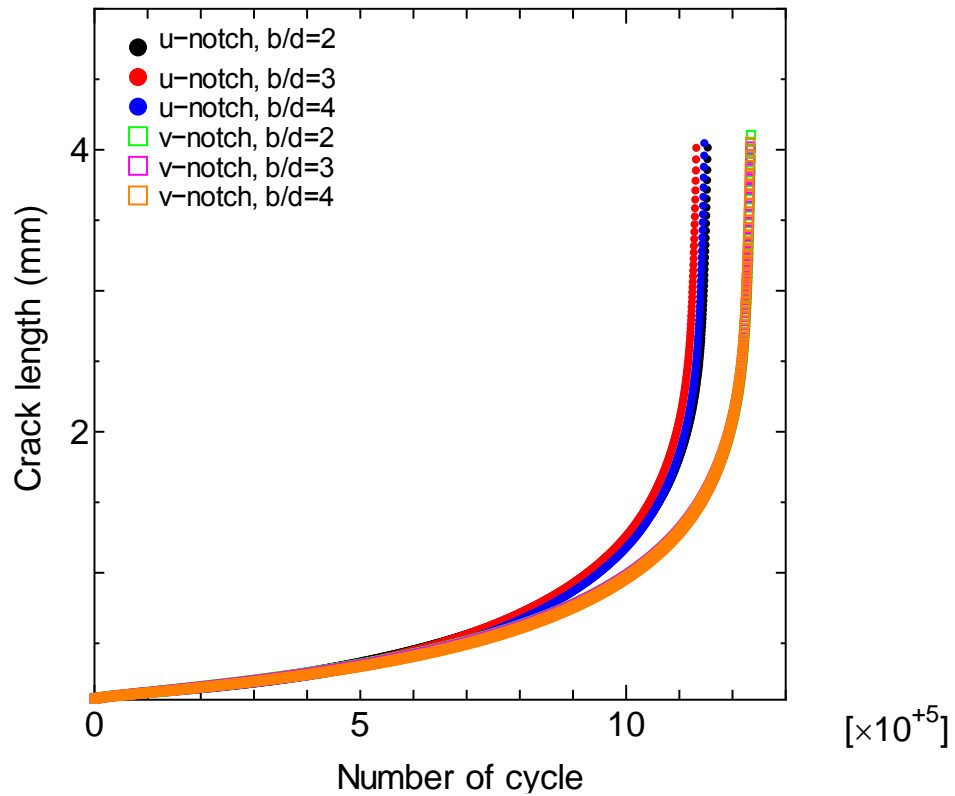
Fig. 3.33(a) Fatigue life for model without weld bead height
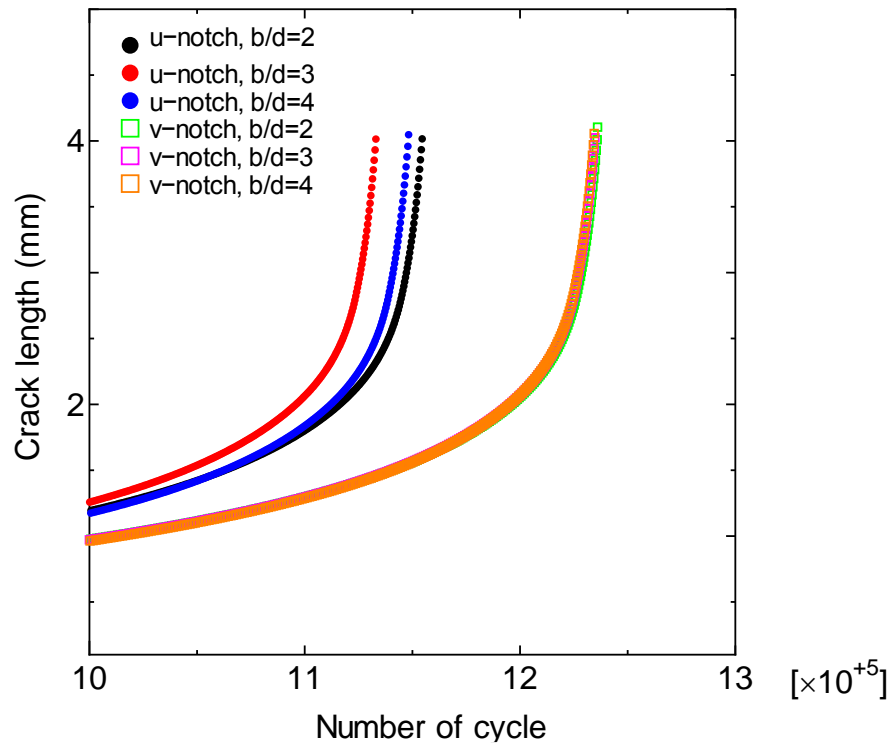
Fig. 3.33(b) Enlarge of Fig. 3.34(a)
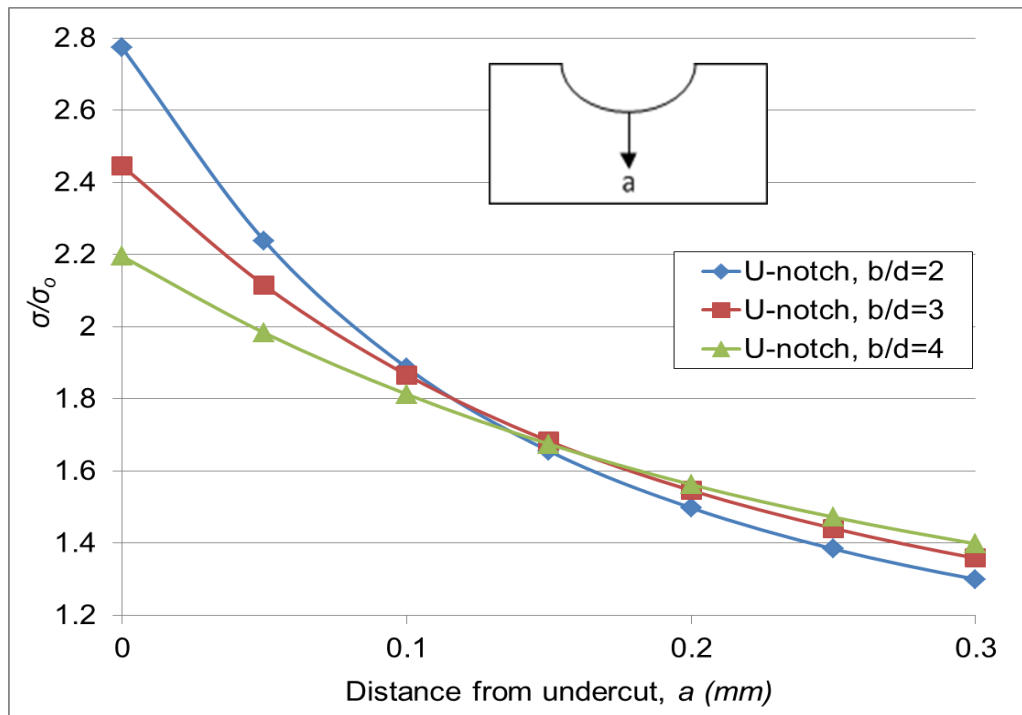
Fig. 3.34 Stress distribution up to 0.3 mm from undercut

60

Further investigations has been made to confirm the shape factor within same shape ratio, *b/d*. As illustrates in Figs. 3.37 to 3.39, V-notch model presents higher *SCF* compare to U-notch model. However, stress gradient for V-notch model found higher compare to U-notch model (Fig. 3.36). By enlarging scale of the graph with focusing stress distribution up to 0.3 mm distance from undercut root, it shows significant information related to the effect of stress gradient to fatigue strength. As we can see at Fig.3.37, stress distribution rapidly decrease by V-notch model while differently behaviour found at U-notch model. At distance point of about 0.06 mm from undercut root, both stress distribution for V and U-notch are at same level. Next, the stress levels keep decreasing for V-notch level and converge to the end of plate thickness. This means that stress found higher for V-notch model up to distance of about 0.06 mm and then maintain low compare to U-notch model. This phenomenon also occurred for shape ratio, *b/d* =3 and 4 where intersection point are at about 0.07 mm and 0.09 mm respectively. All of this results explained why V-notch model gives higher fatigue life as shown in Figs. 3.33(a) and (b).
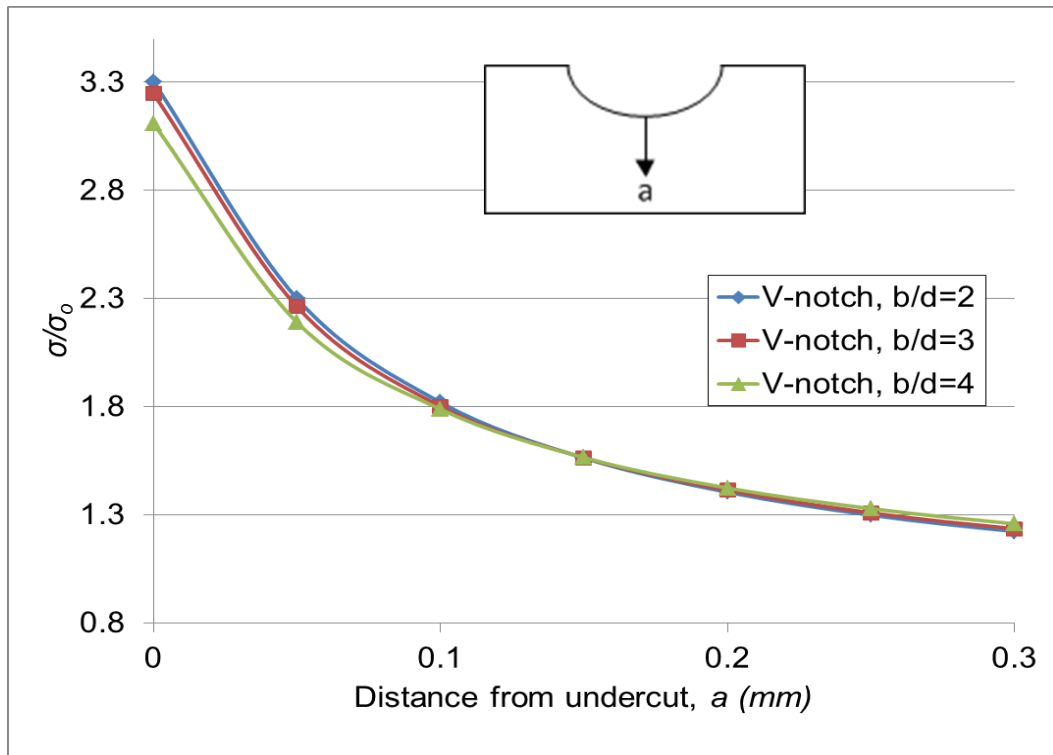
Fig. 3.35 Stress distribution for V-notch model up to 0.3 mm from undercut root
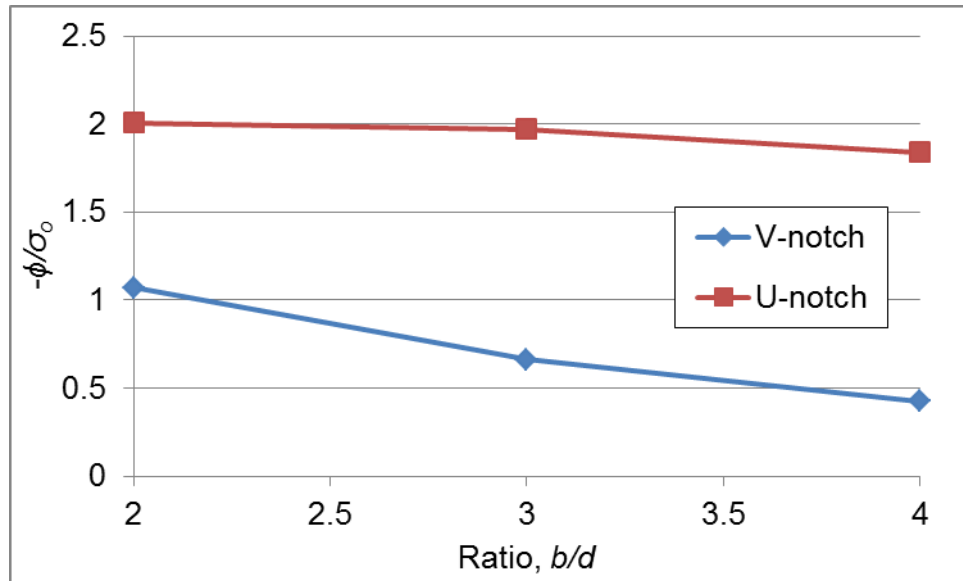
Fig. 3.36 Comparison of ϕ for model with no weld bead
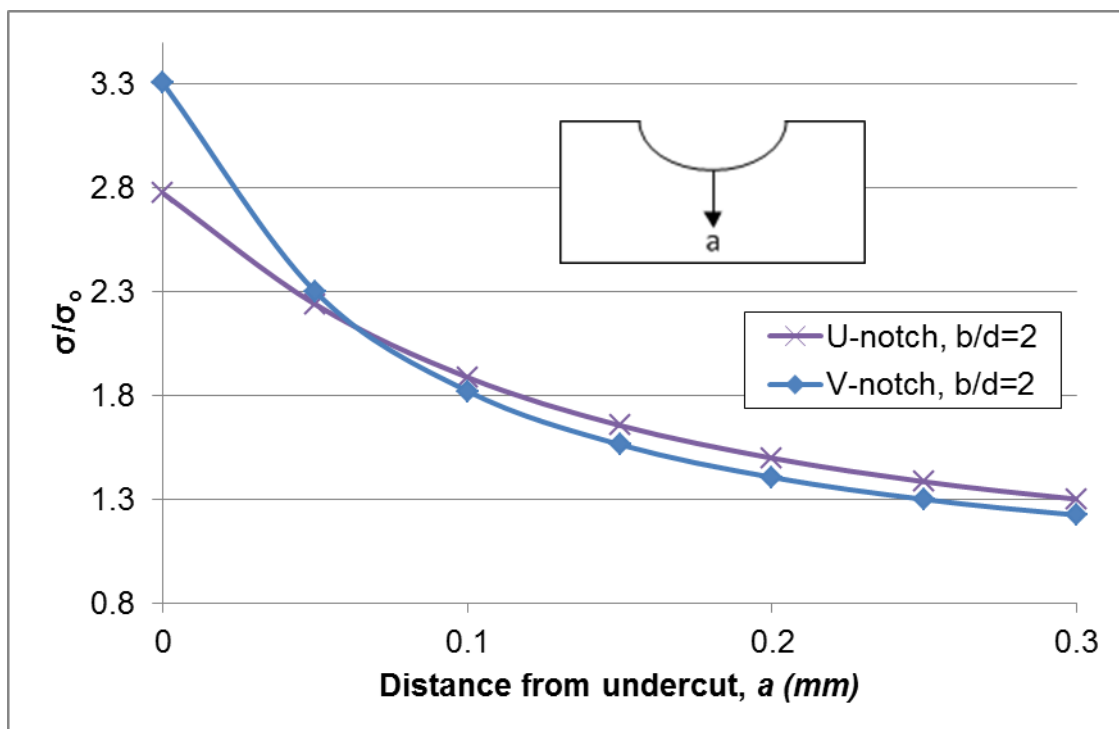
Fig. 3.37 Stress distribution of shape ratio $b/d=2$ up to 0.3 mm from undercut
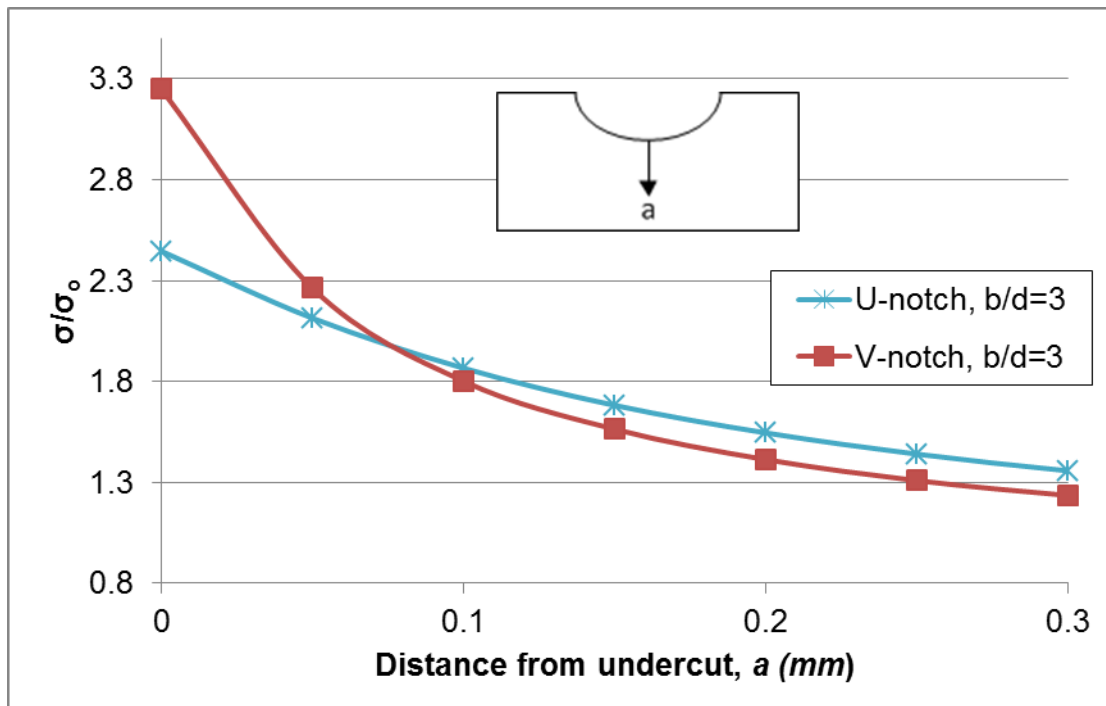
Fig. 3.38 Stress distribution of shape ratio *b/d*=3 up to 0.3 mm from undercut
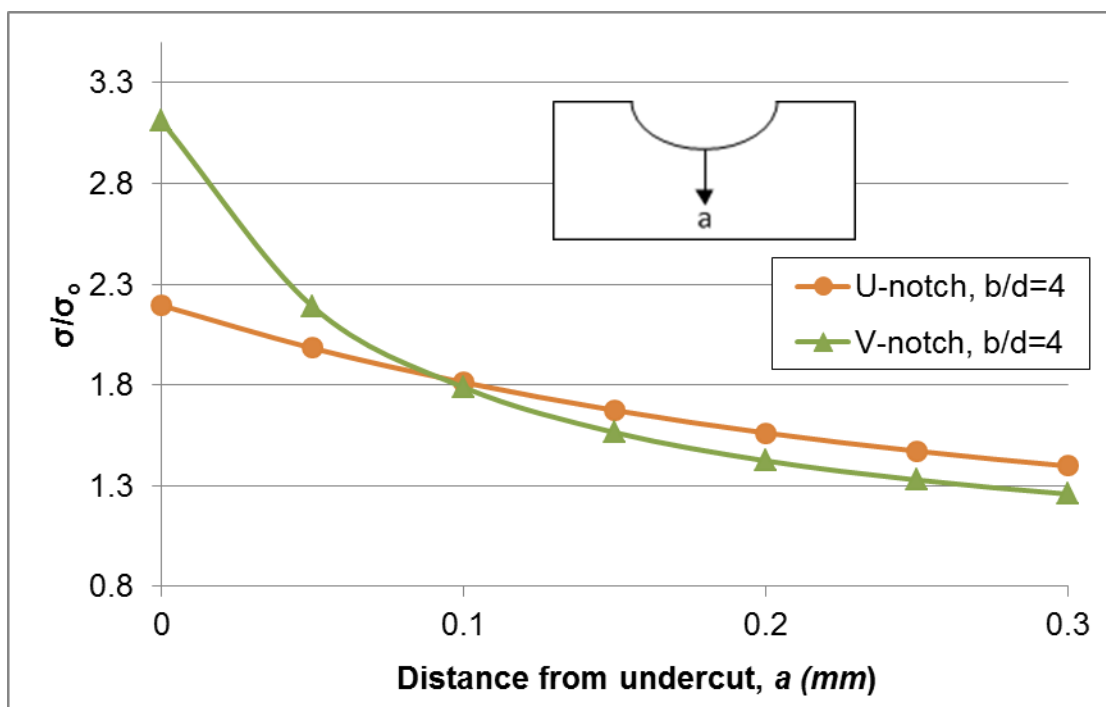
Fig. 3.39 Stress distribution of shape ratio *b/d*=4 up to 0.3 mm from undercut

In the case of welded joint with weld bead height (h = 2.5, 5, 7.5 and 10 mm), Fig. 3.40 represents fatigue life calculation results for model with weld bead height of 2.5 mm and flank angle of 90°. This case presents similar pattern as Fig. 3.33(a) and (b) which V-notch model gives higher fatigue life compare to U-notch model. For U-notch model, is shows lower shape ratio, *b/d* gives lower fatigue life. However, these results found in contrast with model without weld bead where lower ratio *b/d* presents higher fatigue life. In other cases, similarly results found for V-notch model where higher ratio illustrates higher fatigue life and not much significant differences found in the model without weld bead height.
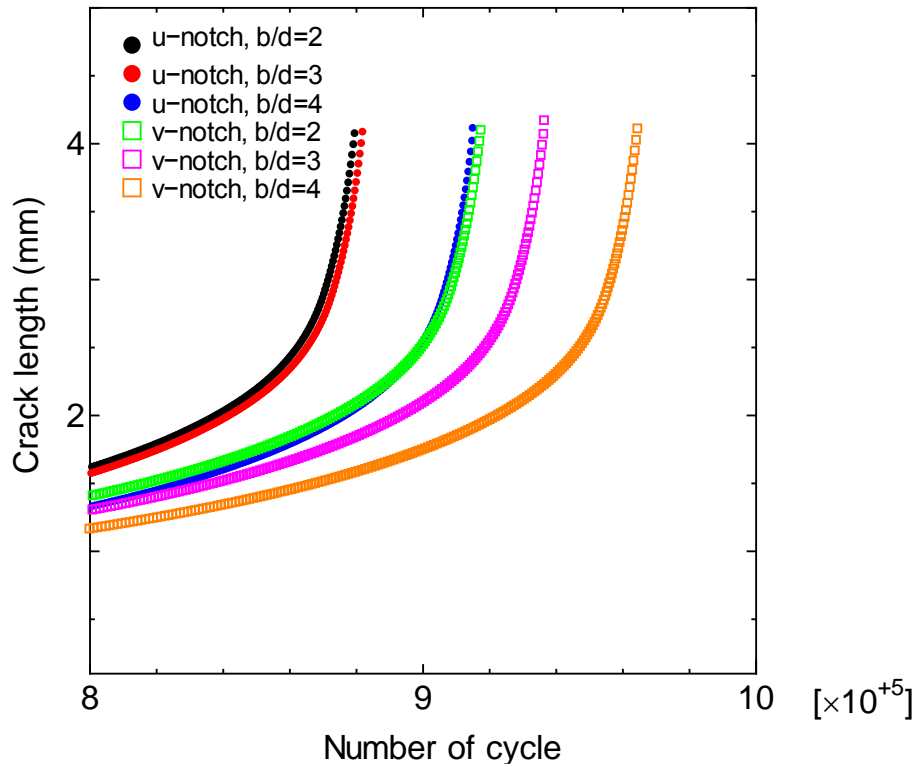
Fig. 3.40 Fatigue life for model with weld bead height, *h*=2.5 mm and flank angle, θ of 90° (enlarge scale)

Referring to Fig. 3.41 will explained about fatigue life result which is shown in Fig. 3.40. Stress found higher for U-notch model with lower shape ratio, *b/d* at undercut root radius but then start decreasing at a transition point at about 0.17 mm. Again, no significant differences found in V-notch model as presented in Fig. 3.42. Next comparison between U and V-notch model at same shape ratio, *b/d* where Fig. 3.43 illustrates V-notch model

gives higher *SCF* compare to U-notch model. However, at about transition point of 0.07 mm from undercut root, stress level for V-notch model become lower then U-notch model. This phenomenon confirms stress gradient plays important role in order to evaluate fatigue life for the structure as can be seen in Fig. 3.31. In addition, this study found by introducing weld bead height, *SCF* found significantly increase for V-notch model compare to U-notch type. Again, stress gradient for U-notch model found rapidly decrease compare to V-notch model as can be seen in Fig. 3.44.
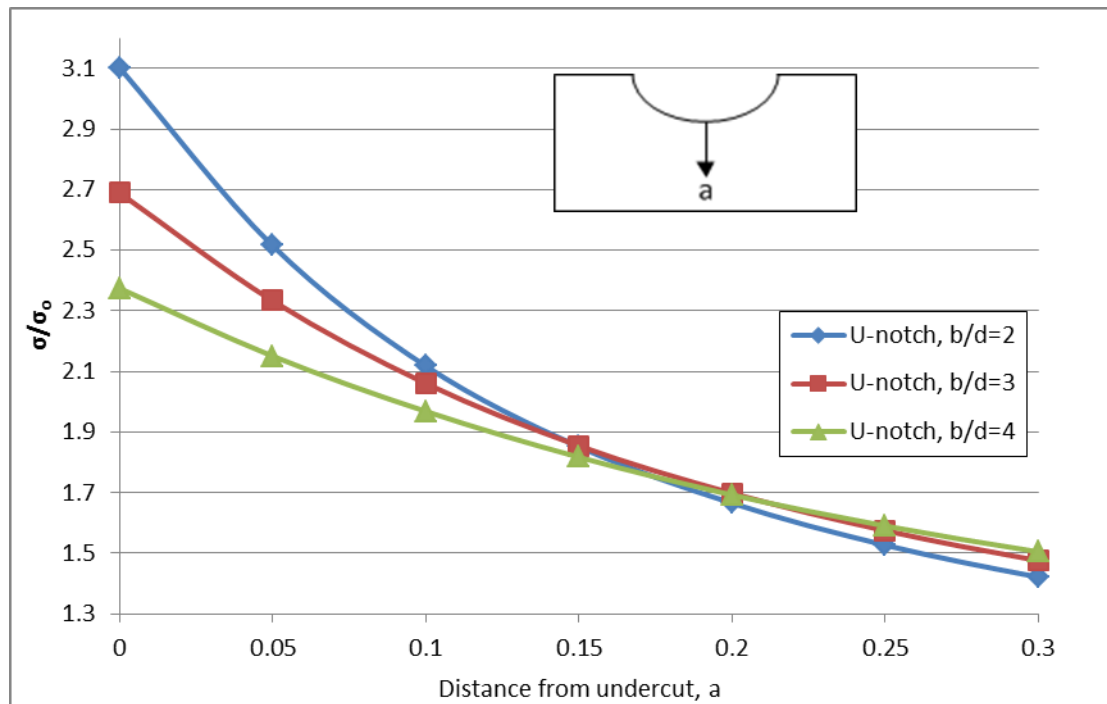
Fig. 3.41 Stress distribution of U-notch model up to 0.3 mm distance of undercut root
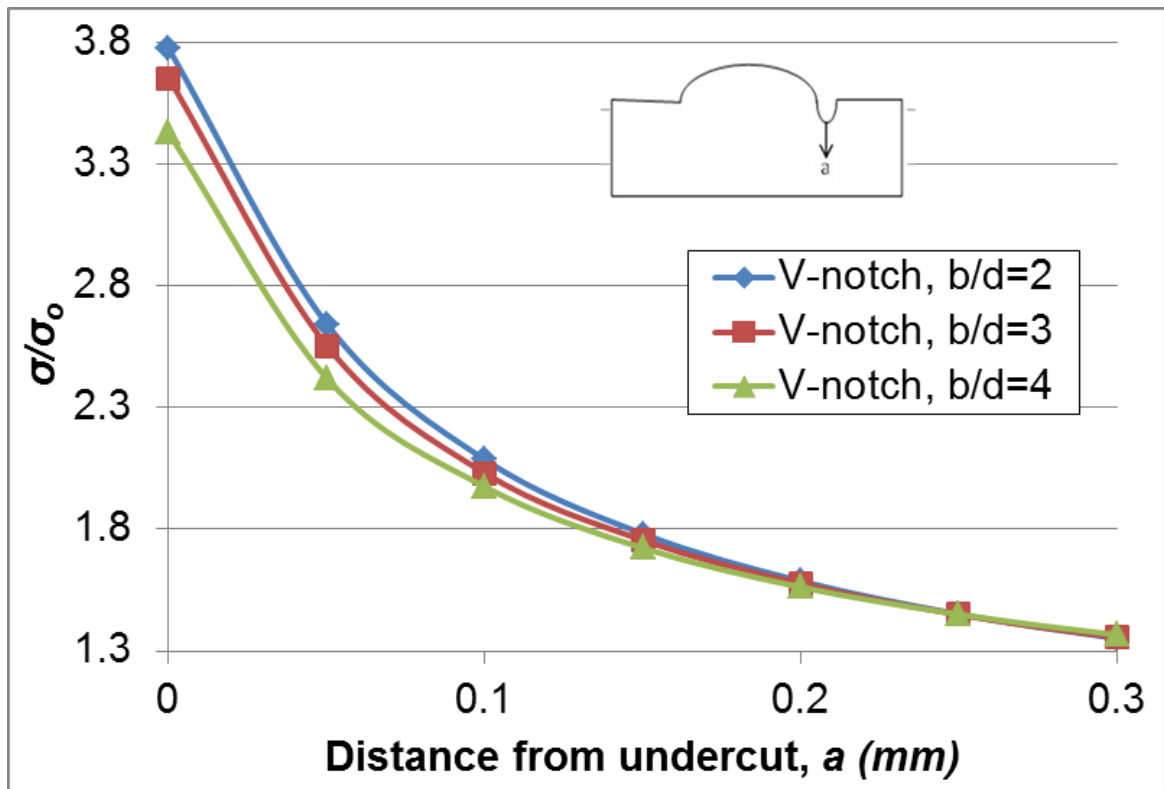
Fig. 3.42 Stress distribution of V-notch model up to 0.3 mm of undercut root
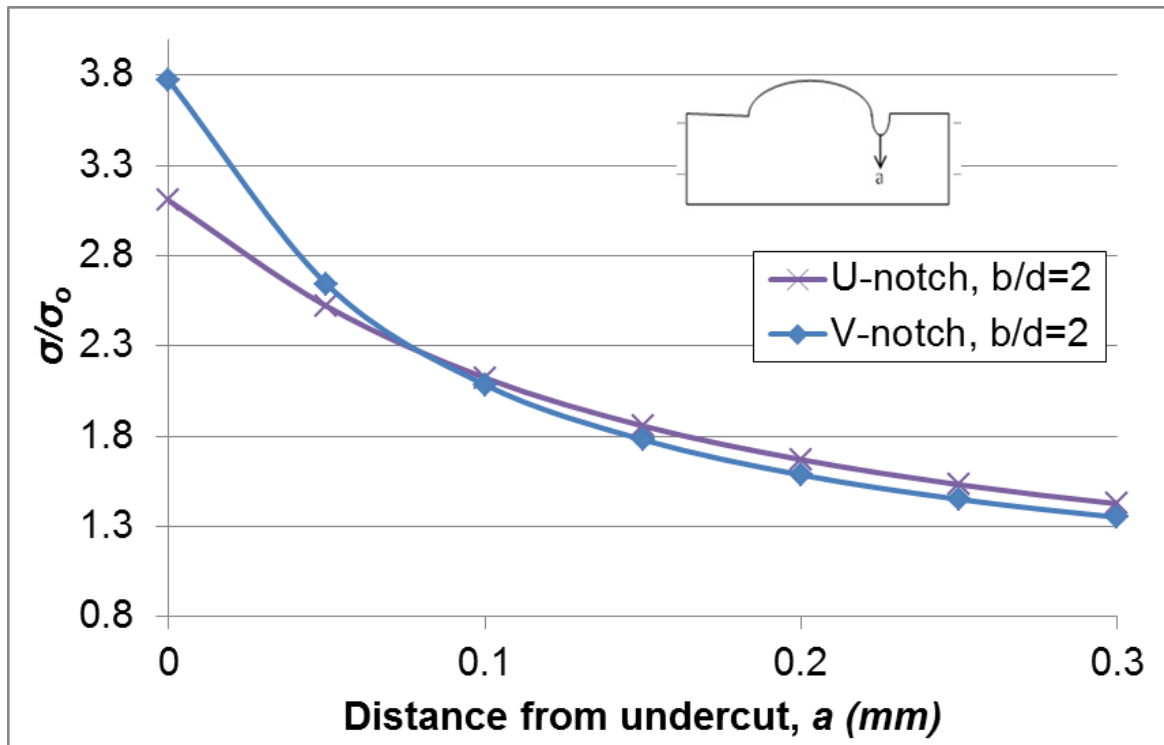
Fig. 3.43 Stress distribution of shape ratio *b/d*=2 up to 0.3 mm from undercut
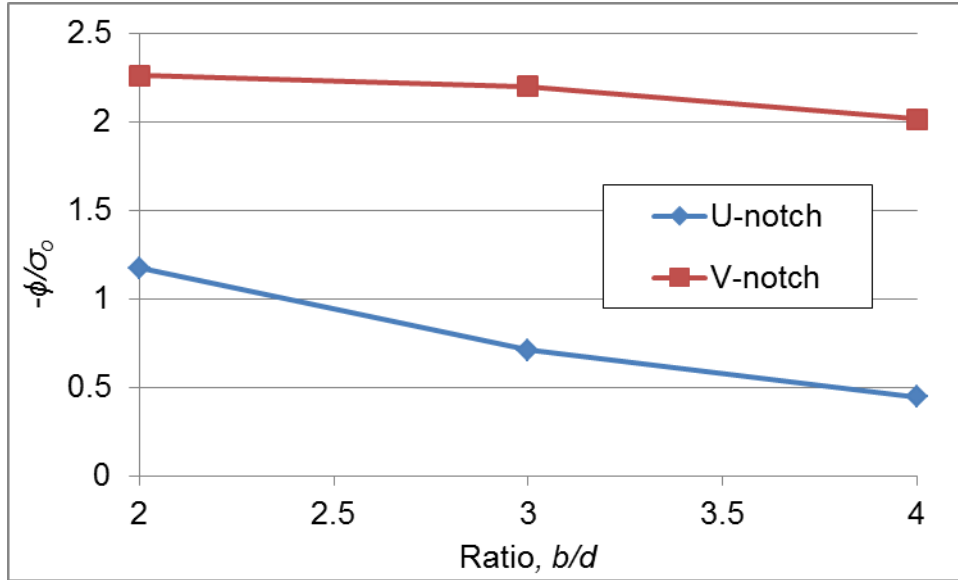
Fig. 3.44 Comparison of ϕ for model with weld bead height, h=2.5 mm and flank angle, Ѳ of 90°

Fig. 3.45 illustrates selected cases for fatigue life at different weld bead height and undercut depth. As can be seen, model with no weld bead (h=0 mm) with lower undercut depth (d=0.25 mm) shows higher fatigue life compare to others. Furthermore, model with weld bead height of 2.5 mm with undercut depth of 1mm presents lower fatigue life compare to others. Therefore, the result confirms deeper undercut depth will reduce the fatigue life of any welded joint structures. However, this case shows the stress concentration factor has significant effect even though stress gradient at higher side for deeper undercut depth (see Fig. 3.46).
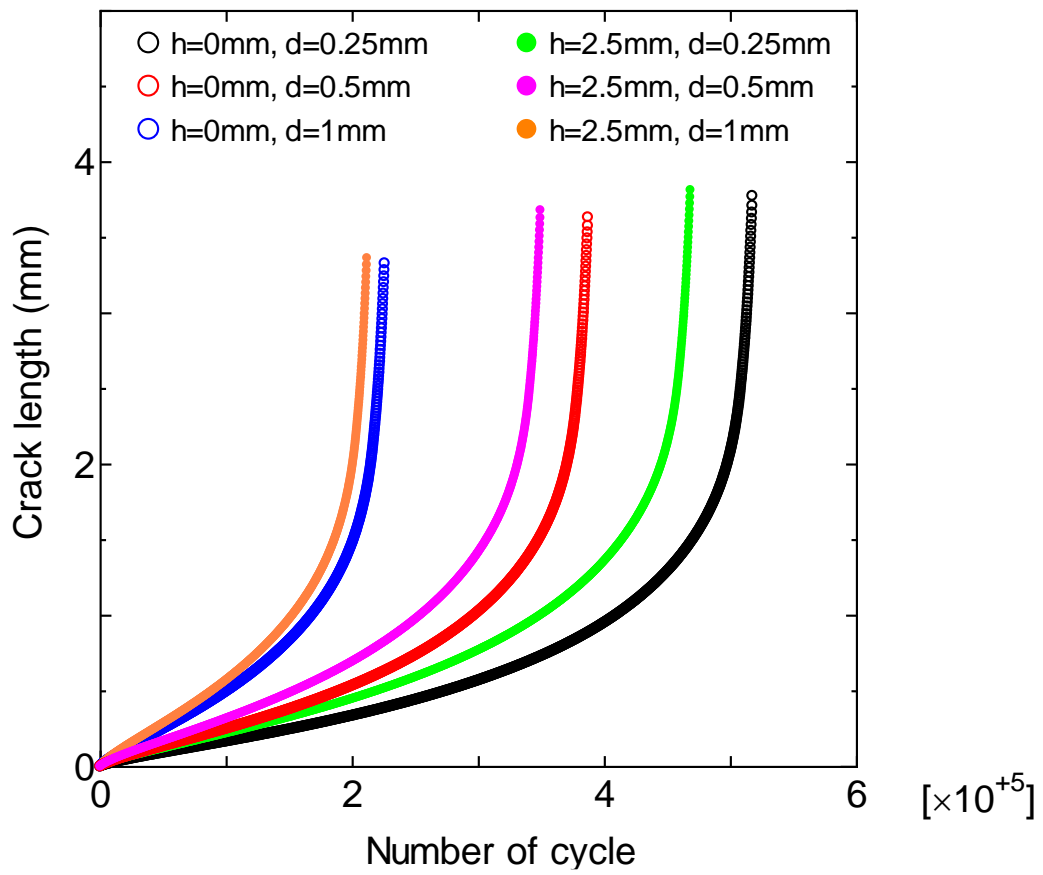
Fig. 3.45 Fatigue life at different undercut depth, *d*
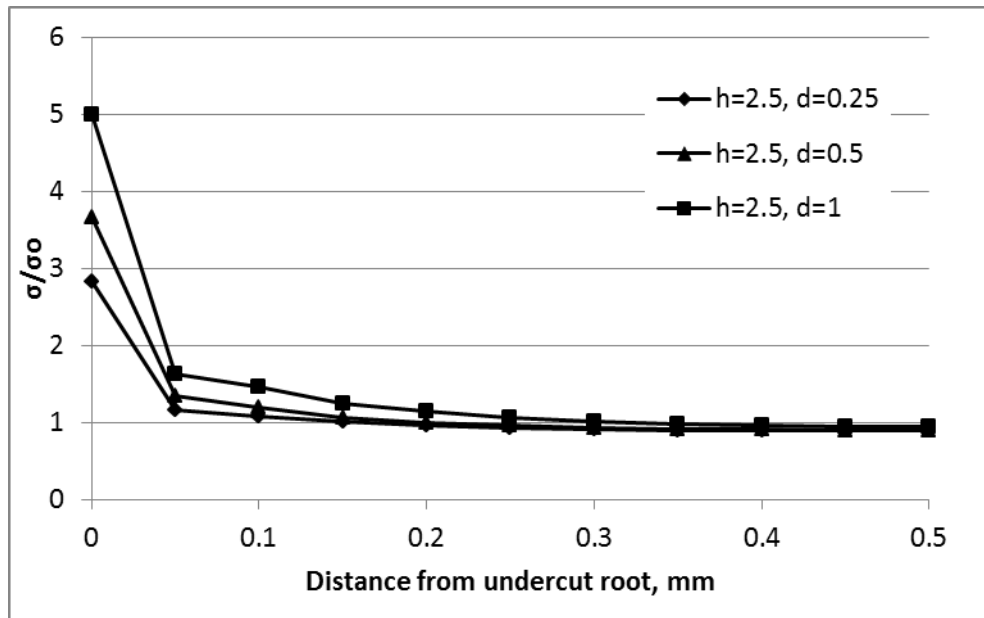
Fig. 3.46 Stress distribution for *h*=2.5 mm at different undercut depth
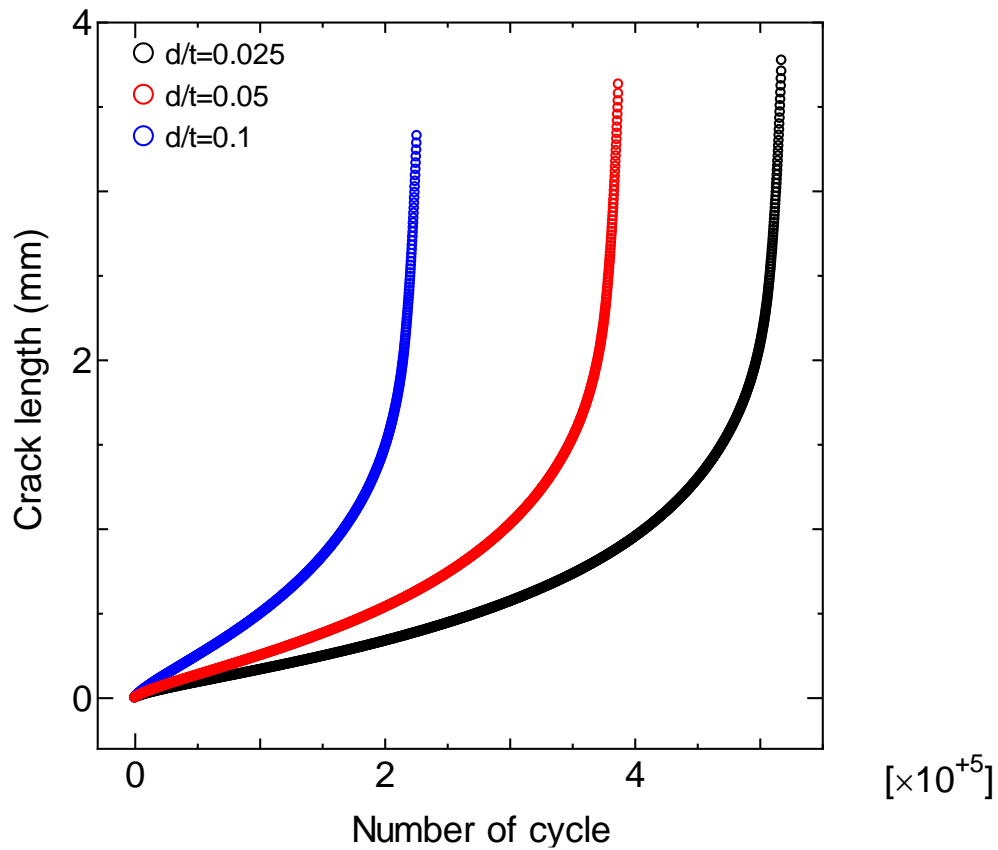
Fig. 3.47 Fatigue life at different *d/t*

The relationship between undercut depth and the plate thickness is important in order to estimate the fatigue life. Fig. 3.47 shows fatigue life at higher *d/t* present lower fatigue life. The undercut over plate thickness ratio can be considered in the improvement of the JSQS. The figure presents a significant effect of different ratio where the different fatigue life at *d/t*=0.05 and 0.1 is about 300,000 cycles. Comparison between different type of notch shape at same shape ratio, *b/d*=4 shows about 80,000 cycles. Therefore, undercut depth, especially *d/t* ratio plays more significant effect in contributing to the fatigue performance on welded structure.

69

3.4 Conclusion

When the above results are taken into consideration, this study has primarily yielded the following conclusions. The amount of reinforcement metal and weld toe radius have an important effect on stress distribution. Higher flank angles and small toe radius cause higher values of SCF. Plate thickness, which is another factor, should also be considered and *h/t* ratio is recommended in the evaluation of stress distribution in butt welded structure. As for weld joints with undercut defects, the ratio of undercut depth to plate thickness, *d/t* are the main parameters controlling the severity of SCF. In addition to excessive reinforcement weld metal with undercut gives rise to increase in the SCF. Finally, in order to predict the SCF for the joints with and without undercut defect, practical formula based on Neuber equation was established with dimensionless parameter. Besides, allowable limit also presented for practical used of engineers and inspectors as a simple guide for performing their job. Below are several conclusions which can draw from this study:

a) The study shows a significant effect of undercut depth (*d*) and weld bead height (*h*) over plate thickness (*t*). Therefore, non-dimensional parameters such as undercut and weld bead height over plate thickness ratio (*d/t*) and (*h/t*) was introduced in this study. In addition, the study found stress concentration factor increase by increments of plate thicknesses.

b) Practical formula is established for the purpose as a tool for evaluation of structural welded defect with the crack-like undercut type. In addition, allowable limit of strength and other member based on JSQS and IACS Rec. 47 is available as references. This will be valuable especially for inspection engineers to decide the next action of structural maintenance.

c) The study found V-notch undercut type gives higher fatigue life compare to U-notch undercut type at constraint of same shape ratio, *b/d*. This will be more practical approach for inspection engineer in considering width, *b* and depth, *d* of undercut rather the shape itself.

d) Studies highlighted stress gradient, ϕ is the important criteria in assessing fatigue strength of the butt welded structure.

e) Weld bead height or reinforcement gives influence in increasing stress concentration factor (SCF).

CHAPTER 4

CHAPTER 4

Comprehensive study of structural integrity of non-load-carrying fillet welded joint effect with large gap size

4.1 Introduction

Recently, the semi-automatic CO_2 gas shielded arc welding is mainly used in large welded built up structures such as ships and offshore structures construction instead of manual arc welding because of its high performance and cost benefit. In general, CO_2 gas shielded welding enables the manufacturing of welded joints with large gaps. Even though excess of filler metal for large gap welded joint may contribute to increase production cost, but in industrial practise total cost not only depends to the amount of filler metal used. Most of the production time is consumed during the structural arrangement and the preparation of fabrication. Again, due to the allowable limitation of gap size of the hull construction quality standards such as JSQS and IACS Rec. 47, more time consuming is needed when any welding works were rejected by the inspector. The redundant welding works will increase much time and cost in the production itself. Therefore, allowable limits on the gap size for the joints made by CO_2 gas shielded welding should be modified.

Most of the hull construction and quality standards requirements and available standards for fatigue test have been explained in Chapter 2. As mention earlier, the purpose of this study is to confirm the mechanical performance of non-load-carrying fillet welded joint with large gap sizes. Hardness, tensile, bending, fatigue capacities and residual stress distribution will be investigated in order to ensure the welding quality. This study is limited to sound welded joints which no defect like undercut, blow hole, root cracking and incomplete fusion are contained in application of large gap sizes. Besides, a skill welder was performed the welding job in order to maintain the weld quality and to ensure consistency of welded specimen performance. The experimental work has been carried out in room temperature varies from 7 degree to 34 degree Celsius.

71

4.2 Experimental methodology

4.2.1 Welded specimen configurations

The welded specimens were constructed by a qualified person who works in a Japanese shipbuilding company in order to avoid inconsistency due to welder skill effect. Plate 300 x 800 x t mm was welded with different gap sizes 0, 20 and 25mm to construct the tee joint. In this case, all welded specimens were constructed without groove. Fig. 4.1 shows that the long tee welded joint plate was cut into several sections of specimens for different mechanical tests and macro observation. The cut specimen with a length of 30mm was used in a fatigue test. Single pass welding was applied to specimen with zero gap. However, about 25 passes of welding works are performed to the specimen with 20 and 25mm gap sizes, see Fig. 4.2. Details of the chemical and mechanical properties of the base metal and weld material are specified in Tables 4.2 to 4.5. In addition, welded specimen was fabricated by two types of welding positions which are the vertical and horizontal positions.

Table 4.1 Welded specimen's configuration

Thickness, t (mm)	Material	Gap size (mm)	Welding position	Specimen ID	Number of specimen
10	Mild steel (*Class NK Grade KAS*)	0	Horizontal	10M0H	4
		20		10M20H	
		25		10M25H	
		0	Vertical	10M0V	4
		20		10M20V	
		25		10M25V	
	High tensile steel (*ClassNK Grade KA36*)	0	Horizontal	10H0H	4
		20		10H20H	
		25		10H25H	
		0	Vertical	10H0V	4
		20		10H20V	
		25		10H25V	
15	Mild steel (Class NK Grade KAS)	0	Horizontal	15M0H	4
		20		15M20H	
		25		15M25H	
		0	Vertical	15M0V	4
		20		15M20V	
		25		15M25V	

		0		15H0H	
	High tensile steel *(ClassNK Grade KA36)*	20	Horizontal	15H20H	4
		25		15H25H	
		0		15H0V	
		20	Vertical	15H20V	4
		25		15H25V	
20	Mild steel *(Class NK Grade KAS)*	0		20M0H	
		20	Horizontal	20M20H	4
		25		20M25H	
		0		20M0V	
		20	Vertical	20M20V	4
		25		20M25V	
	High tensile steel *(ClassNK Grade KA36)*	0		20H0H	
		20	Horizontal	20H20H	4
		25		20H25H	
		0		20H0V	
		20	Vertical	20H20V	4
		25		20H25V	
25	Mild steel (*Class NK Grade KAS*)	0		25M0H	
		20	Horizontal	25M20H	4
		25		25M25H	
		0		25M0V	
		20	Vertical	25M20V	4
		25		25M25V	
	High tensile steel (*ClassNK Grade KA36*)	0		25H0H	
		20	Horizontal	25H20H	4
		25		25H25H	
		0		25H0V	
		20	Vertical	25H20V	4
		25		25H25V	

Fig. 4.1 Schematic illustration of welded specimen used

(a) Zero gap　　　　　(b) 20mm gap　　　　　(c) 25mm gap

Fig. 4.2 Photographs of the specimens

(a) Zero gap

74
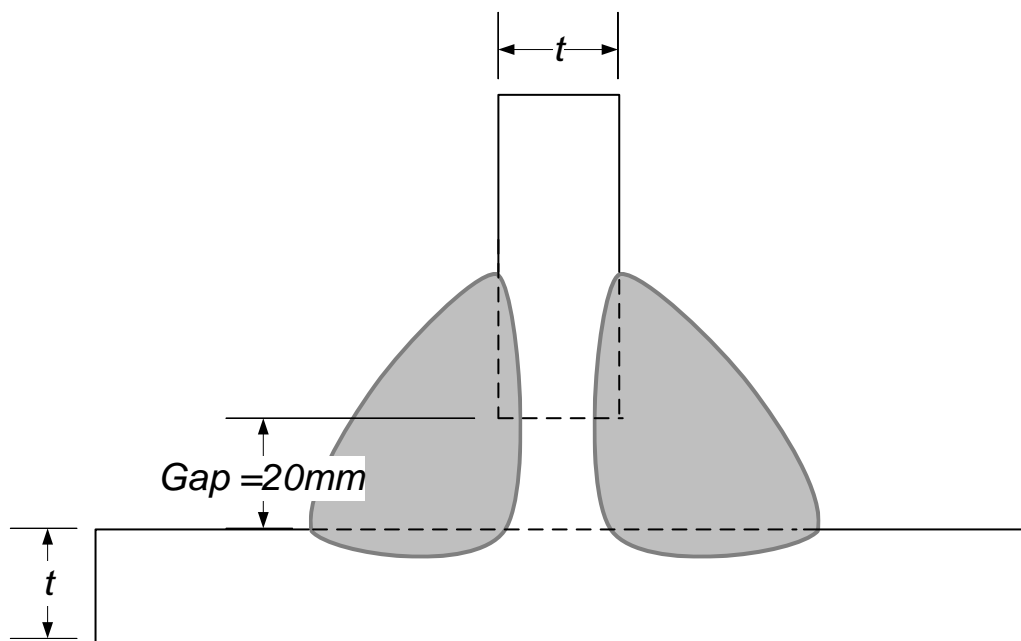
(b) 20 mm gap
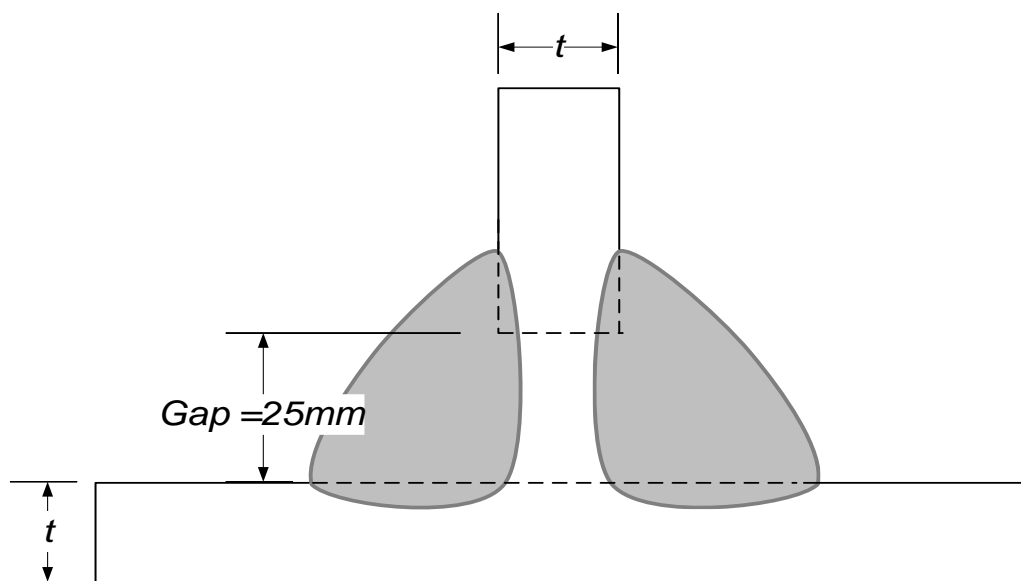
(c) 25 mm gap

Fig. 4.3 Schematic configuration of the welded specimens

Table 4.2 Chemical composition of base metal (%)

Materials	C	Si	Mn	P	S	Cu	Ni	Cr
High tensile steel (ClassNK Grade KA36)	0.16	0.23	1.04	0.0182	0.068	0.1	0.1	0.2
Mild steel (ClassNK Grade KAS)	0.17	0.12	0.77	0.011	0.07	0	0	0

Table 4.3 Mechanical properties of base metal

Materials	Yield strength (MPa)	Tensile strength (MPa)	Elongation (%)
High tensile steel (ClassNK Grade KA36)	410	525	23
Mild steel (ClassNK Grade KAS)	316	455	29

Table 4.4 Chemical composition of weld material (%)

Shield gas	C	Si	Mn	P	S
CO_2	0.06	0.50	1.40	0.015	0.010

Table 4.5 Mechanical properties of weld material

Yield strength (MPa)	Tensile strength (MPa)	Elongation (%)	Charpy 2V-notch at 0ºC, (J)
520	580	28	91

The effect of geometrical condition is very important in studying the fatigue performance of welded specimens. As discussed in chapter 2, such parameters to be considered are flank angle, weld toe and weld throat thickness. The definitions of flank angle, Θ and weld toe radius, ρ are described in Fig. 4.4. Each specimen's flank angle and weld toe radius were measured under a stereo microscope and all data was tabulated in Table 4.5. Here, all of the data were presented within the limits of IACS Rec. 47 and JSQS requirements where the flank angle, $\Theta^o \leq 90^o$. Weld toe radius, ρ for specimens was measured only at base metal at which presume for crack initiation at right and left position and ranging between 0.79 to 3.51 mm.
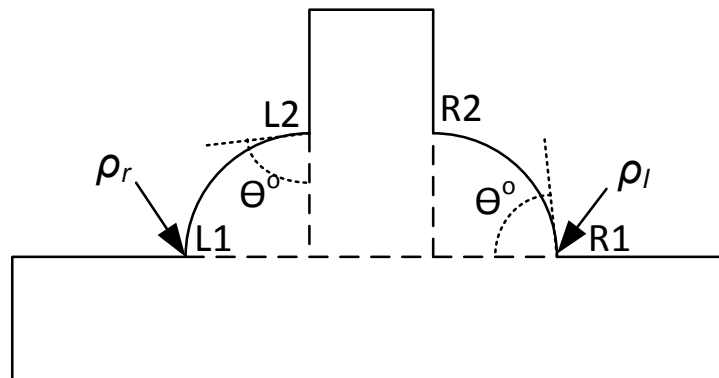
Fig. 4.4 Definitions and location of flank angle, Θ^o and weld toe radius, ρ

Table 4.6 Measured flank angle and weld toe radius of the welded specimens

Specimen ID	Flank angle (deg.)				Weld toe radius, ρ (mm)	
	L1	R1	R2	L2	ρ_r	ρ_l
10M0H	45.65	50.28	51.03	47.43	2.06	1.56
10M20H	43.65	40.98	54.50	48.90	2.88	2.42
10M25H	35.53	39.65	54.50	50.15	2.96	3.22
10M0V	60.64	69.92	55.20	66.22	1.32	1.50
10M20V	54.74	51.98	54.80	37.84	1.94	2.47
10M25V	65.98	59.58	35.22	43.30	1.64	1.95
10H0H	60.74	62.96	48.72	54.60	1.35	1.93
10H20H	31.62	43.78	47.73	51.66	3.12	2.82
10H25H	41.00	44.57	55.33	57.32	2.94	3.51
10H0V	54.10	70.00	54.33	61.51	0.90	0.79
10H20V	47.70	57.94	35.00	31.34	1.92	2.05
10H25V	52.10	54.18	42.54	33.80	1.98	1.86
15M0H	51.05	49.33	48.95	51.05	1.71	1.65
15M20H	46.20	43.70	47.33	48.90	2.91	3.49
15M25H	41.50	52.48	48.43	41.50	2.62	2.11
15M0V	90.40	83.70	62.68	54.54	1.56	1.07
15M20V	61.90	33.00	65.78	40.20	2.22	2.90
15M25V	71.00	39.84	57.62	38.12	1.99	2.28
15H0H	71.84	72.48	78.44	71.84	1.84	1.85
15H20H	39.40	52.20	44.32	49.18	3.14	2.22
15H25H	41.90	68.06	72.92	80.86	2.43	1.66
15H0V	58.70	41.92	59.58	44.90	1.24	1.17
15H20V	56.80	54.94	61.98	56.66	1.58	1.16
15H25V	56.70	46.28	59.78	37.42	2.05	1.20

Note: Specimen ID for example 10**M**0H means type of material; **M** = mild steel, **H** = high tensile steel, 10M0<u>H</u> means type of welding position; <u>H</u> = horizontal, <u>V</u> = vertical, **10**M<u>0</u>H means size; **10** = plate thickness and <u>0</u> = gap sizes.

4.2.2 Welding parameter

The tee fillet welded joint specimen was prepared by using a semi-automatic CO_2 gas welding. The welding parameters for the welded specimen are presented in Tables 4.6 and 4.7. Some values in the table are varied in order to maintain the quality of the welded joint parameters. However the variation is small in average.

Table 4.7 Welding parameters of mild steel specimen

Specimen ID	Current (A)	Voltage (V)	Travelling speed (mm/s)	No. of pass	Heat input (kJ/cm)
10M0H	260	30	6.61	1	11.8
10M0V	180	26	1.84	1	25.4
10M20H	280	32	7.27	25	13.7
10M20V	200	27	1.70	6	35.1
10M25H	290	32	7.15	25	14.7
10M25V	220	28	1.71	7	39.7
15M0H	290	32	6.53	1	14.2
15M0V	200	27	1.84	1	29.4
15M20H	280	33	6.70	21	12.1
15M20V	220	29	1.89	7	31.2
15M25H	300	32	7.18	30	12.2
15M25V	220	27	2.01	9	27.4

Table 4.8 Welding parameters of high tensile steel specimen

Specimen ID	Current (A)	Voltage (V)	Travelling speed (mm/s)	No. of pass	Heat input (kJ/cm)
10H0H	310	31	6.25	1	15.4
10H0V	200	22	2.26	1	19.4
10H20H	290	28	7.70	18	11.0
10H20V	190	22	1.50	5	33.5
10H25H	310	28	8.01	23	11.6
10H25V	240	24	1.53	5	42.2
15H0H	290	32	5.51	1	16.8
15H0V	200	26	2.17	1	24.0
15H20H	300	34	7.56	20	12.8
15H20V	220	28	2.20	8	26.9
15H25H	300	32	7.39	23	11.7
15H25V	210	28	2.17	10	26.0

The nominal value of heat input in Tables 4.7 and 4.8 is defined as below:

$$\text{Heat input} = 60EI / 1000S \qquad (4.1)$$

where,

H = heat input (kJ/cm),
E = voltage (V),
I = current (A) and
S = welding speed (mm/min).

4.2.3   *Mechanical test – hardness and tensile*

Hardness of the cross-section of welded specimens was examined by Vickers hardness with an indentation load of 10 kgf. All mechanical tests were carried out based on the Rules for the Survey and Construction of Steel Ships, part M – Welding requirements by ClassNK (2013). The location points of hardness indentation are presented in Figs. 4.5 and 4.6 along the dashed line. The number in a circle presented the location point. Additional indentation at the centre (Fig. 4.6) was done for specimen with 20 and 25 mm gap sizes to confirm the mechanical property. The test was performed at a distance of less than 2 mm from the specimen surface.
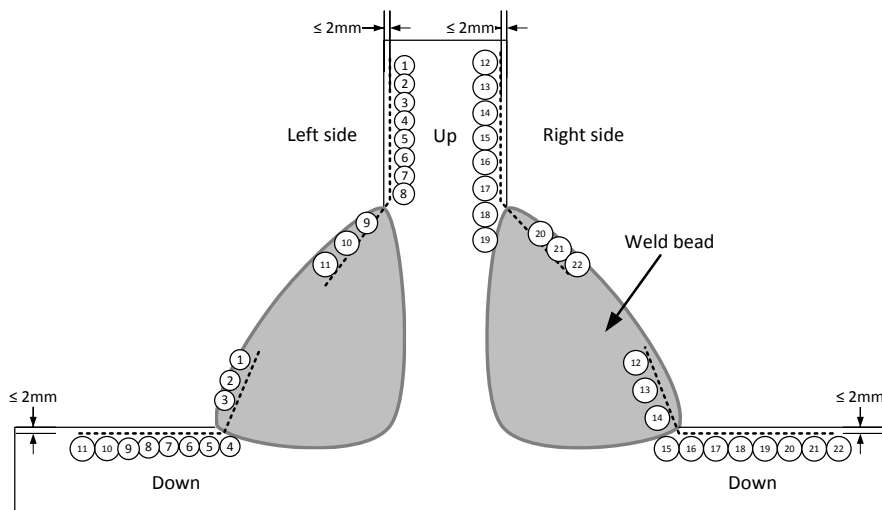
Fig. 4.5 Location of indentation point for zero gap specimens
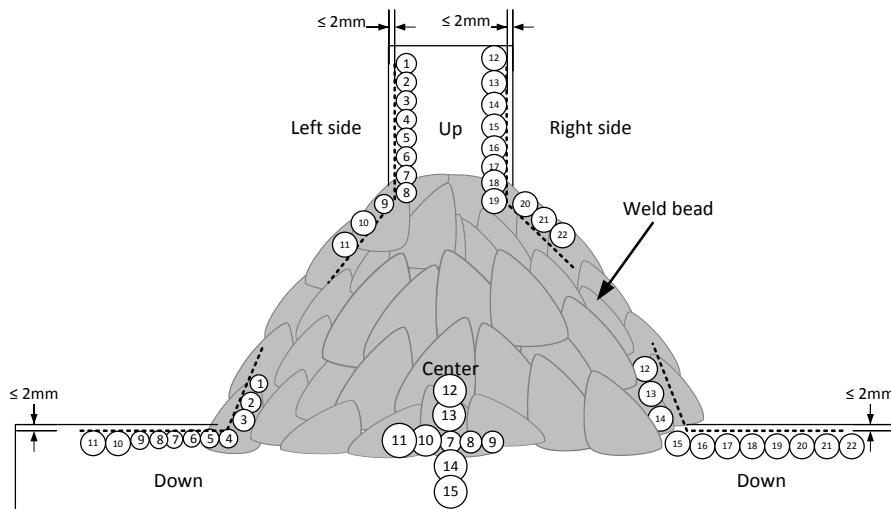
Fig. 4.6 Location of indentation point for 20 and 25 mm gap specimens
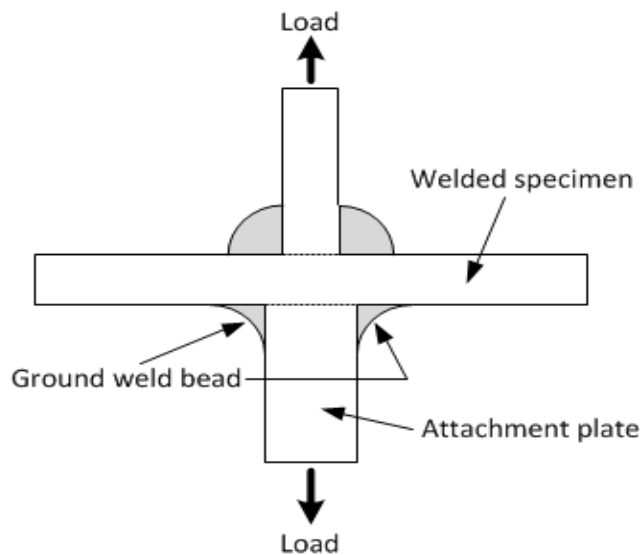
Fig. 4.7 Attachment plate to welded specimen for tensile test

Next, a tensile test was conducted by attaching a piece of steel by welded joint to the specimen as shown in Fig. 4.7. The weld bead at the attaching plate was ground to avoid breaking at the attachment to the specimen. The purpose of this test is to locate the breaking area, whether at the base metal, a specimen's weld toe or weld bead (Fig. 4.8). It is vital to confirm the quality of welded joints at the fracture surface, to determine whether any weld defects was presented. Macro observation was performed by polishing the cross-section of welded joint specimens in order to check any defect. All specimens were observed before any mechanical tests take place.
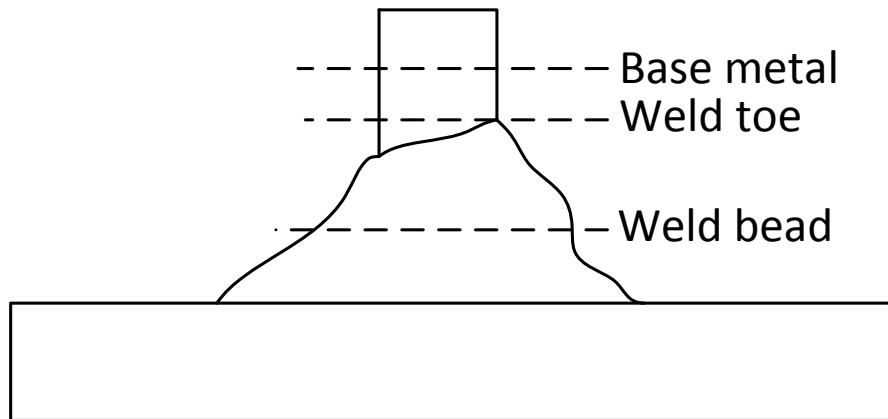
Fig. 4.8 Breaking part location

4.2.4 Bending test

Bending tests were carried out in order to confirm the quality of welded joints. As mention in Chapter 2, it is important to conduct fracture test such as bending of stiffener plate to defects any defect of the welded joint especially at the weld toe. Fig. 4.9 shows the specimen configuration on jig fixtures in order to perform bending tests. The web plate of the welded specimen was bending to 45° to 60°. Following magnetic particle inspection was applied in order to detect any cracks by visual examination.
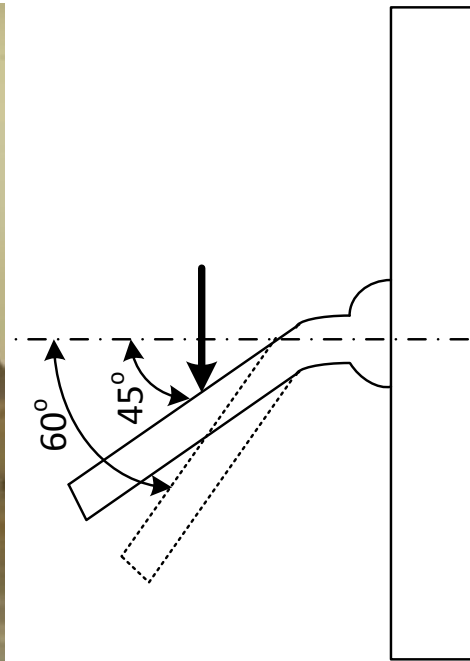
(a) Holding jig   (b) Angle of bending test

Fig. 4.9 Configuration of bending test

4.2.5   Macro observation

In welding procedure and qualification tests of steels for hull construction and marine structures by IACS code, the test specimen is examined by preparing the specimen's surface for etching to clearly reveal the weld metal, fusion line, root penetration and heat affected zone. This examination is vital in confirming the welding quality and to verify any defect like porosity or lack of fusion was presented.

4.2.6   Fatigue test

S-N curves proposed by the International Institute of Welding (IIW) Fatigue Design recommendations are based on the nominal stress range and the curves are normally used to classify fatigue resistance of structural details. It was noted in the IIW documents where fatigue class (FAT) recommendation for non-load-carrying fillet welded joint for as welded is FAT80 while toe ground is FAT100. This recommendation is applicable for steel with non-corrosive conditions. The similar fatigue design curve also established in Japanese Society of Steel Construction (1995) based on nominal stress. Here, curve D in

JSSC is equivalent to IIW-FAT100 while curve E for IIW-FAT80. In addition, UK HSE basic S-N curves that were published in IACS Rec. 56 (1999) defined stress range can be categorized to nominal stress, hot spot stress and notch stress. Stress concentration factor due to geometrical configuration and weld geometry is taken into account.

Fatigue tests of the tee fillet welded joint was carried out on a specimen with dimension of 300 x 30 x 10 mm at room temperature. The three point bending test (Fig.4.10) was performed on a Dynamic Servo Hydraulic Machine in accordance to ISO/TR 14345 (2012) and JSME Standard 002 (1984). Furthermore, the specimen's configuration as shown in Fig. 4.11 with constant amplitude at stress ratio, $R = 0$ was applied to the frequency of 15Hz. There are many definitions of failure criterion as mention in ISO/TR 14345 such as the detectable crack of specific length and through thickness cracking. In this case, failure criteria are defined when the specimens broke with a crack propagated up to 80% of specimen's thickness. In other words, fatigue test machine will stop at a certain limit after specimen's broke, see Fig. 4.25 in the following section. Ferreira and Branco (1989) stated that the fatigue test will be terminated when the cracks propagate more than half of the plate thickness. In all cases, the crack was started from weld toe and no crack found started from weld root. In order to compare the fatigue performance of welded specimen with large gap sizes, fatigue design recommendations as established in IIW and UK HSE were used as reference curves.
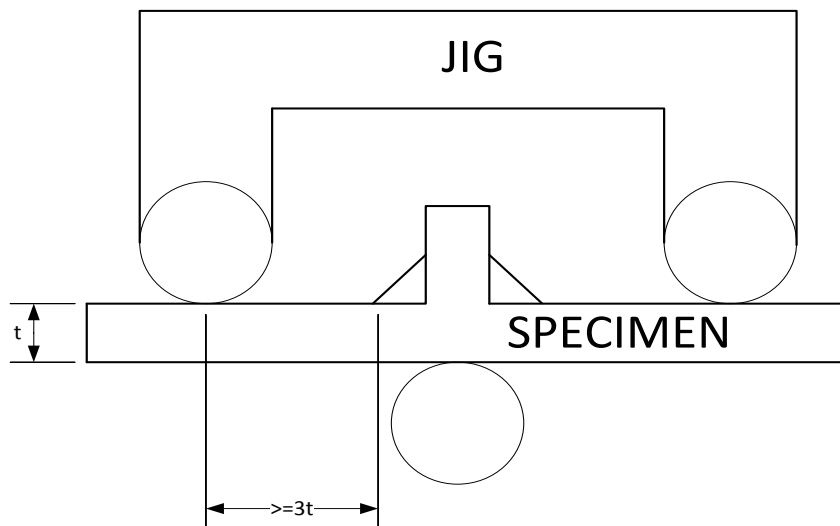
Fig. 4.10 Schematic of three point bending fatigue test (available span length of 56 mm and 75 mm)

83

Fig. 4.11 Specimen's configurations of the fatigue test machine

4.2.6.1 Hot spot stress

There are many ways to determine stress values in order to plot the S-N curve such as nominal stress, hot spot stress and effective notch stress. The most popular method for expressing fatigue performance is nominal stress range. In this study, nominal stress will calculate based on the beam theory to determine the stress range for tee fillet welded specimen. As mention earlier, three point bending of fatigue test will be conducted in this study with stress range, $R = 0$.
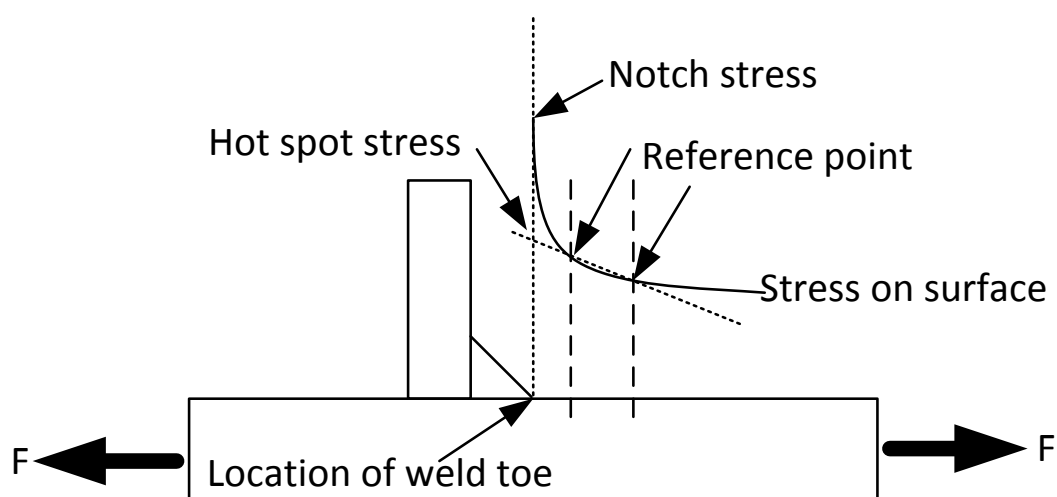
Fig. 4.12 Definitions of hot spot stress

The hot pot stress is applied to explain the fatigue strength for welded structure which contains the structural stress concentration sites. The hot spot stress can be determined by finite element method and its characteristic, see Fig. 4.12. The hot spot stress was calculated by using reference point and extrapolation method. In this case below formula (Hobbacher, 2008) was used to calculate hot spot stress since this study is using fine mesh with an element length not more than 0.4 of plate thicknesses:

$$\sigma_{hs} = 1.67. \, \sigma_{0.4t} - 0.67\sigma_{1.0t}. \tag{4.2}$$

Here; σ_{hs} = hot spot stress, t = plate thickness, $\sigma_{0.4t}$ = stress at the nodal point with a distance of $0.4t$ from weld toe, $\sigma_{1.0t}$ = stress at the nodal point with a distance of t from weld toe.

Below are the procedures in calculating structural stress in order to verify the validity of equation (4.2):

1. Sample of calculation:
   Based on equation (2), hot spot stress was calculated as below:
   σ_{hs} = 1.67(395.124) - 0.67(325.491)
      = 441.78 MPa

2. Based on node coordinate at 0.4t and 1.0t (See Fig. 4.13), find the curve equation. Next, from the equation, get the y value (structural stress) when x=0.
   For example;

   At 0.4t: x= 4, y=395.124
   At 1.0t: x=10, y=325.491
   Slope = -10.9633
   Structural stress, at x=0, y= 435.124 MPa
   % difference compares to hot spot stress: 1.56 %

3. Based on a linear curve on stress distribution as shown in Fig. 4.12. From the straight line, structural stress at x=0, y= 439.52 MPa

   % difference compares to hot spot stress: 0.511 %

Based on the example of calculation as above, both methods of calculation in (2) and (3) shows by using equation (4.2) is significant with very low differences. Therefore, hot spot stress calculation of the equation will be applied in plotting S-N curve based on hot spot stress since very little difference in comparison with present structural stress.

Another formula as described in Chapter 2 for 3 reference points and coarse mesh element with higher order gives similar results as equation 4.2 with error less than 5%.
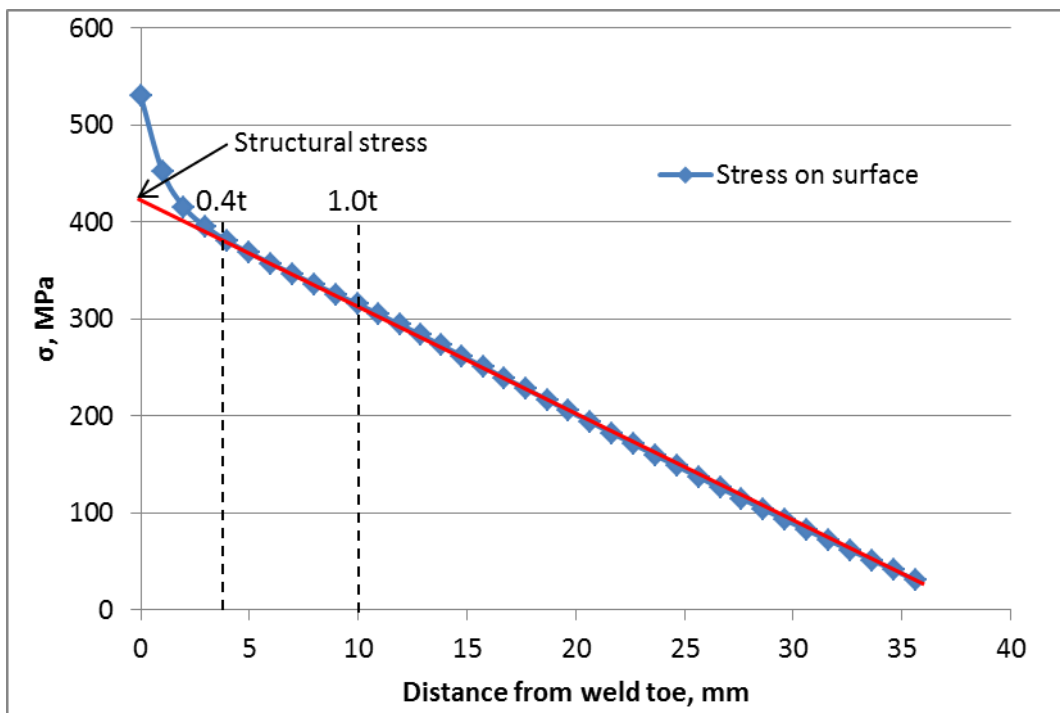
Fig. 4.13 Example of stress distribution on plate surface

4.3 Results and discussion

4.3.1 *Mechanical test – hardness and tensile*

Experimental results are shown here is for specimen thickness of 10 and 15 mm with material of high tensile steel (HTS) and mild steel (MS). Figs. 4.14 to 4.19 illustrate the results from the Vickers hardness test. The results of the test are referring to Figs. 4.5 and 4.6 where the point of indentation was located. In this case, location of indentation point can be referred as x-axis coordinate. All figures present results based on location, type of material and gap size. As can be seen in Fig. 4.20, the highest hardness value found at both specimen thickness of with 309 Hv. The value is still under the limitation of ClassNK (2013) where for steel with minimum yield strength of 420 MPa, the hardness test should not exceed 350 Hv10. The higher hardness value is present at the weld bead location compared to the base metal. The results are similarly found in the mechanical properties studied by Okayasu et. al. (2013).
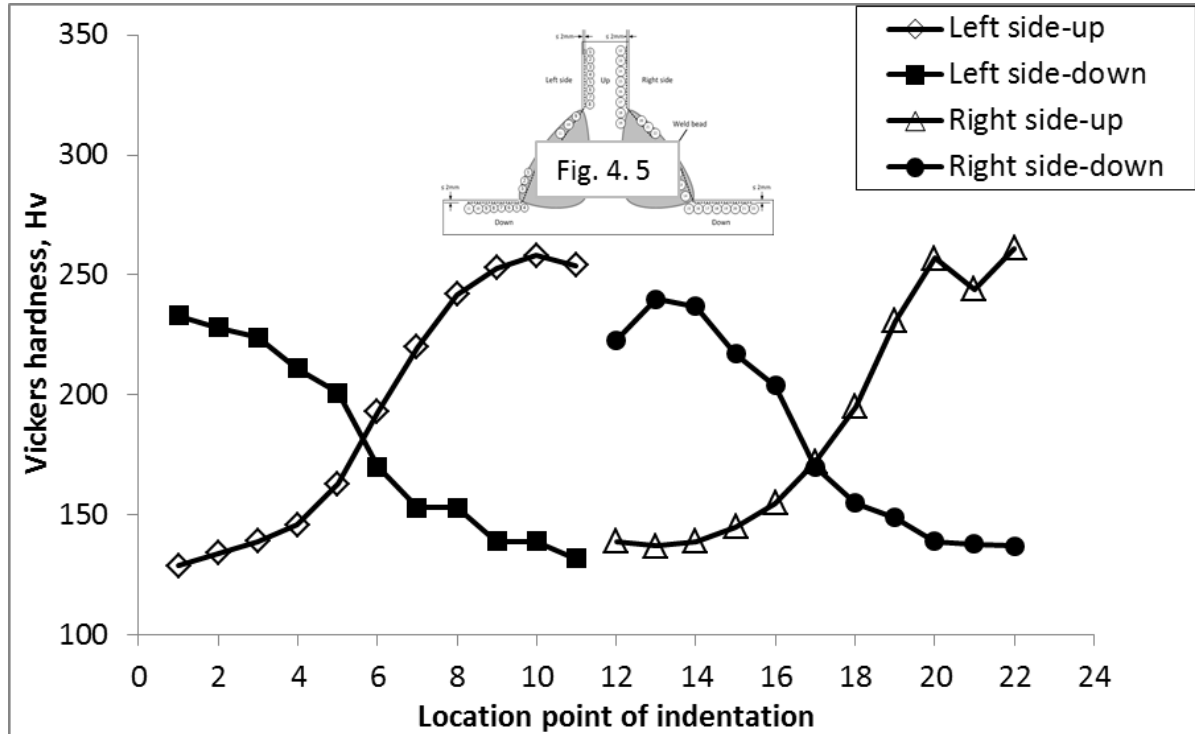
Fig. 4.14 Vickers hardness profile of welded specimen of mild steel with zero gaps
(indentation load: 10 kgf)
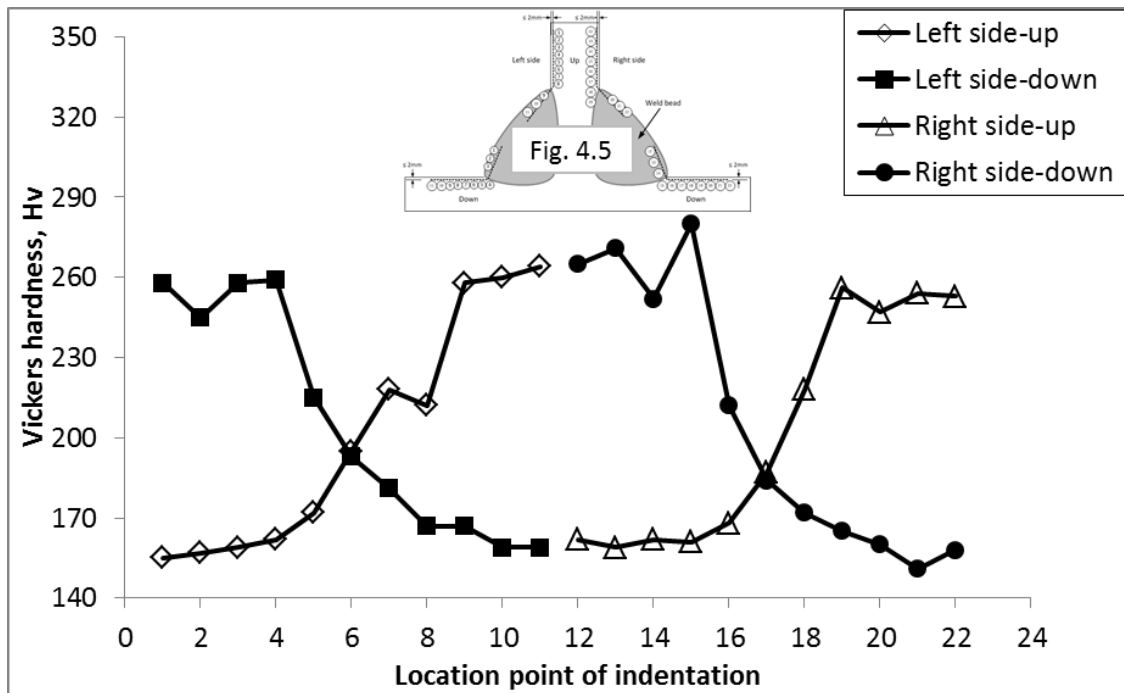
Fig. 4.15 Vickers hardness profile of welded specimen of high tensile steel with zero gaps
(indentation load: 10 kgf)
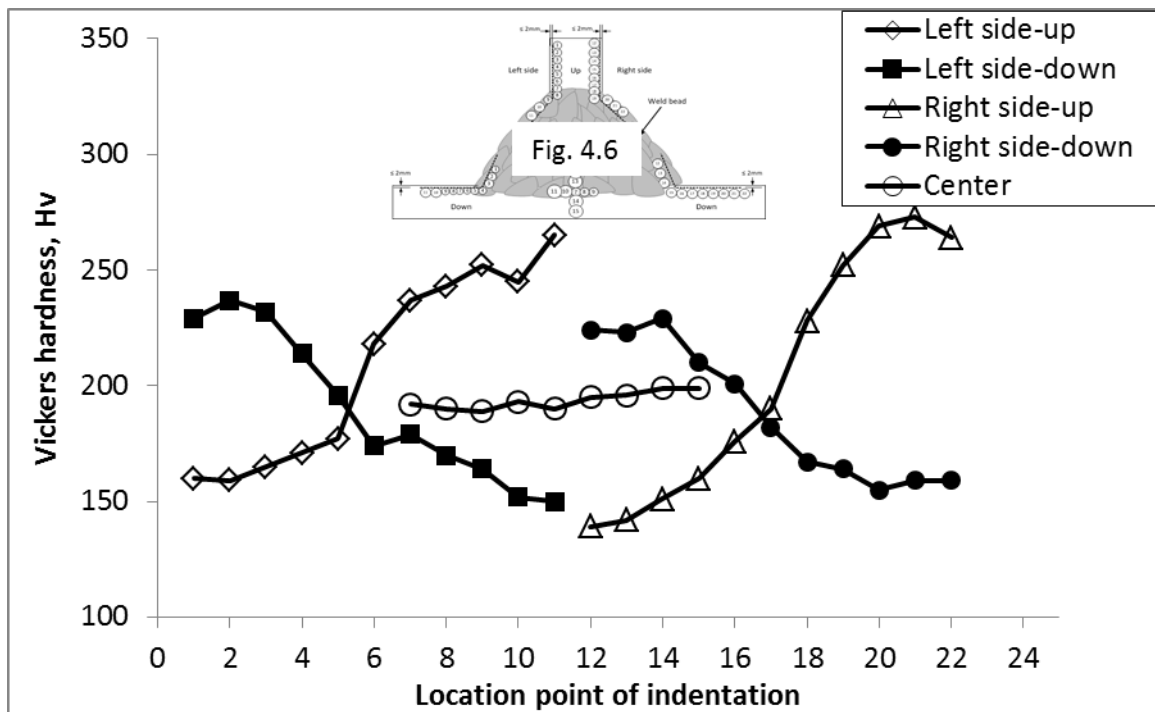
Fig. 4.16 Vickers hardness profile of welded specimen of mild steel with 20mm gaps
(indentation load: 10 kgf)
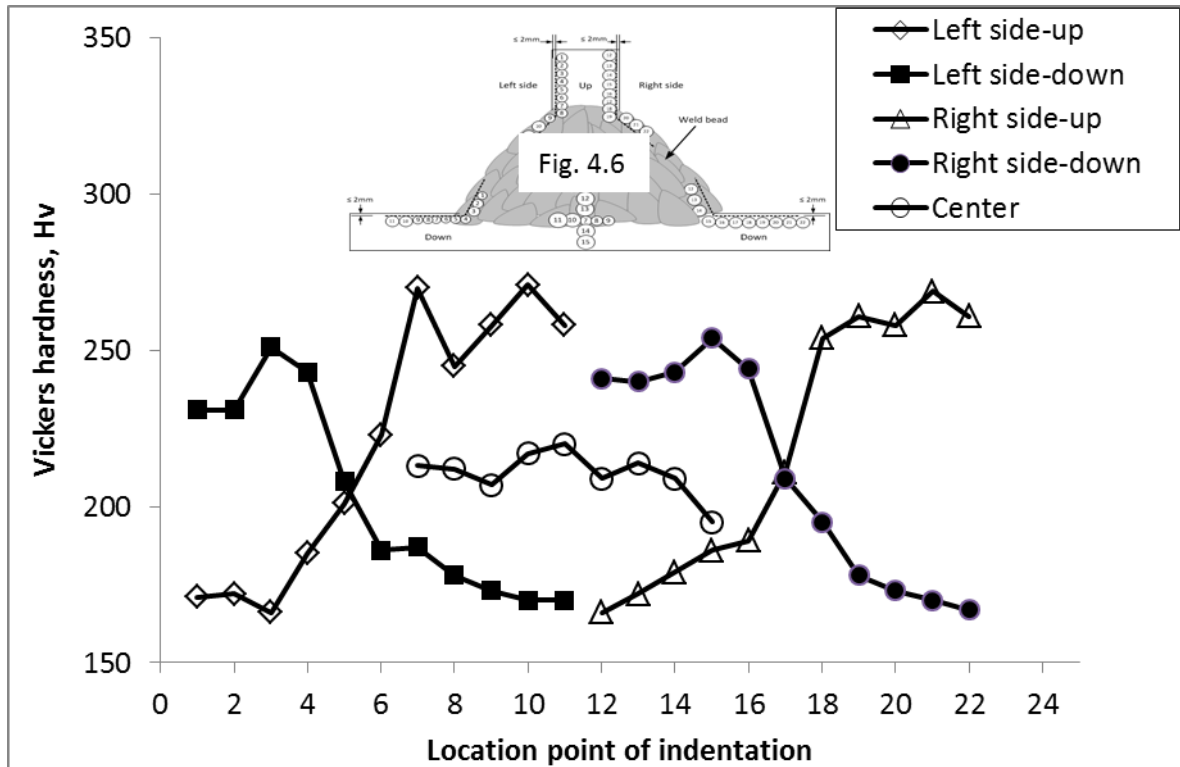
Fig. 4.17 Vickers hardness profile of welded specimen of high tensile steel with 20 mm gaps (indentation load: 10 kgf)
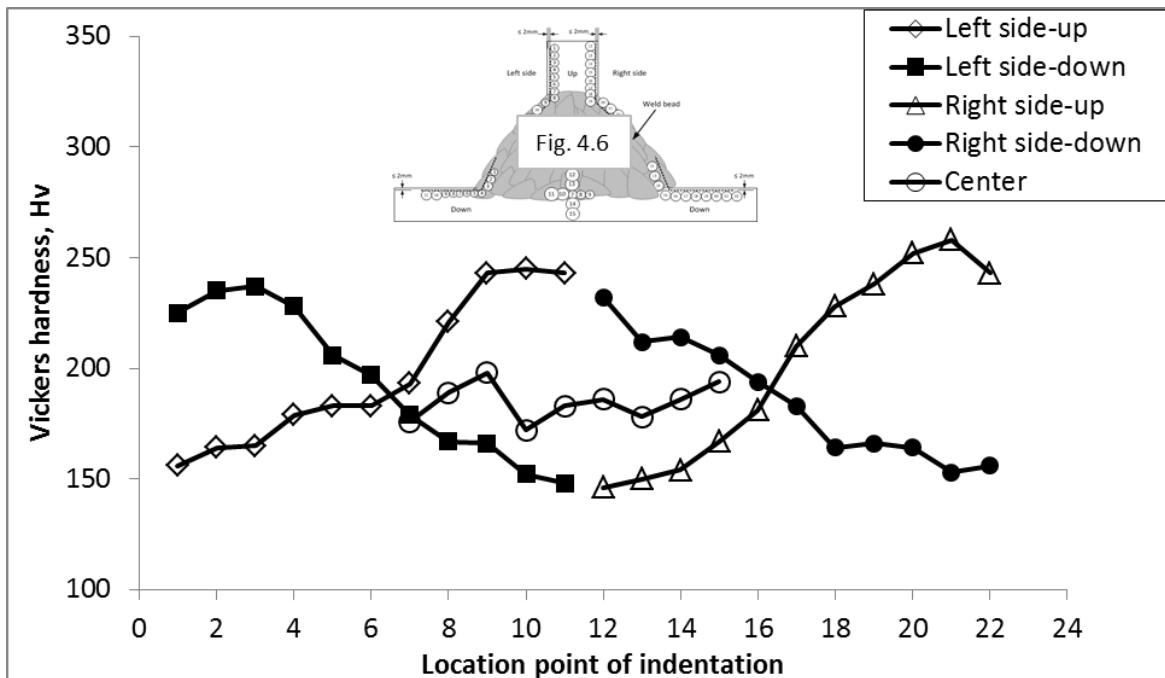
Fig. 4.18 Vickers hardness profile of welded specimen of mild steel with 25 mm gaps (indentation load: 10 kgf)

89
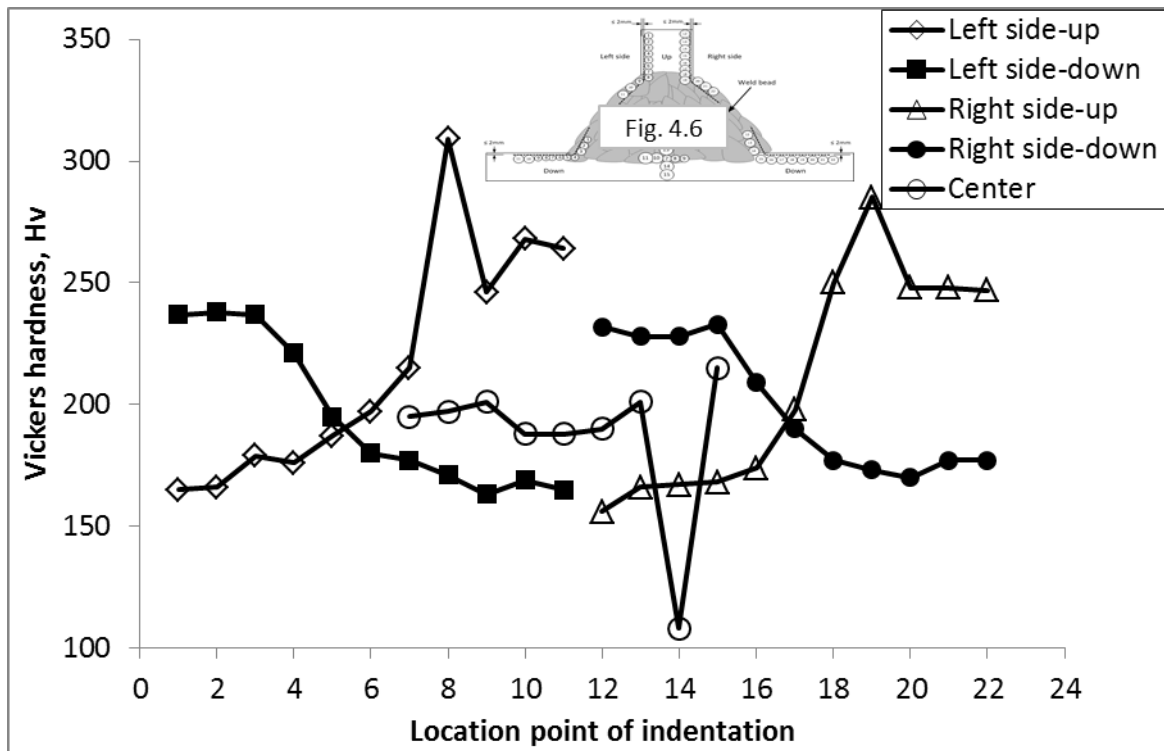
Fig. 4.19Vickers hardness profile of welded specimen of high tensile steel with 25 mm gaps (indentation load: 10 kgf)
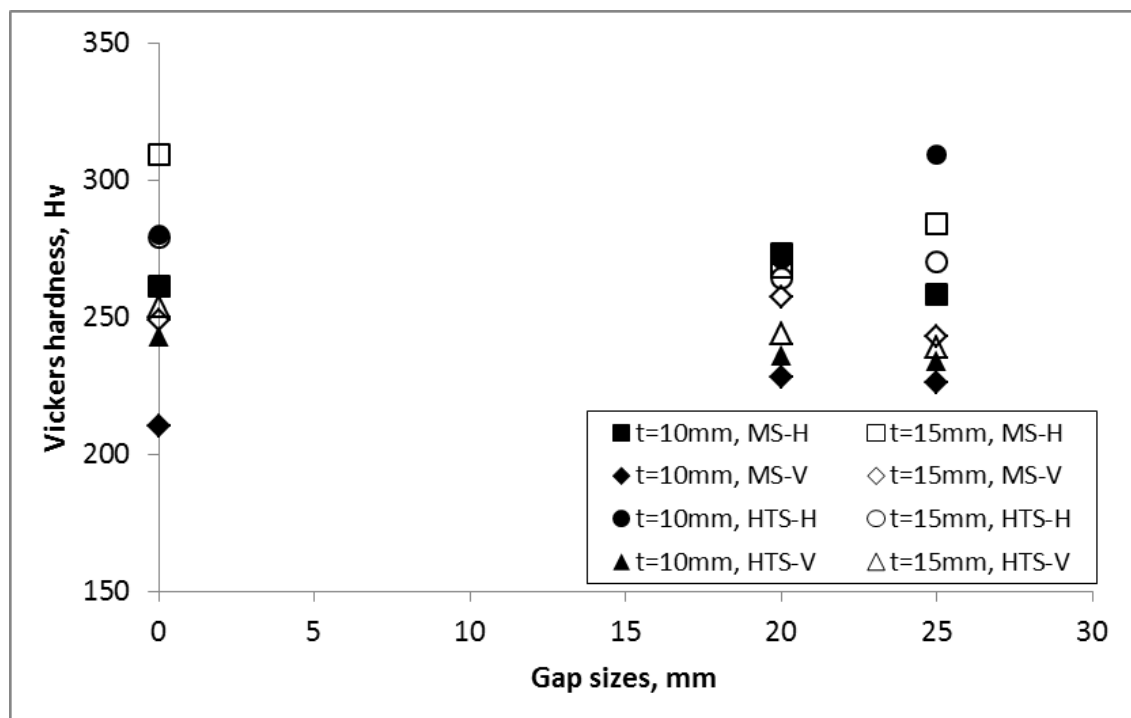
Fig. 4.20 Maximum hardness profile for all specimens (indentation load: 10 kgf)

Fig. 4.21 presents the breaking stress for tensile test. The breaking part takes place at the base metal as can be referred in Fig. 4.8. The nominal breaking stress was calculated based on the initial cross sectional area before the welded specimen breaks. The figure shows that the welded specimens with high tensile steel material give higher load compared to mild steel. However, there is no significant effect of different welding positions and gaps. The results also indicate higher strength takes place at the positions of the weld toe and the weld metal compared to the base metal.
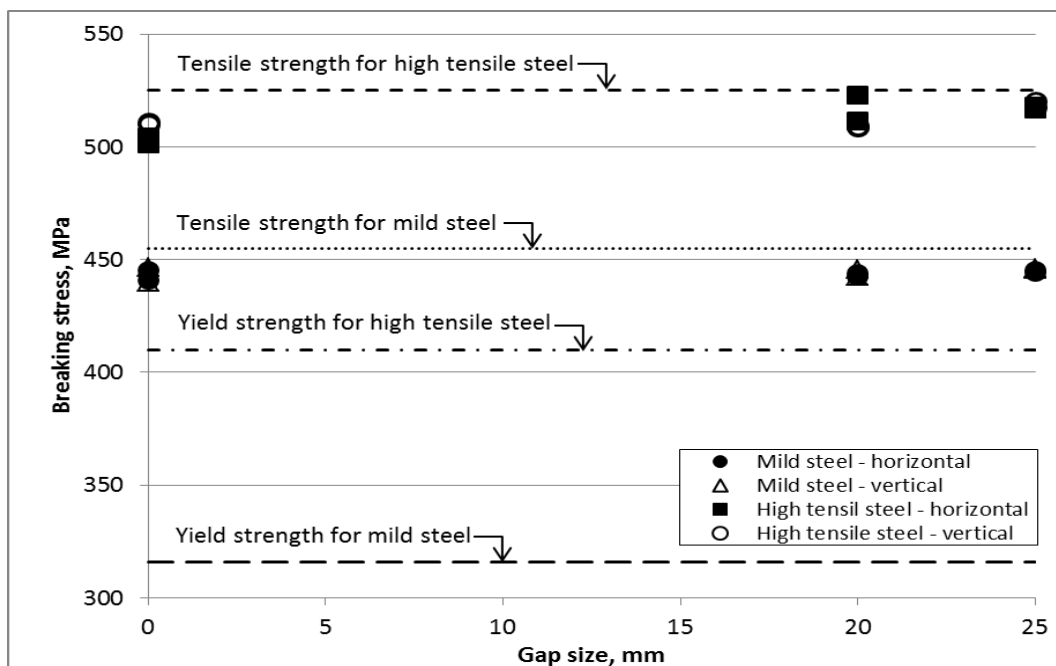
Fig. 4.21 Breaking stress of welded specimen

4.3.2 Bending test

Fig. 4.22 presents welded area of specimens after bending test. Magnetic particle inspection was used in order to detect any cracks or defect at the weld toe location. Based on visual observation, there are no defects or any cracks found on the welded specimen of 10 and 15 mm thickness.

(a) $\Theta = 45^o$, gap = 0 mm	(b) $\Theta = 60^o$, gap = 0 mm	(c) $\Theta = 90^o$, gap=0 mm
(d) $\Theta = 45^o$, gap = 20 mm	(e) $\Theta = 60^o$, gap =20 mm	(f) $\Theta = 90^o$, gap =20 mm
(f) $\Theta = 45^o$, gap = 25 mm	(g) $\Theta = 60^o$, gap = 225m	(h) $\Theta = 90^o$, gap=25 mm
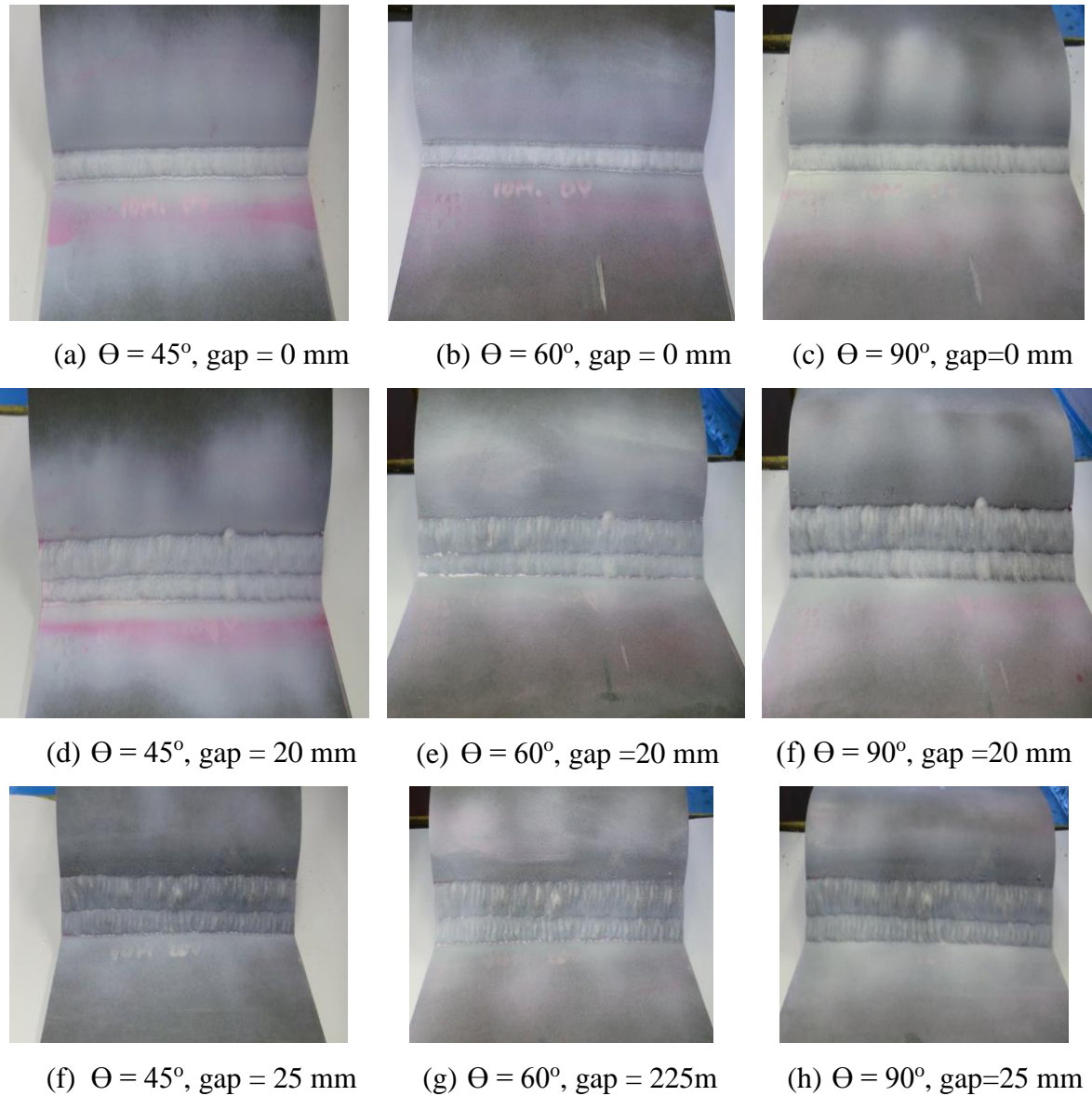
Fig. 4.22 Weld toe condition after bending test for 10 mm thickness

4.3.3 Macro observation test

As mentioned in ClassNK (2012), the macro observation is done by etching the weld face in order to confirm the quality of welded joints. Any defect like pore, inclusion and lack of fusion will be revealed during the observation. Based on the observation (Figs. 4.23 and 4.24), there are no clearly defects found on welded surface. Therefore, all welded specimens show good welding quality which will not affect the fatigue test results.
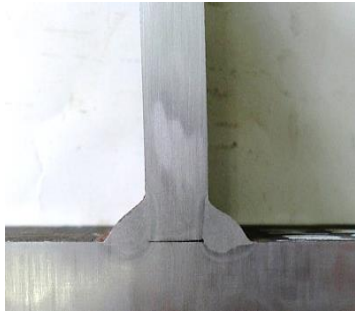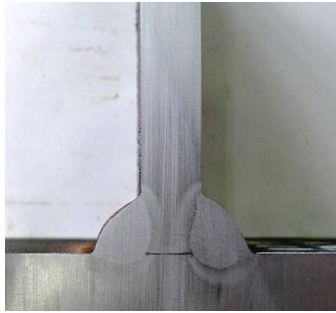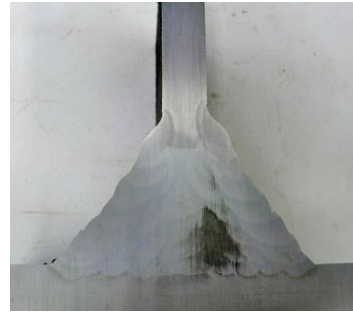
(a) 10 mm-H   (b) 10 mm-V   (c) 20 mm-H

(d) 20 mm-V   (e) 25 mm-H   (f) 25 mm-V

Fig. 4.23 Weld face of mild steel with different gaps for 10 mm thickness
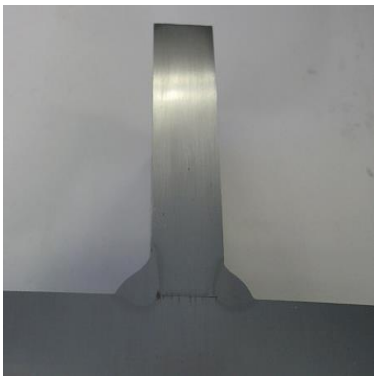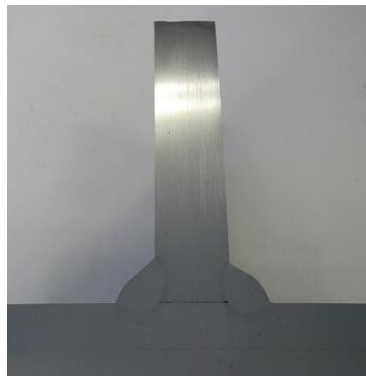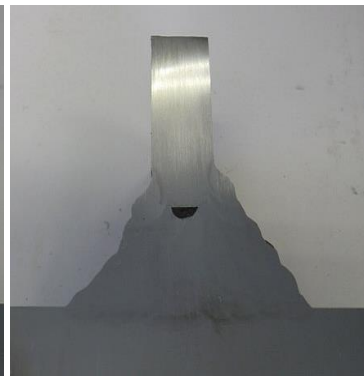
(a) 10 mm-H   (b) 10 mm-V   (c) 20 mm-H
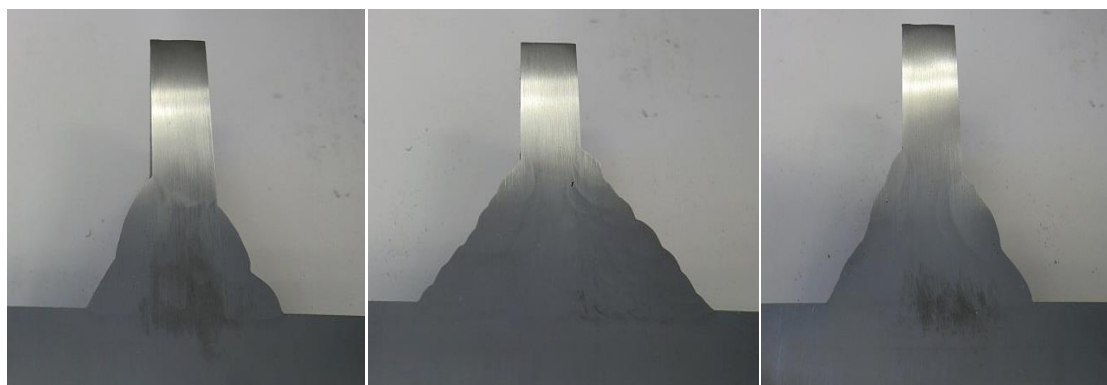
(c) 20 mm-H   (d) 25 mm-V   (e) 25 mm-H

Fig. 4.24 Weld face of mild steel with different gaps for 15 mm thickness

4.3.4 Fatigue test

S-N curve based on the nominal stress

The nominal stress range is used as a testing procedure in order to plot the S-N curve. As can be seen in Fig. 4.25, the specimen was broken with the cracks propagate up to 80% of the plate thickness. The fatigue test result is obtained from 4 specimens of each individual geometrical parameter. The study has been done in laboratory scale in order to confirm the fatigue performance of large gap size on non-load-carrying fillet welded joint even though based on the requirements of ISO/TR 14345 (2012) which need at least 8 to 10 specimens with 2 or more specimens per stress range to construct the fatigue line. Fig. 4.26 shows examples of the fracture surface resulted from fatigue test. Crack initiation for all of the specimens start from the weld toe as can be seen in the figure.
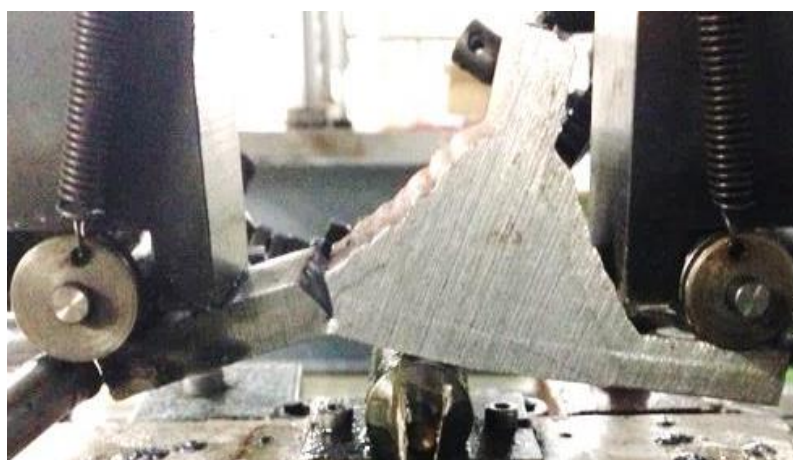
Fig. 4.25 Definitions of failure criterion

Figs. 4.27 and 4.28 show the experimental results for all welded specimens with 10 mm and 15 mm thickness respectively. Detail of the results can be seen at Appendix A. The fatigue class design curve in this that represents the upper boundary is IIW-FAT100 and the bottom boundary is IIW-FAT80 based on the recommendation of IIW. Here, all welded specimens illustrate higher fatigue performance by comparing to both design curves.
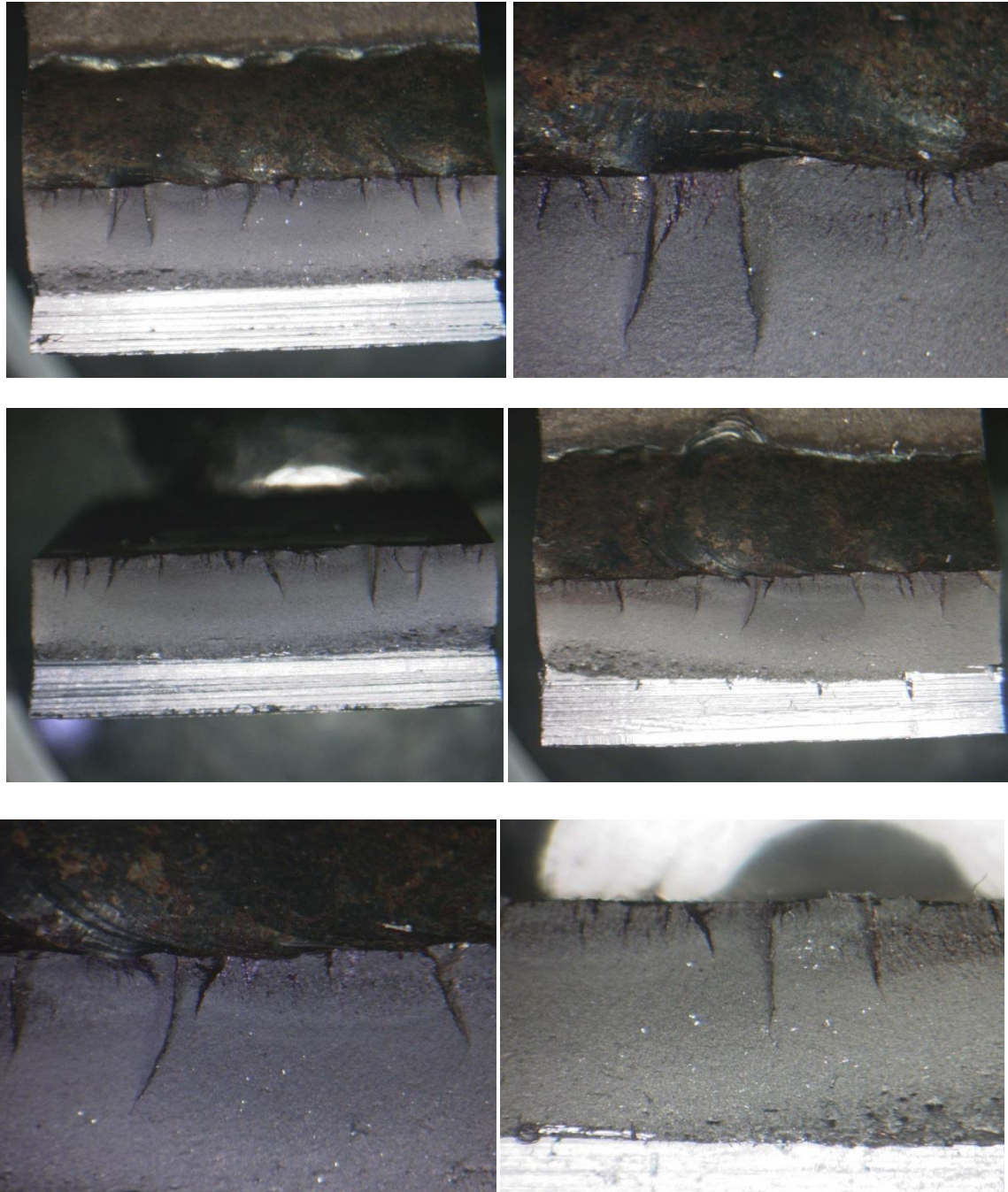
Fig. 4.26 Examples of fracture surface from 10 mm plate thickness with zero gap
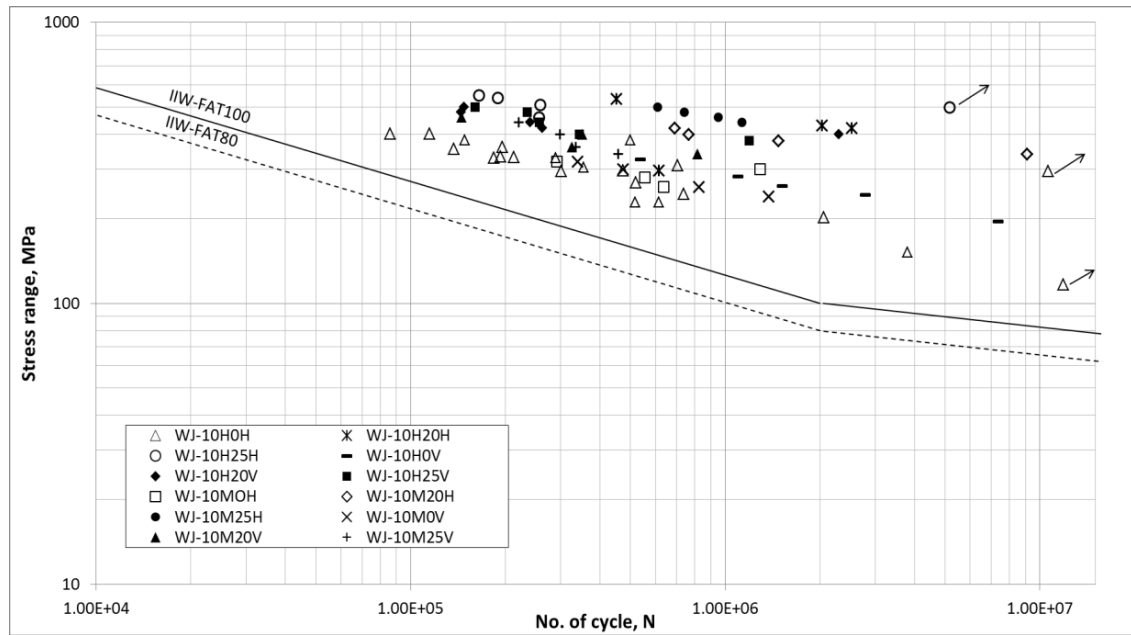
Fig. 4.27 S-N curve for all specimens of 10 mm thickness
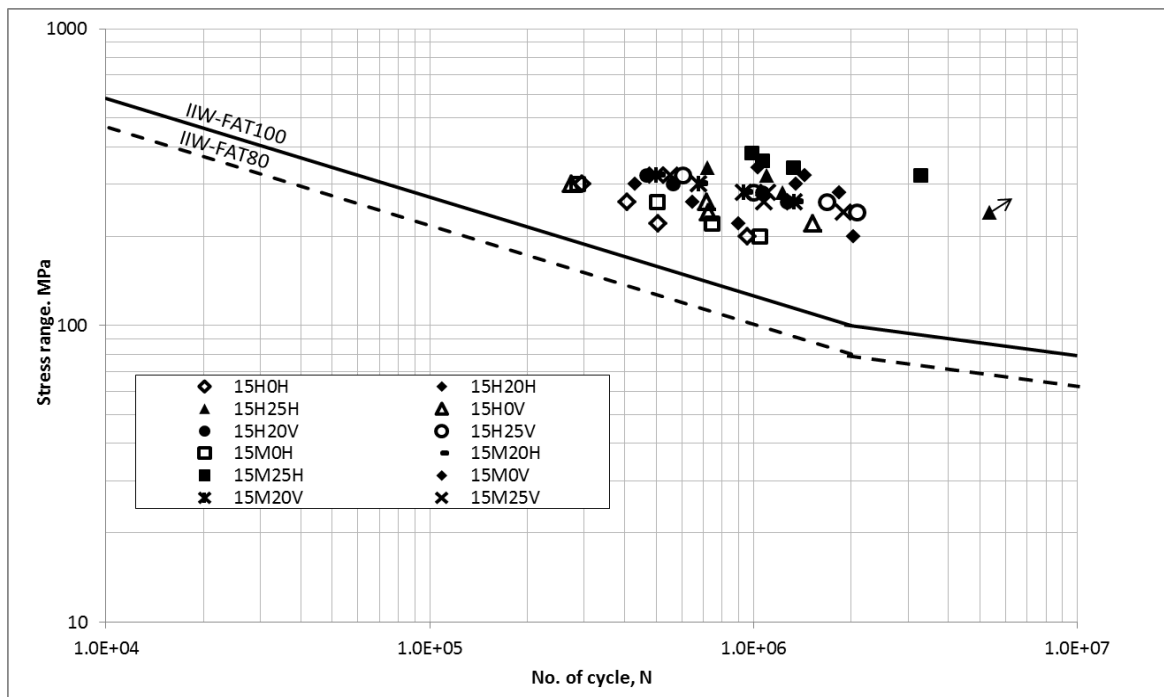
Fig. 4.28 S-N curve for all specimens of 15 mm thickness

4.3.5 Effect of welded specimen geometry

Figs. 4.29, 4.30 and 4.31 present the comparison between the welded joint specimen with zero gap and with a gap of 20 mm and 25 mm. Here, the figure clearly shows welded joint specimens with gap illustrates the higher fatigue performance compared to zero gap specimens. Based on least square fitting method, specimen with 25 mm gap shows little higher fatigue life compare to 20 mm gap. Figs. 4.32 to 4.34 show the comparison of welded joint specimen with different welding positions. Based on the average line drawn in the figure, the results indicate that there are no significant differences between both welding positions for plate thickness of 10 mm and 15 mm which contribute to the fatigue performance. However, there is a significant contribution to the fatigue performance of plate thickness of 20 mm for horizontal and vertical welding position. Following in Fig. 4.35, specimen with plate thickness of 10 mm shows higher performance compared to 15 mm and 20 mm. The effect of plate thickness was studied by Nguyen and Wahab (1995) where fatigue performance increased with the decrement of the plate thickness.
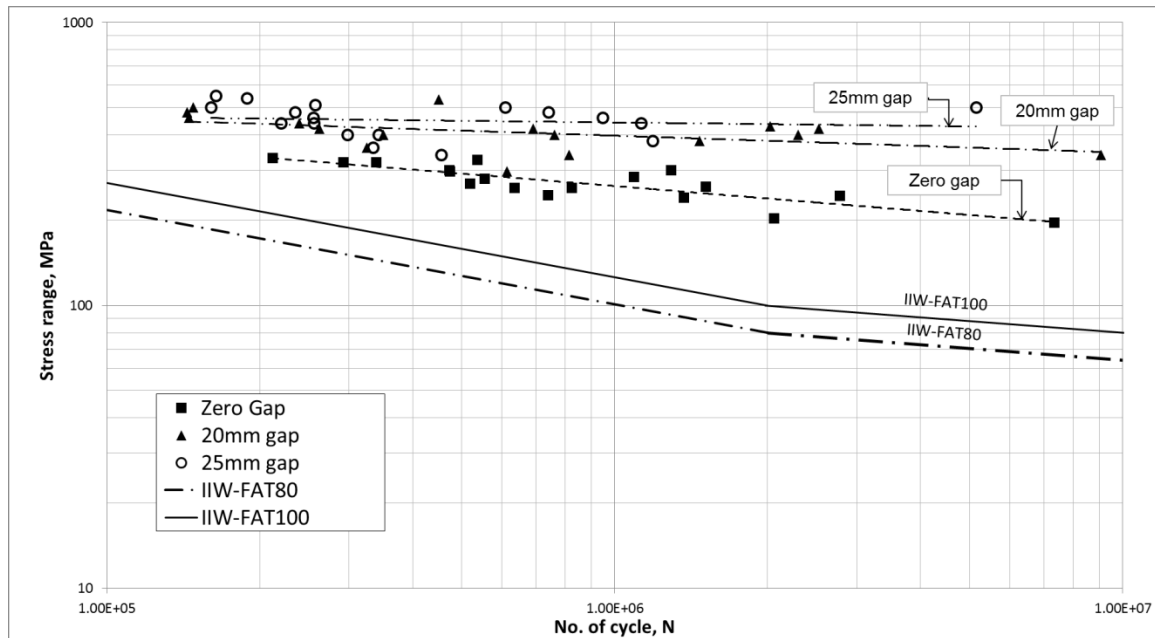
Fig. 4.29 Comparison of S-N curve between welded joint specimen with zero gap, 20 mm and 25 mm gap for plate thickness of 10 mm
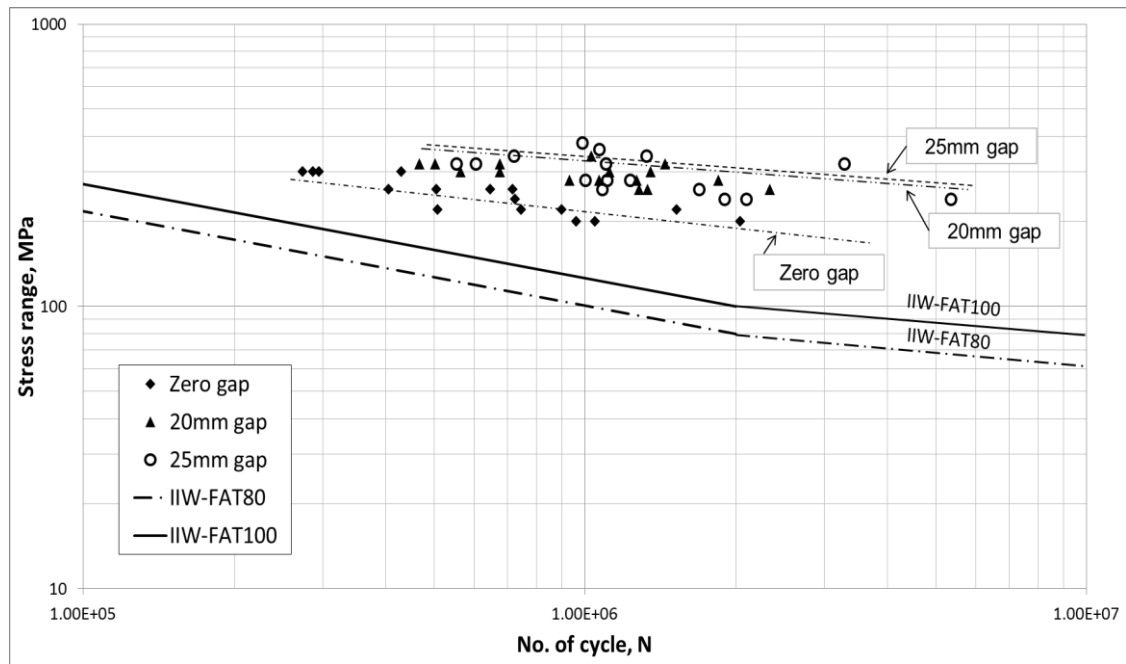
Fig. 4.30 Comparison of S-N curve between welded joint specimen with zero gap, 20 mm and 25 mm gap for plate thickness of 15 mm
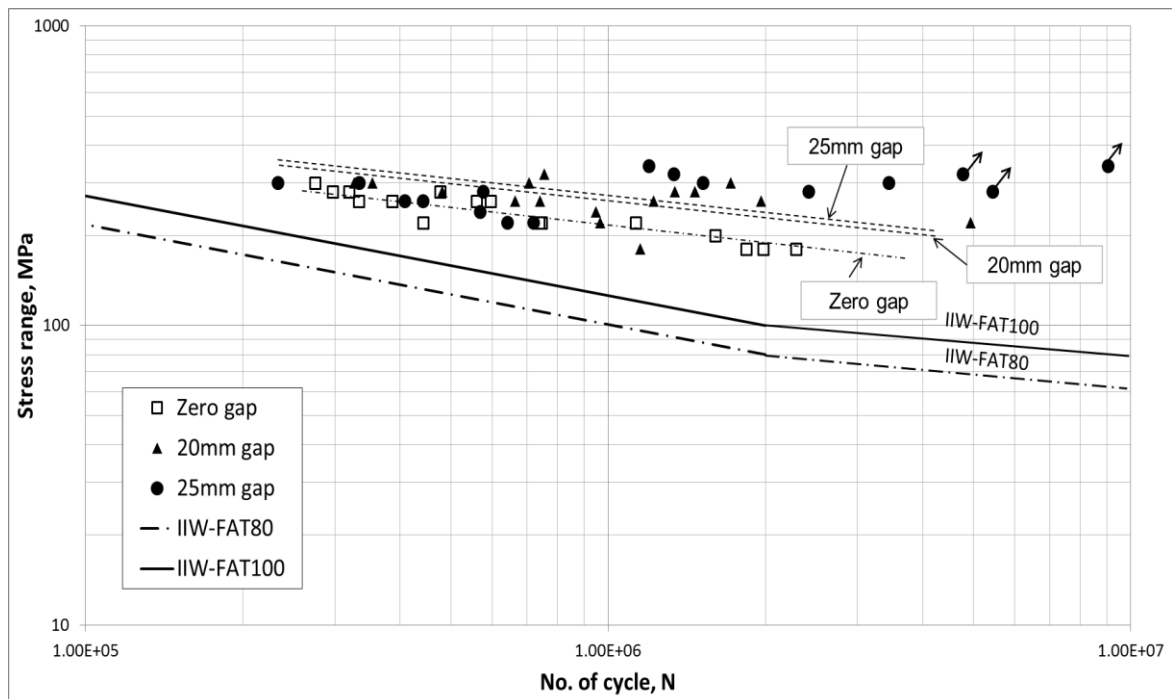
Fig. 4.31 Comparison of S-N curve between welded joint specimen with zero gap, 20 mm and 25 mm gap for plate thickness of 20 mm
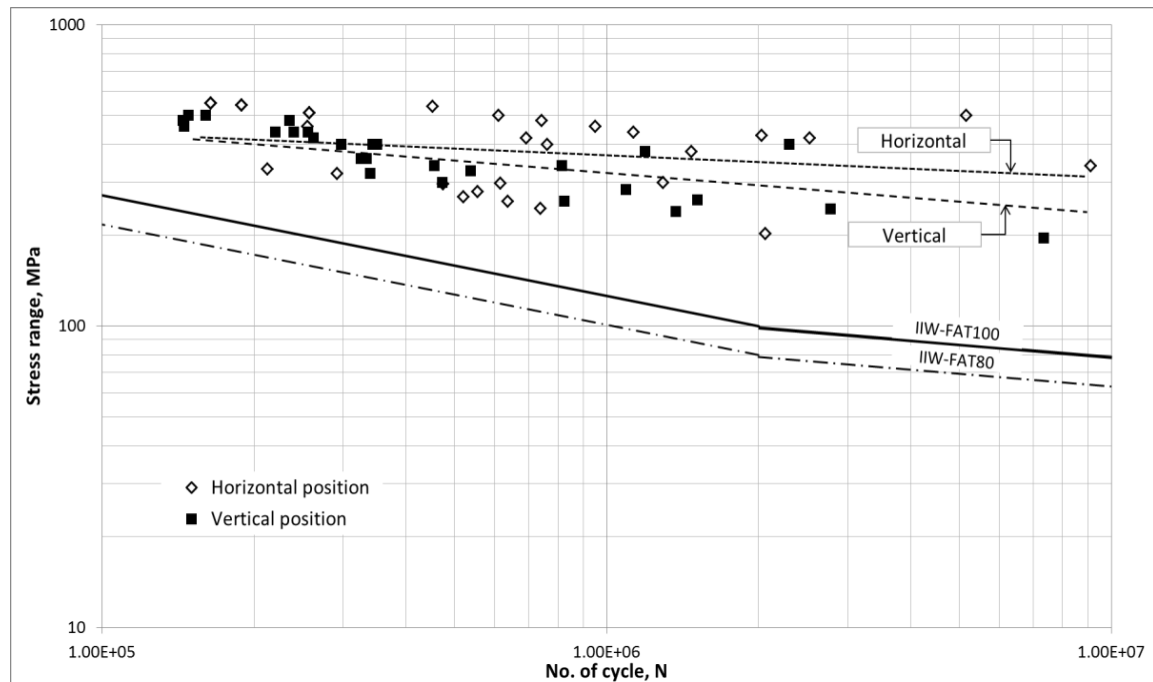
Fig. 4.32 Comparison of S-N curve for horizontal and vertical welding position for 10 mm
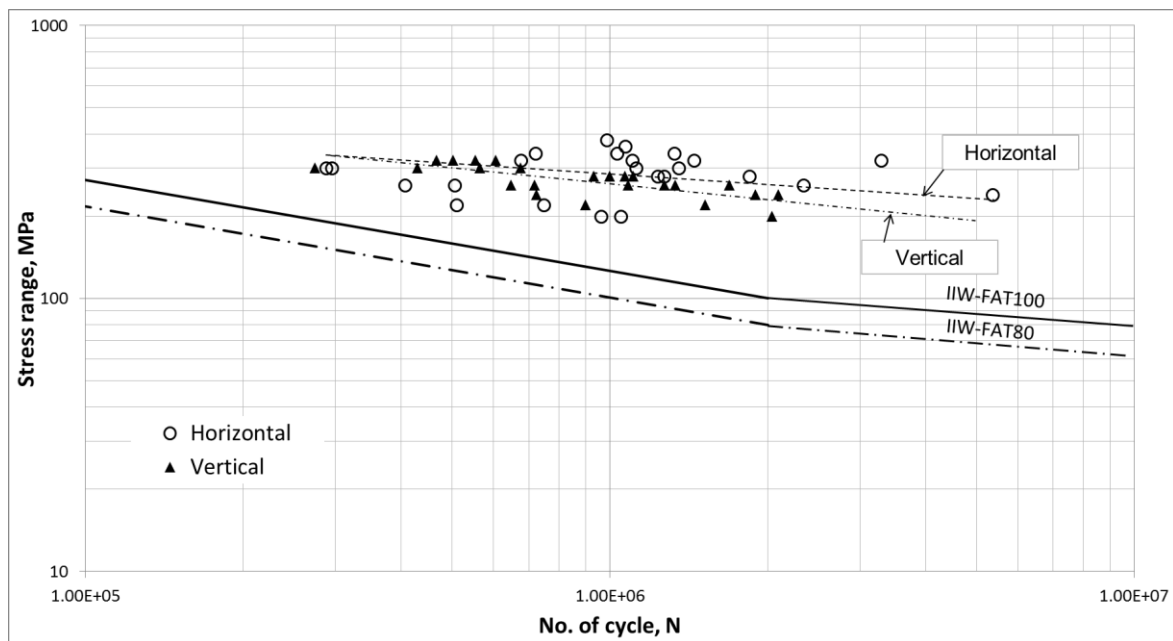
Fig. 4.33 Comparison of S-N curve for horizontal and vertical welding position for 15 mm
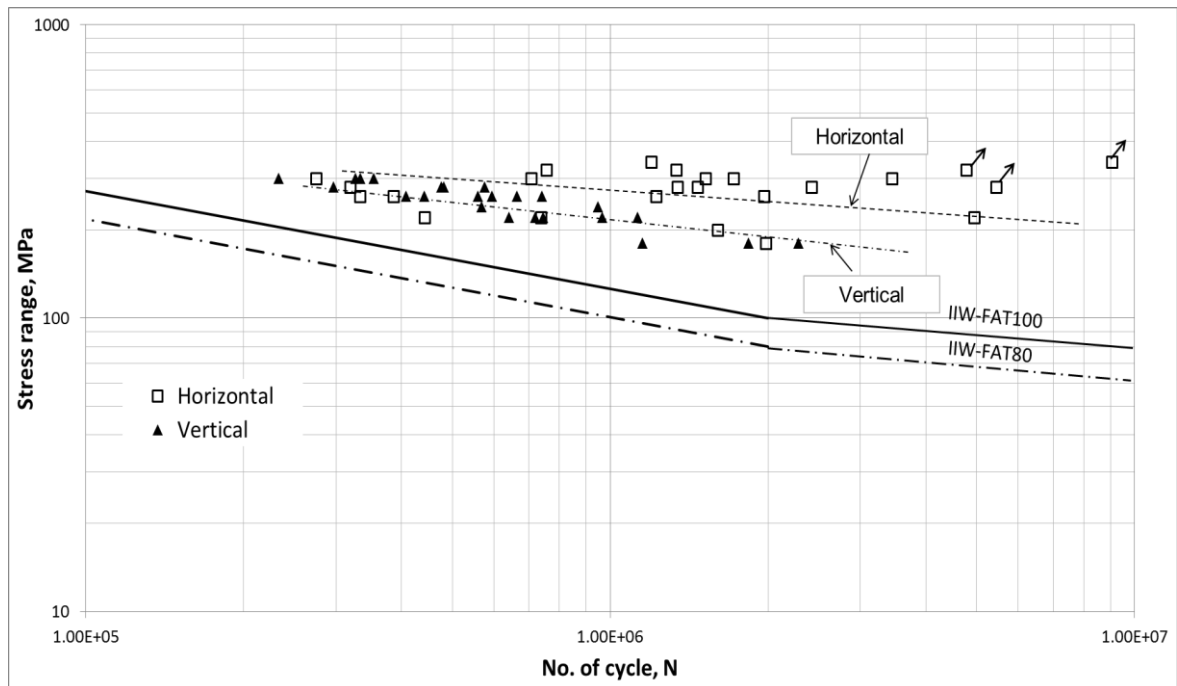
Fig. 4.34 Comparison of S-N curve for horizontal and vertical welding position for 20 mm
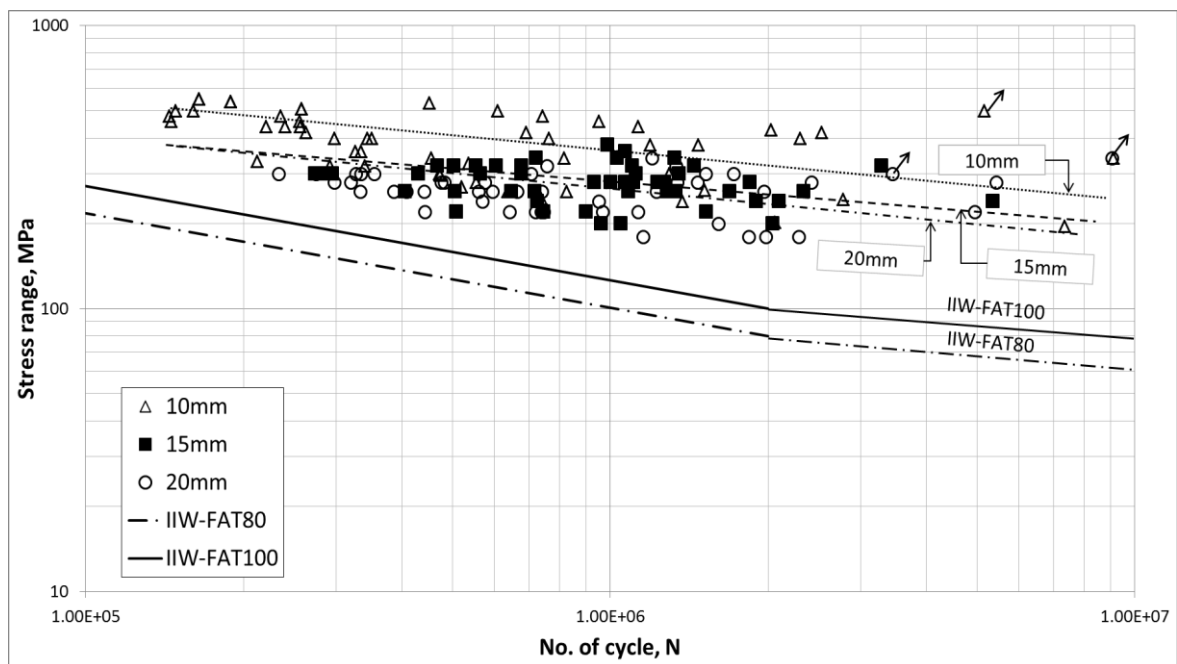
Fig. 4.35 S-N curves at different plate thickness

Fig. 4.36 presents S-N curve based on the hot spot stress. Design curves of UK-HSE were introduced since the stress range for the design curve is defined by the hot spot stress. Here, UK-HSE Curve C is categorized for fillet welded joint classification. In addition, UK-HSE Curve D is normally used as a reference design curve for ship hull structures. Based on both design curves, the fatigue strength of all welded specimens presents a good performance.
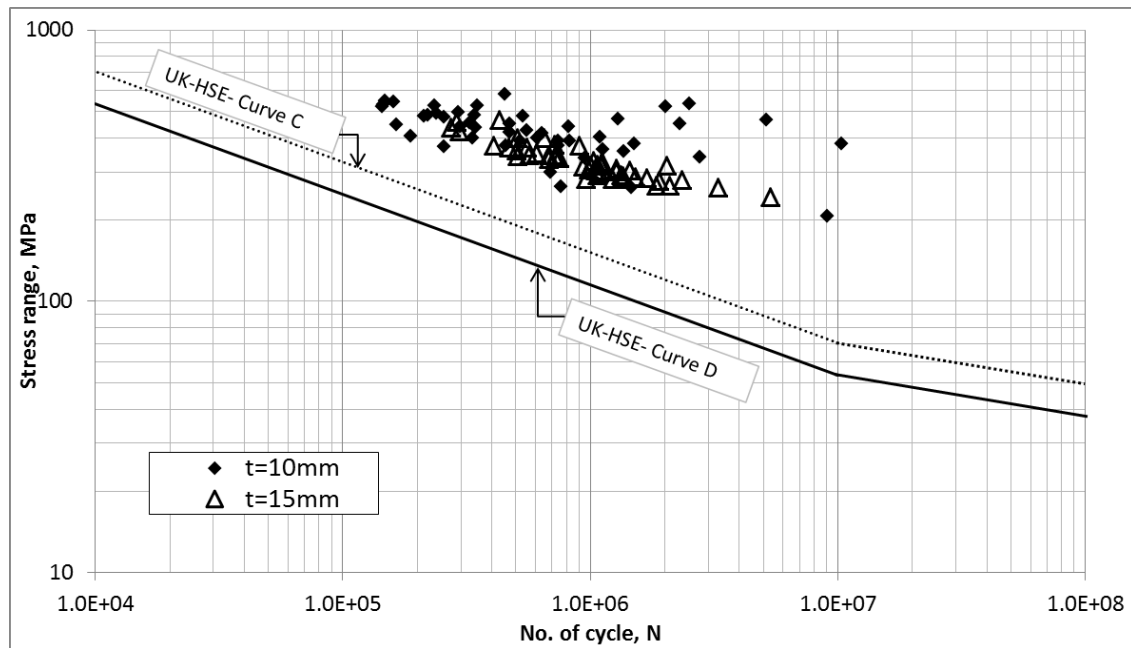
Fig. 4.36 S-N curve based on hot spot stress

The study gives an overview about the effect of gap in non-load-carrying fillet welded joint. In industrial practice, most of engineers prefer the welded joint with no gap. However, based on the studies, welded joint with a certain gap shows higher fatigue performance. The experimental results might contribute to the improvement of the structural integrity of large welded structures. Furthermore, study by Miki et. al. (1993) has achieved similar results. However, the experimental result is not universal for all applications since the skill of welders may contribute to the quality of welded joints. In this case, a high skill welder was performed the welding works. In addition, the most important factor which affects the fatigue performance of welded joint as reported by many researchers as mention in Chapter 2 such as toe radius, flank angle, defect and surface finish at the weld toe was found not significant in this study. This is because all

geometrical parameters are not maintained in single stress range to evaluate the geometrical parameter. Besides, more specimens are needed in order to conduct such experimental work.

4.4 Conclusion

Non-load-carrying tee fillet welded joint with various gaps, welding positions and materials are applied in this study. The study achieved the objective where non-load-carrying fillet welded joint with gap shows higher fatigue performance compared to zero gaps. In addition, all semi-automatic CO_2 welded specimens presents higher performance in accordance to fatigue class design (FAT) as mentioned in the IIW document and UK-HSE. In this case, suitable parameter should be proposed in order to improve the quality standards such as JSQS and IACS. In addition, several conclusions can be drawn as follows:

a) Plate thickness of 10 mm presents higher fatigue performance compared to 15 mm and 20mm.

b) There is no significant effect of fatigue performance for horizontal and vertical positions of a welded joint for plate thickness of 10 mm and 15 mm. However, horizontal welding position illustrates the higher fatigue performance for plate thickness of 20 mm.

c) Fatigue performance of 20 mm gap size has little significant difference compared to 25 mm for 10 mm plate thickness. However, no significant difference found in 15 mm and 20 mm plate thickness.

d) The S-N curves which are plot based on hot spot approach shows better performance compared to UK-HSE basic design curve.

e) The strength of weld metal may contribute to the structural integrity of the non-load-carrying welded joint with large gap size.

CHAPTER 5

CHAPTER 5

Conclusion

As mention earlier in Chapter 2, the objective of the thesis is to suggest for the improvement of the hull construction quality standards. Some allowable limit needs to be revised for the consistency with the industrial needs and rapid growth in design technology as well as a safety concern to put into consideration. Besides, it will be beneficial to the industry player in getting better cost with optimum safety and integrity of the build structure. Moreover, specialist worker such as design engineer and inspector will be more realistic in performing their job. Overall study will give an overview to readers on the importance of code and standards with periodically reviewed. In current modern situation, many inventors and invention has been published to enhance the customer need without jeopardized the safety issue.

5.1 Numerical study on butt welded joint with undercut

Numerical studies had been done in order to verify the influence of geometrical parameter to the fatigue performance of the butt welded joint with undercut defect. Furthermore, the study was extended to confirm the effect of undercut shape which contributes to the structural performance. Below are the conclusions of the numerical studies:

a) Studies are done to investigate the effect of geometrical parameter over stress concentration factor. The study shows a significant effect of undercut depth (d) and weld bead height (h) over plate thickness (t). Therefore, non-dimensional parameters such as undercut and weld bead height over plate thickness ratio (d/t) and (h/t) was introduced in this study. In addition, the study found stress concentration factor increase by increments of plate thicknesses.

b) Practical formula is established for the purpose as a tool for evaluation of structural welded defect with the crack-like undercut type. In addition, allowable limit of strength and other member based on JSQS and IACS Rec. 47 is available as references in terms of stress concentration factor. This will be valuable, especially for inspection engineers to decide the next action of structural maintenance.

c) The study found V-notch undercut type gives higher fatigue life compare to U-notch undercut type of constraint on the same shape ratio, *b/d*. This will be a more practical approach for inspection engineer in considering width, *b* and depth, *d* of undercut rather the shape itself.

d) The studies highlighted stress gradient, *χ* is the important criteria in assessing fatigue strength of the butt welded structure.

e) Weld bead height or reinforcement gives influence in increasing stress concentration factor (SCF).

5.2 Experimental work on structural integrity of non-load-carrying fillet welded joint with large gap size

Experimental work was conducted to confirm the structural performance of fillet welded joint with large gaps.

f) Plate thickness of 10 mm presents higher fatigue performance compared to 15 mm and 20 mm.

g) There is no significant effect of fatigue performance for horizontal and vertical positions of a welded joint for plate thickness of 10 mm and 15 mm. However, horizontal welding position illustrates the higher fatigue performance for plate thickness of 20 mm.

h) Fatigue performance of 20 mm gap size has little significant difference compared to 25 mm for 10 mm plate thickness. However, no significant difference found in 15 mm and 20 mm plate thickness.

i) The S-N curves which are plot based on hot spot approach shows better performance compared to UK-HSE basic design curve.

j) The yield strength of weld metal which is higher than based metal may contribute to the structural integrity of the non-load-carrying welded joint with large gap sizes.

k) A skill welder worker is a significant factor in contributing to the structural performance of welded joint with large gap sizes.

5.3 Recommendation for the future work

a) Numerical work can be extended to validate the experimental results of non-load-carrying fillet welded joint with large gap sizes.

b) Established practical formula for SCF should validate with other type of model.

c) The tensile fatigue test should be conducted to the welded specimen with large gap size to validate the experimental results by 3 point bending type test.

d) Hot spot stress can be measured with strain gauge located on welded specimen to validate the FEA extrapolation work.

REFERENCES

Almar-Naess, A. (1985), *Fatigue Handbook – Offshore steel structure*, Norway: Tapir Publisher.

AWS D1.1/D1.1M:2006, *Structural welding code – steel*, American welding society.

Bell R., Vosikovsky O. and Bain S.A (1989), The significance of weld toe undercuts in the fatigue of steel plate T-joints, *International Journal of Fatigue* 11 No. 1, pp 3-11.

BS EN 1011-2:2001, *Welding. Recommendations for welding of metallic materials. Arc welding of ferritic steels.*

BS EN 1993-1-1:2005, *Eurocode 3: Design of steel structures – Part 1-9, Fatigue.*

ClassNK (2013) *Rules for survey and construction of steel ships*, Part M – Welding.

Dugdale D.S (1960), Yielding of steel sheets containing slits, *Journal of Mechanics and Physics of Solids*, Vol. 8, Issue 2, pp 100-104.

Elber W. (1971), The significance of fatigue crack closure. Damage Tolerance in Aircraft Structures, *ASTM STP* 486: 230-242.

Ferreira J.A.M and Branco C.A.M (1989), Influence of the radius curvature at the weld toe in the fatigue strength of fillet welded joints, *International Journal of Fatigue* 11 No. 1, pp 29-36.

Fillippini M. (2000), Stress gradients calculations at notches, *International Journal of Fatigue* 22, 397-409

Fricke W. (2003), Fatigue analysis of welded joints: state of development, *Marine Structures* 16, pp 185-200.

Gotoh K. and Harada K. (2010), Numerical Simulation of fatigue crack growth based on strip yield model considering work hardening of materials, *Proceedings of OMAE* 2010, 20726.

Gurnet, T.R (1979), *Fatigue of welded structures*, Cambridge: Cambridge University Press.

Hobbacher A. (2006), Problem of effect of weld imperfections on fatigue and their consideration in design codes, *Steel structures* 6, 289-298

Huang H. (2008), Influence of mesh type and size on crack growth modeling, *Journal of Pressure Equipment and System*, 88-91.

IACS No. 47 – Rev. 5 (2010), *Shipbuilding repair quality standard*, International Association of Classification Societies.

IACS Rec. 56 (1999) *Fatigue assessment of ship structures.*

IIW document, IIW-1823-07 ex XIII-2121r4-07/XV-1254r4-07 (2008), *Recommendations for fatigue design of welded joints and components*, International Institute of Welding.

ISO 5817:2003, *Welding – fusion welded joints in steel, nickel, titanium and their alloys (beam welding excluded) – Quality levels for imperfections*

ISO/TR 14345: 2012 , *Fatigue – fatigue testing of welded components - Guidance*

Jang C.D and Hong S.Y (2009), *Proceedings of the 17th International Ship and Offshore Structures Congress*, Volume 3, Seoul National University.

JSME Standard 002 (1984) -*Standard Method of Statistical Fatigue Testing*.

JSQS (2010), *Japan Shipbuilding and Quality Standard – Hull Part*, Japan Society of Naval Architects and Ocean Engineers.

JSSC (1995)- *Fatigue design recommendation for steel structures*, Japan Society of Steel Corporation.

Kainuma S. and Mori T. (2006), A fatigue strength evaluation method for non-load carrying fillet welded cruciform joints, *Int. Journal of Fatigue* 28, pp 864-872.

Kihl D.P and Sarkani S. (1997), Thickness effects on the fatigue strength of welded steel cruciform, *Int. Journal of Fatigue* Vol 19, Supp. No. 1, pp 311-316.

Kim M.H, Kim S.M, Kim Y.N., Kim S.G, Lee K.E. and Kim G.R (2009), A comparative study for the fatigue assessment of a ship structure by use of hot spot stress and structural stress approaches, *Ocean Engineering* 36, pp 1067-1072.

Lee C.H, Chang K.H, Jang G.C and Lee C.Y (2009), Effect of weld geometry on the fatigue life of non-load-carrying fillet welded cruciform joints, *Engineering Failure Analysis* 16, pp 849-855.

Maddox S.J (2011), *Fatigue design rules for welded structures*, Fracture and fatigue of welded joints and structure – Chapter 7, Woodhead Publishing, UK, pp 168-206.

Mahmud S.M.I and Sumi Y. (2011), Thickness effect on fatigue strength of plates with semi-elliptical side notches and weld joints*, Journal of the Japan Society of Naval Architects and Ocean Engineers.*

Mashiri F.R, Zhao X.L and Grundy P. (2001), Effects of weld profile and undercut on fatigue crack propagation life of thin-walled cruciform joint, *Thin-Walled Structures* 39, pp 261-285.

McDonald K.A. (2011), *Fracture and fatigue of welded joints and structures*, Woodhead publishing in limited, Cambridge, UK.

Miki C., Tateishi K., Fan H. D. and Tanaka M. (1993), Fatigue strengths of fillet-welded joints containing root discontinuities, *Int. Journal of Fatigue* 15 no.2, pp 133-140.

Nguyen N.T and Wahab M.A (1996), The effect of undercut and residual stresses on fatigue behavior of misaligned butt joints, *Engineering Fracture Mechanics*, vol. 55, no. 3, pp 453-469.

Nguyen N.T, Wahab M.A, A Theoretical Study of The Effect of Weld Geometry Parameters on Fatigue Crack Propagation Life, *Engineering Fracture Mechanics* 1995;51(1):1–18.

Nykanen T., Marquis G.and Bjork T. (2007), Fatigue analysis of non-load-carrying fillet welded cruciform joints, *Engineering Fracture Mechanics* 74, pp 399-415.

Offshore technology report 2001/015, Steel, HSE, UK.

Okayasu M., Ohkura Y., Sakamoto T., Takeuchi S., Ohfuji H. and Shiraishi T. (2013), Mechanical properties of SPCC low carbon steel joints prepared by metal inert gas welding, *Material Science & Engineering* A 560, pp 643-652.

Onozuka M. and Sugiyama S. (1989), An Experimental Study on Plate Thickness Effect on Fatigue Strength, Proceedings of EVALMAT89, ISIJ, pp 55-62.

Pang H.L.J. (1993), *Analysis of weld toe profiles and weld toe cracks*, International Journal of Fatigue 15 No. 1, pp 31-36.

Paris P.C. and F. Erdogan (1963), A critical analysis of crack propagation laws, Journal of Basic Engineering, Transactions of the ASME, Series D 85, pp. 528–534.

Radaj D., Sonsino C.M and Fricke W. (2009), Recent developments in local concepts of fatigue assessment of welded joints, *International Journal of Fatigue* 31, pp 2-11.

Schijve J. (2009), *Fatigue of structures and materials*, Netherlands, Springer science+business.

Tchankov D. S., Ohta A., Suzuki N. and Maeda Y. (1999), Random loading life assessments for notched plates, *International Journal of Fatigue* 21, pp 941-946.

Technical Report ISO/TR 14345:2012, *Fatigue – Fatigue testing of welded components – guidance*, ISO and IIW.

Tokihiko K., Rinsei I. and Koichi Y. (2007), *Development of ultra-low spatter CO$_2$ gas shielded arc welding process "J-STAR® Welding*, JFE Technical Report no. 10, pp 50-53.

Toyosada M., Gotoh K. and. Niwa T. (2004), Fatigue crack propagation for a through thickness crack: a crack propagation law considering cyclic plasticity near the crack tip, *International Journal of Fatigue,* Vol. 26, Issue 9, pp 983-992.

Toyosada M., Gotoh K. and. Niwa T. (2004), Fatigue life assessment for welded structures without initial defects: an algorithm for predicting fatigue crack growth from a sound site, *International Journal of Fatigue,* Vol. 26, Issue 9, pp 993-1002.

Website: http://www.twi-global.com/ accessed on 2 Jun 2014.

Williams H.E., Ottsen H., Lawrence F.V. and Munse W.H. (1970), *The effect of weld geometry on the fatigue behavior of welded connections*, Interim Report on Phase 2.1, IHR-64, Behavior of Welded Highway Structures, Univ. of Illinois, USA.

Yamaguchi I., Terada Y. and Nitta A. (1964), On the fatigue strength of steels for ship structure, *Journal of The Society of Naval Architects of Japan.*

APPENDIX A

Experimental data

Specimen model		Stress range, Mpa	Load on fatigue machine	Date	Time	Temperature (ºC)	Humidity (%)	Fatigue life, N_f	Comment
10H0H	1	300	5.871	5/9	1427-1823	27.5	62	212309	
10H0H	2	260	5.174	5/9-6/9	1944-0430	28	63	473434	
10H0H	3	240	4.841	6/9-7/9	1452-0030	28	60	519916	
10H0H	4	220	4.441	9/9-10/9	1009-1251	28	60	738891	
10H0H	5	180	3.683	10/9-12/9	1002	29	59	2059173	
10H20H	1	300	7.577	18/10-20-10	1015-0910	22.5	56	2525132	
10H20H	2	260	7.787	20/20-22/10	1137-1307	24	66	2023918	
10H20H	3	320	9.499	22/10-23/10	2103-0524	24.5	70	451177	
10H20H	4	260	6.737	23/10-31/10	1738-1643	22.5	84	10318088	stop-not break
10H20H	5	340	8.378	31/10-1/11	1656-0420	24	52	615164	
10H25H	1	500	9.184	1/11-5/11	1116-1052	23	56	5158593	stop- no break
10H25H	2	550	10.280	5/11-5/11	1058-1401	22	58	164221	
10H25H	3	540	9.738	5/11-5/11	1843-2213	22	58	188705	
10H25H	4	510	9.522	6/11-6/11	0049-0535	19	60	257405	
10H25H	5	460	8.774	6/11-6/11	1048-1532	22	60	255178	

Specimen model		Stress range, Mpa	Load on fatigue machine	Date	Time	Temperature (°C)	Humidity (%)	Fatigue life, N_f	Comment
10H0V	1	300	5.867	7/10-8/10	1531-0128	27.3	66	536718	
10H0V	2	260	5.098	8/10-9/10	0831-0445	25	80	1092117	
10H0V	3	240	4.645	9/10-10/10	0704-1102	25	82	1510505	
10H0V	4	220	4.356	10/10-12/10	1116-1442	29	76	2777344	
10H0V	5	180	3.554	12/10-18/10	1752-0942	28	44	7335445	stop- no break - bending
10H20V	1	500	9.227	6/11-6/11	1643-1929	24		148188	
10H20V	2	480	8.790	7/11-7/11	1146-1427	24		144307	
10H20V	3	440	8.307	7/11-8/11	2010-0037	23		239403	
10H20V	4	400	7.550	8/11-10/11	1119-0553	23		2298597	stop- no break - bending
10H20V	5	420	7.774	10/11-10/11	0603-1056	21.5		262562	
10H25V	1	500	9.409	11/11-11/11	0955-1253	20	44	160366	
10H25V	2	480	9.093	11/11-11/11	1436-1858	20	44	235119	
10H25V	3	440	8.294	11/11-12/11	2044-0129	17	52	255901	
10H25V	4	400	7.554	12/11-12/11	1030-1652	17	54	343506	
10H25V	5	380	7.196	12/11-13/11	1713-1515	19	46	1189260	

Specimen model		Stress range, Mpa	Load on fatigue machine	Date	Time	Temperature (°C)	Humidity (%)	Fatigue life, N_f	Comment
10M0H	1	300	5.546	14/11-15/11	1201-1157	20	52	1300190	
10M0H	2	320	5.945	15/11-16/11	1952-0118	19.5	62	291991	
10M0H	3	280	5.152	16/11-17/11	2320-0937	17.5	61	554514	
10M0H	4	260	4.911	17/11-18/11	1730-0518	17.5	56	636077	
10M0H	5					sending for residual stress measurement			
10M20H	1	340	6.276	18/11-25/11	1059-1117	14	49	9087756	stop-not break
10M20H	2	400	7.456	25/11-26/11	1135-0142	17	68	762359	
10M20H	3	420	7.777	26/11-27/11	1634-0523	17	47	691209	
10M20H	4	380	7.178	27/11-28/11	1017-1332	14	66	1471149	
10M20H	5					sending for residual stress measurement			
10M25H	1	440	8.149	28/11-29/11	1504-1159	16	54	1129077	
10M25H	2	460	8.491	29/11-30/11	1438-0813	13.5	55	949438	
10M25H	3	480	8.911	30/11-1/12	0825-0959	15	62	741727	
10M25H	4	500	9.199	1/12-2/12	1042-2200	14	72	609410	
10M25H	5					sending for residual stress measurement			

Specimen model		Stress range, Mpa	Load on fatigue machine	Date	Time	Temperature (°C)	Humidity (%)	Fatigue life, N_f	Comment
10M0V	1	320	5.994	9/12-9/12	1320-1830	17	56	339622	
10M0V	2	300	5.593	10/12-10/12	1040-0336	15	76	472160	
10M0V	3	260	4.815	10/12-11/12	1337-0452	15	54	854072	
10M0V	4	240	4.415	11/12-12/12	1630-1752	13	60	1369583	
10M0V	5					sending for residual stress measurement			
10M20V	1	460	8.575	13/12-13/12	0947-1228	12	64	145519	
10M20V	2	400	7.529	13/12-14/12	2159-0428	12	54	350700	
10M20V	3	360	6.645	16/12-16/12	1021-1640	11	56	325686	
10M20V	4	340	6.338	17/12-18/12	1415-0520	12	54	815187	
10M20V	5					sending for residual stress measurement			
10M25V	1	440	8.201	18/12-18/12	1612-2017	16	56	220307	
10M25V	2	400	7.456	19/12-19/12	1401-1930	16	54	297704	
10M25V	3	360	6.799	20/12-20/12	1046-1640	14	46	334493	
10M25V	4	340	6.369	22/12-22/12	1048-1850	16	54	455546	
10M25V	5					sending for residual stress measurement			

Specimen model		Stress range, Mpa	Load on fatigue machine	Date	Time	Temperature (°C)	Humidity (%)	Fatigue life, N_f	Comment
15H0H	1	300	12.378	2/2-2/2	1214-1742	19	76	295026	
15H0H	2	260	10.941	3/2-3/2	1122-1654	16	78	406598	
15H0H	3	220	10.000	4/2-4/2	1010-1930	17	38	509021	
15H0H	4	200	8.279	5/2-5/2	2030-2010	17	38	960659	
15H0H	5					sending for residual stress measurement			
15H20H	1	320	13.246	7/2-8/2	0943-1227	11	66	1443751	
15H20H	2	300	12.562	8/2-9/2	2105-2208	21	40	1352782	
15H20H	3	280	11.629	10/2-11/2	1008-2019	20	44	1845551	
15H20H	4	340	14.331	11/2-12/2	2126-1632	19	32	1030935	
15H20H	5					sending for residual stress measurement			
15H25H	1	320	13.555	13/2-14/2	1132-0756	21	30	1101191	
15H25H	2	280	12.095	14/2-15/2	1044-0932	18	40	1231229	
15H25H	3	340	14.450	19/2-20/2	1736-0700	21	34	721290	
15H25H	4	240	10.333	15/2-19/2	1420-1730	22	34	5354947	stop-no break
15H25H	5					sending for residual stress measurement			

Specimen model		Stress range, Mpa	Load on fatigue machine	Date	Time	Temperature (ºC)	Humidity (%)	Fatigue life, N_f	Comment
15H0V	1	300	12.708	20/2-20/2	1617-2122	23	34	273891	
15H0V	2	260	11.013	25/2-26/2	1114-0033	23	40	718392	
15H0V	3	240	10.116	21/2-21/2	1015-2341	21	38	724756	
15H0V	4	220	8.389	23/2-24/2	2212-0223	21	40	1521960	
15H0V	5					sending for residual stress measurement			
15H20V	1	320	13.269	26/2-26/2	1158-2037	19	62	467459	
15H20V	2	300	12.480	27/2-28/2	1414-0042	21	66	565330	
15H20V	3	280	11.534	1/3-2/3	1050-0935	20	60	1068237	
15H20V	4	260	11.158	28/2-1/3	1050-1034	21	60	1271587	
15H20V	5					sending for residual stress measurement			
15H25V	1	320	13.378	3/3-3/3	1127-2240	17	44	605704	
15H25V	2	280	12.056	4/3-5/3	1217-1000	19	42	1000483	
15H25V	3	260	10.870	5/3-6/3	1500-2242	19	40	1687988	
15H25V	4	240	10.133	7/3-9/33	1157-02450	19	30	2094841	
15H25V	5					sending for residual stress measurement			

Specimen model		Stress range, Mpa	Load on fatigue machine	Date	Time	Temperature (°C)	Humidity (%)	Fatigue life, N_f	Comment
15M0H	1	300	13.213	24/12-24/12	1148-1710	17	47	287141	
15M0H	2	260	11.544	25/12-25/12	1229-2315	17	43	505887	
15M0H	3	220	9.782	26/12-27/12	1235-0202	17	48	747151	
15M0H	4	200	8.793	27/12-28/12	2227-1935	15	36	1047268	
15M0H	5					sending for residual stress measurement			
15M20H	1	300	13.254	5/1-6/1	2256-1939	18	48	1119235	
15M20H	2	320	13.957	7/1-7/1	1117-2349	19	47	676600	
15M20H	3	260	11.340	8/1-10/1	1130-0705	18	54	2338111	
15M20H	4	280	12.213	10/1-11/1	1030-1001	14	34	1268865	
15M20H	5					sending for residual stress measurement			
15M25H	1	320	13.957	11/1-14/1	2023-1224	15	44	3290019	jig break left side
15M25H	2	340	14.999	14/1-15/1	1303-1335	17	42	1325650	
15M25H	3	360	15.524	15/1-16/1	1944-1531	11	54	1068749	
15M25H	4	380	16.227	16/1-17/1	1551-1008	14	48	986908	
15M25H	5					sending for residual stress measurement			

Specimen model		Stress range, Mpa	Load on fatigue machine	Date	Time	Temperature (°C)	Humidity (%)	Fatigue life, N_f	Comment
15M0V	1	300	12.896	17/1-17/1	1036-1840	10		430000	
15M0V	2	260	11.122	17/1-18/1	2232-1032	10		647477	
15M0V	3	220	10.350	18/1-19/1	2049-1328	11		899130	
15M0V	4	200	8.752	19/1-21/1	2306-1322	9		2036664	
15M0V	5					sending for residual stress measurement			
15M20V	1	320	13.688	21/1-22/2	1747-0302	9		502411	
15M20V	2	300	12.811	22/1-22/1	1042-2314	7		676350	
15M20V	3	280	11.939	23/1-24/1	1148-0504	14.5		932242	
15M20V	4	260	11.084	24/1-25/1	1100-1142	16		1334194	
15M20V	5					sending for residual stress measurement			
15M25V	1	280	11.977	27/1-28/1	1142-0732	16		1107601	
15M25V	2	260	11.158	28/1-29/1	0959-0602	16		1082784	
15M25V	3	240	10.333	29/1-30/1	1002-2109	16		1896607	
15M25V	4	320	13.778	25/1-26/1	2007-0623	20		554697	
15M25V	5					sending for residual stress measurement			

Specimen model		Stress range, Mpa	Load on fatigue machine	Date	Time	Temperature (°C)	Humidity (%)	Fatigue life, N_f	Comment
20H0H	1	280	15.381	4/5-4/5	0750-1345	18	54	319585	
20H0H	2	260	14.097	5/5-5/5	1003-1614	20	62	333500	
20H0H	3	220	11.928	5/5-6/5	1647-0627	24	38	737796	
20H0H	4	180	9.760	6/5-7/5	0930-1512	19	48	1603922	
20H0H	5					sending for residual stress measurement			
20H20H	1	300	16.000	29/5-30/5	1454-2241	34	52	1716314	
20H20H	2	280	14.983	31/5-1/6	0209-0259	25	68	1341550	
20H20H	3	260	14.190	1/6-3/6	2249-1109	28	60	1961965	
20H20H	4	320	17.067	3/6-4/6	1131-0131	28	60	756310	
20H20H	5					sending for residual stress measurement			
20H25H	1	300	15.627	12/7-13/7	1446-1853	27	52	1517824	
20H25H	2	280	14.386	14/7-16/7	1414-1100	27	60	2417557	
20H25H	3	340	17.892	18.7-19/7	1530-1342	30	50	1198231	
20H25H	4	320	16.725	17/7-18/7	1103-1146	28	60	1334217	
20H25H	5					sending for residual stress measurement			

Specimen model		Stress range, Mpa	Load on fatigue machine	Date	Time	Temperature (°C)	Humidity (%)	Fatigue life, N_f	Comment
20H0V	1	300	15.132	8/2-8/5	0944-1834	24	60	476377	
20H0V	2	260	13.543	8/5-9/5	2031-0733	19	62	595465	
20H0V	3	220	11.580	9/5-10/5	1104-0757	25	57	1127824	
20H0V	4	180	9.696	10/5-12/5	1236-0658	25	48	2287713	
20H0V	5					sending for residual stress measurement			
20H20V	1	300	16.480	4/6-4/6	0930-1604	25	76	354708	
20H20V	2	280	14.784	4/6-5/6	1734-0552	26	68	664447	
20H20V	3	260	13.820	5/6-6/6	1044-0438	25	74	967135	
20H20V	4	220	11.616	6/6-7/6	1120-0842	23	84	1154166	
20H20V	5					sending for residual stress measurement			
20H25V	1	300	16.427	8/7-8/7	1620-2039	29	54	233117	
20H25V	2	260	14.001	9/7-9/7	1130-1941	27	70	441813	
20H25V	3	240	13.056	10/7-10/7	1152-2225	27	70	569611	
20H25V	4	220	11.968	11/7-11/7	1112-2305	28	56	641614	
20H25V	5					sending for residual stress measurement			

Specimen model		Stress range, Mpa	Load on fatigue machine	Date	Time	Temperature (°C)	Humidity (%)	Fatigue life, N_f	Comment
20M0H	1	300	16.000	30/4-30/4	1358-1903	21	70	274884	
20M0H	2	260	13.860	30/4-1/5	2300-0609	20	74	386370	
20M0H	3	220	11.730	1/5-1/5	1107-1918	22	66	442182	
20M0H	4	180	9.600	1/5-3/5	2320-1157	21	62	1977359	
20M0H	5					sending for residual stress measurement			
20M20H	1	300	15.840	16/5-16/5	0935-2240	25	61	706772	
20M20H	2	260	14.000	17/5-18/5	0945-0803	25	53	1222793	
20M20H	3	220	11.655	18/5-22/5	2151-1722	27	52	4941875	stop - not break
20M20H	4	280	14.884	22/5-23/5	1731-2040	29	58	1466186	
20M20H	5					sending for residual stress measurement			
20M25H	1	300	16.267	7/6-10/6	1645-0334	26	82	3446312	
20M25H	2	280	15.083	27/6-1/7	1049-1536	26	74	5441912	stop - not break
20M25H	3	340	18.496	1/7-8/7	1543-1512	29	52	9043285	stop - not break
20M25H	4	320	17.410	10/6-14/6	0954-0730	26	76	4770241	stop - not break
20M25H	5					sending for residual stress measurement			

Specimen model		Stress range, Mpa	Load on fatigue machine	Date	Time	Temperature (°C)	Humidity (%)	Fatigue life, N_f	Comment
20M0V	1	280	15.033	12/5-12/5	0938-1508	23	68	297144	
20M0V	2	260	13.820	12/5-13/5	2250-0912	21	68	560167	
20M0V	3	220	11.733	13/5-14/5	1534-0522	29	54	745138	
20M0V	4	180	9.728	14/5-16/5	1457-0059	23	65	1837700	
20M0V	5					sending for residual stress measurement			
20M20V	1	300	16.267	26/5-26/5	1207-1810	26	76	326740	
20M20V	2	280	15.033	23/5-24/5	2150-0645	23	70	482014	
20M20V	3	260	14.052	27/5-27/5	0945-2329	24	56	740672	
20M20V	4	240	12.970	28/5-29/5	1033-0409	29	44	949627	
20M20V	5					sending for residual stress measurement			
20M25V	1	300	16.053	14/6-18/6	0736-1340	24	74	334363	
20M25V	2	280	15.431	18/6-19/6	1625-0250	23	82	577045	
20M25V	3	260	14.010	19/6-20/6	1539-0241	27	60	408215	
20M25V	4	220	11.968	23/6-24/6	1437-0356	27	33	720264	
20M25V	5					sending for residual stress measurement			